State of Illinois
Rod. R. Blagojevich, Governor
Illinois Department of Natural Resources
Illinois State Geological Survey

Declining Specific Capacity of High-Capacity Wells in the Mahomet Aquifer: Mineralogical and Biological Factors

Samuel V. Panno, Keith C. Hackley, Edward Mehnert,
David R. Larson, Dylan Canavan, and Timothy C. Young

Circular 566 2005

Illinois Department of Natural Resources

1905-2005 ISGS Illinois State Geological Survey

Disclaimer

Front Cover: *Drilling operations with rotasonic drill rig immediately adjacent to the well house for NIWC 57.*

Released by the authority of the State of Illinois 10/05

Declining Specific Capacity of High-Capacity Wells in the Mahomet Aquifer: Mineralogical and Biological Factors

Samuel V. Panno, Keith C. Hackley, Edward Mehnert,
David R. Larson, Dylan Canavan, and Timothy C. Young

Circular 566 2005

Illinois Department of Natural Resources
ILLINOIS STATE GEOLOGICAL SURVEY
William W. Shilts, Chief
615 E. Peabody Drive
Champaign, Illinois 61820-6964
217-333-4747
www.isgs.uiuc.edu

Contents

Tables

Figures

Abstract

Over the last three decades, Illinois-American Water Company (IL-AWC) personnel have observed progressive decreases in the specific capacities of most of the company's high-capacity wells screened in the Mahomet aquifer at Champaign, Illinois. Based on a preliminary study, Illinois State Geological Survey investigators hypothesized that the loss of specific capacity was largely due to calcite precipitating adjacent to the wells as a result of decreased hydrostatic pressure around the wells and a concomitant loss of CO_2 caused by outgassing.

To test this hypothesis, a high-capacity well (IL-AWC well NIWC 57) was extensively analyzed. Well NIWC 57 has been in operation since 1964, has a pumping rate of 2.68 million gallons per day, and has experienced a loss of 76% of its total specific capacity. Two boreholes were drilled to bedrock near well NIWC 57 using the rotasonic technique, which requires only a limited use of drilling fluids. Drill cores collected from the surface down to and into bedrock were examined in the field and in the laboratory using a variety of physical, chemical, and biological techniques. Two monitoring wells were installed in each completed borehole. Groundwater samples were collected from NIWC 57, two other production wells, and the two new monitoring wells. Additionally, suspended solids entrained in the water of the high-capacity wells were trapped on a 0.5-μm filter for examination by scanning electron microscopy.

Several factors were potentially responsible for the loss of specific capacity in the production wells. Examination of the materials retained in the filters showed that calcite, in the form of euhedral crystals that were about 5 μm in diameter, was precipitating in close proximity to the wells. X-ray diffraction results showed that the sand and gravel from the borehole closest to the production well was enriched in clay minerals relative to the borehole farther away. Clay minerals, clay-size particles, and larger mineral fragments of the same composition as those constituting the aquifer (particles up to 100 μm in diameter) were found to have been transported within the aquifer and were discharged from the wells during pumping. Analysis of suspended materials retained by the filters also revealed the presence of iron-depositing bacteria and biofilm fragments. The size and abundance of detrital mineral fragments and bacterially derived materials (e.g., tubercles) found on the filters appeared to be correlated to the pumping rate. That is, the greater the pumping rate, the larger and more abundant were the detrital materials and bacterial debris collected on the filters.

Based on the available evidence, the following conceptual model was proposed: iron-depositing bacteria produced biofilms on the well screens (probably within the gravel pack and possibly within the adjacent aquifer) that entrapped transported mineral fragments, clay minerals, and newly precipitated calcite crystals. These three components apparently combined to produce an insoluble scale on the well screen and potentially in the gravel pack and adjacent aquifer. The model suggests that this process was responsible for the decreased specific capacity of the production wells in the western well field of Champaign, Illinois.

The study results suggest that this type of plugging might be a likely cause of decreases in the specific capacity of other production wells screened in the Mahomet aquifer in east-central Illinois and other bedrock valley aquifers of the Midwest. Inspection of the screens with a downhole camera and collection and analyses of samples of encrustation, if present, could yield valuable information as to the nature of the encrustation. This information could be used to identify appropriate, commercially available remediation techniques.

Introduction

Specific capacity expresses the productivity and efficiency of a well and is defined as the pumping rate in gallons per minute (gpm) divided by the drawdown in feet. Decreases in the specific capacity can force an operator to abandon a production well. Because a high-capacity well typically costs hundreds of thousands of dollars to drill and put into service, a significant loss of specific capacity during the life of a well is an important physical and economic problem. Factors leading to the loss of specific capacity (other than mechanical problems with the pump) include hydraulic influences and reduced porosity of the well screen and/or gravel pack as a result of biological, chemical, and/or physical processes (Borch et al. 1993). The processes often result in the encrustation of deposits of organic and/or inorganic materials on the well screen, in the gravel pack, and/or in the adjacent aquifer (Johnson Division 1982).

Illinois-American Water Company's (IL-AWC) western well field in Champaign, Illinois, includes 12 production wells that have individual pumping capacities ranging from 1.55 to 3.44 $\times 10^6$ gallons per day. These wells supply water to Champaign, Urbana, and surrounding communities, and most have lost specific capacity since the wells were first constructed (fig. 1). The wells averaged a 1.22% loss of specific capacity per year, but the total annual changes range from an increase of 4.17% to a decrease of 4.10%. An evaluation of data available from IL-AWC showed that physical hydraulic interferences at the wells and in the well field had little effect on the observed losses.

Preliminary geochemical studies of selected production wells (Mehnert et al. 1999) suggested that carbonate and iron minerals could be precipitating within the aquifer and reducing the porosity and hydraulic conductivity within 100 feet of each affected well. The authors hypothesized that precipitation of these minerals from groundwater could be associated with outgassing of CO_2 caused by the reduction in hydrostatic pressure in the aquifer adjacent to the well resulting from pumping.

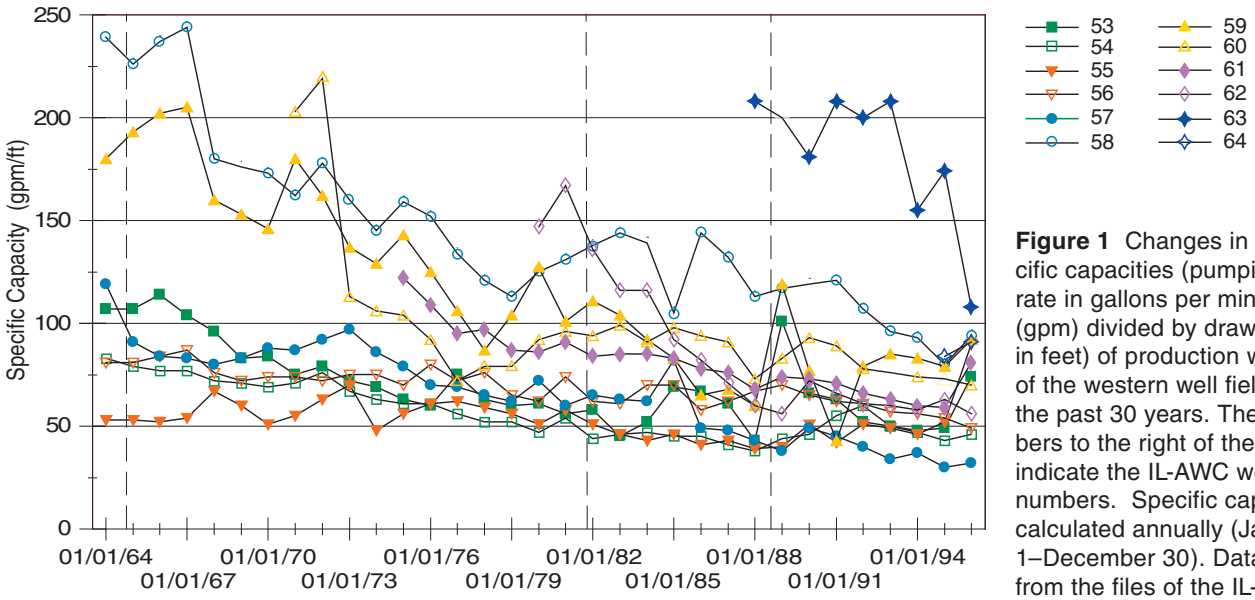

Figure 1 Changes in specific capacities (pumping rate in gallons per minute (gpm) divided by drawdown in feet) of production wells of the western well field over the past 30 years. The numbers to the right of the figure indicate the IL-AWC well numbers. Specific capacity calculated annually (January 1–December 30). Data are from the files of the IL-AWC.

This process could be exacerbated by the presence of dissolved methane gas in the groundwater. Other mechanisms explored by Mehnert et al. (1999) included hydraulic factors such as well interference, entrance velocities exceeding the optimum of 6 feet per minute (Driscoll 1986), and biofouling resulting from the growth of iron-depositing bacteria on and near the well screens.

Objectives

Given the results of the earlier study (Mehnert et al. 1999), this present investigation focused on the potential for loss of specific capacity resulting from secondary mineralization, physical plugging by transported clay and other minerals, and/or biofilm development on the well screen within the gravel pack and within the pore spaces of the Mahomet aquifer. A high-capacity well, NIWC 57, was selected for study. Well NIWC 57 has been in operation since 1964, has an operating pumping rate of 2.68×10^6 gallons per day, and has lost 76% of its original specific capacity. Aquifer materials and groundwater were closely examined for evidence of physical, chemical, and biological factors that could be responsible for the loss of specific capacity in the production wells.

Geology and Hydrogeology of the Study Area

As water use in the midwestern United States has increased in recent years, reliance on local and regional aquifers has increased. Glacial drift aquifers are extensive and offer a prolific source of fresh water for many parts of the midwestern and eastern United States. One such aquifer, the Mahomet aquifer, was deposited in a roughly east-west–trending buried bedrock valley in east-central Illinois and western Indiana that was once thought to be part of the larger Teays drainage system. Studies have found, however, that the Teays is not a single, coherent drainage system (e.g., Melhorn and Kempton 1991a, 1991b).

The Mahomet Sand Member is composed of sand and gravel deposited as glacial outwash within the confines of the Mahomet Bedrock Valley. The outwash was subsequently buried by tills deposited during later Pleistocene continental glaciations (fig. 2). Melhorn and Kempton (1991a) reviewed the geology and hydrogeology of the Teays-Mahomet Bedrock Valley System, which is summarized here.

The Mahomet Bedrock Valley, which was incised in bedrock, is now buried beneath 300 or more feet of Pleistocene glacial drift. Using the 500-foot elevation contour to define its upper limit, the valley ranges in width from 8 to 11 miles (figs. 3 and 4). The deepest part of the valley and many of its tributary channels are filled with clean sand and gravel that averages 100 feet thick and, in places, up to 200 feet thick (figs. 3 and 4). The Mahomet aquifer, which is generally coincident with the Mahomet Sand Member of the Banner Formation, is overlain by the Glasford Formation. Sand and gravel outwash deposits within the Glasford Formation, which are generally most extensive where they are associated with the Vandalia Till Member, also constitute an aquifer that, in the vicinity of the Mahomet aquifer, is locally important. Relatively thin sand deposits in the Wedron Formation typically occur at shallow depths and, in some places, intersect the surface and form springs or seeps.

Horberg (1953) reported that the Mahomet aquifer "... sand and gravel in roughly equal proportions is composed of a wide variety of rocks and minerals, dominantly of sedimentary origin. Silty beds occur throughout. Many horizons are strongly oxidized." The sand of the Mahomet Sand Member is made up predominantly of quartz, lesser amounts of K-feldspar and Ca-Na feldspar (Willman and Frye 1970), and minor amounts of translucent heavy minerals that

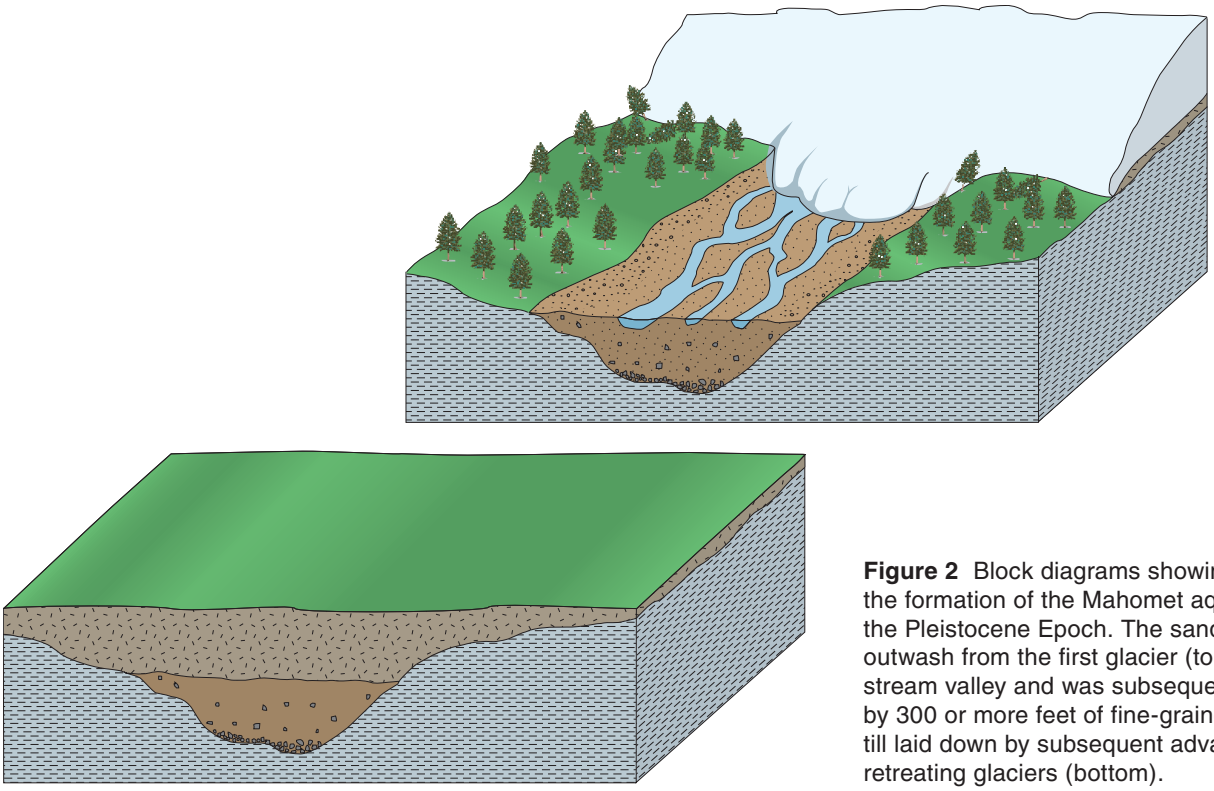

Figure 2 Block diagrams showing stages in the formation of the Mahomet aquifer during the Pleistocene Epoch. The sand and gravel outwash from the first glacier (top) filled a stream valley and was subsequently buried by 300 or more feet of fine-grained glacial till laid down by subsequent advancing and retreating glaciers (bottom).

include (in descending order of abundance) hornblende, garnet, epidote, and hyperenstatite (Manos 1961). Carbonate minerals in these sands are dominated by calcite, which is in contrast to the overlying sands of the Glasford aquifer where dolomite is the dominant carbonate mineral (H. Glass, ISGS, personal communication 1992).

The hydraulic characteristics of the Mahomet aquifer have been determined from pumping tests conducted on high-capacity wells. Transmissivities for the Mahomet Sand Member range from 7×10^{-4} to 8×10^{-2} m^2/s; median hydraulic conductivity is 1.4×10^{-3} m/s. A potentiometric surface prepared from historical records of water levels showed the probable pre-development groundwater flow directions and a hydraulic gradient of approximately 0.0002 (Kempton et al. 1991). The largest hydraulic heads were found near the intersection of northeastern Champaign, northwestern Vermilion, and southern Iroquois Counties (fig. 4). Groundwater flow was originally to the north, east, and southwest from this area prior to the establishment of large pumping centers (Kempton et al. 1991).

Earlier workers (e.g., Visocky and Schicht 1969, Kempton et al. 1982) assumed that recharge to the Mahomet aquifer came from the surface via vertical leakage of precipitation and snowmelt through the overlying glacial deposits. However, an examination of the chemical composition of the groundwater in the Mahomet aquifer (Panno et al. 1994) showed geochemically distinct groundwater regions along several reaches of the aquifer. The existence of these distinct regions revealed that recharge comes at least partly from bedrock sources in some parts of the Mahomet aquifer.

Methods

Construction of Drilling and Monitoring Wells

Two boreholes were drilled near production well NIWC 57 using rotasonic drilling equipment. Rotasonic drilling allows for the recovery of minimally disturbed and essentially complete core without the use of drilling fluid, except to lubricate the outside of the core barrel during drilling in the unsaturated zone (Barrow 1994). A relatively small volume of water may be used to force the core from the core barrel during recovery. The drilling company, Boart Longyear of Schofield, Wisconsin, used a rotasonic drill head mounted on a Gus Pech model GP24-300RS rig.

The first borehole (NIWC 57-1) (fig. 3), located approximately 15 feet north-northeast of NIWC 57, was drilled 3 feet into bedrock to a total depth of 333 feet. The second borehole (NIWC 57-2), located approximately 60 feet southeast of NIWC 57, was drilled to a total depth of 310 feet. The rotasonic drilling method (fig. 6) provided high-quality core with nearly complete recovery of the Quaternary materials underlying this site. The Quaternary materials included soil, dense glacial tills, cobbles within the tills, and sand and gravel. The bedrock was Pennsylvanian System shale. Geological

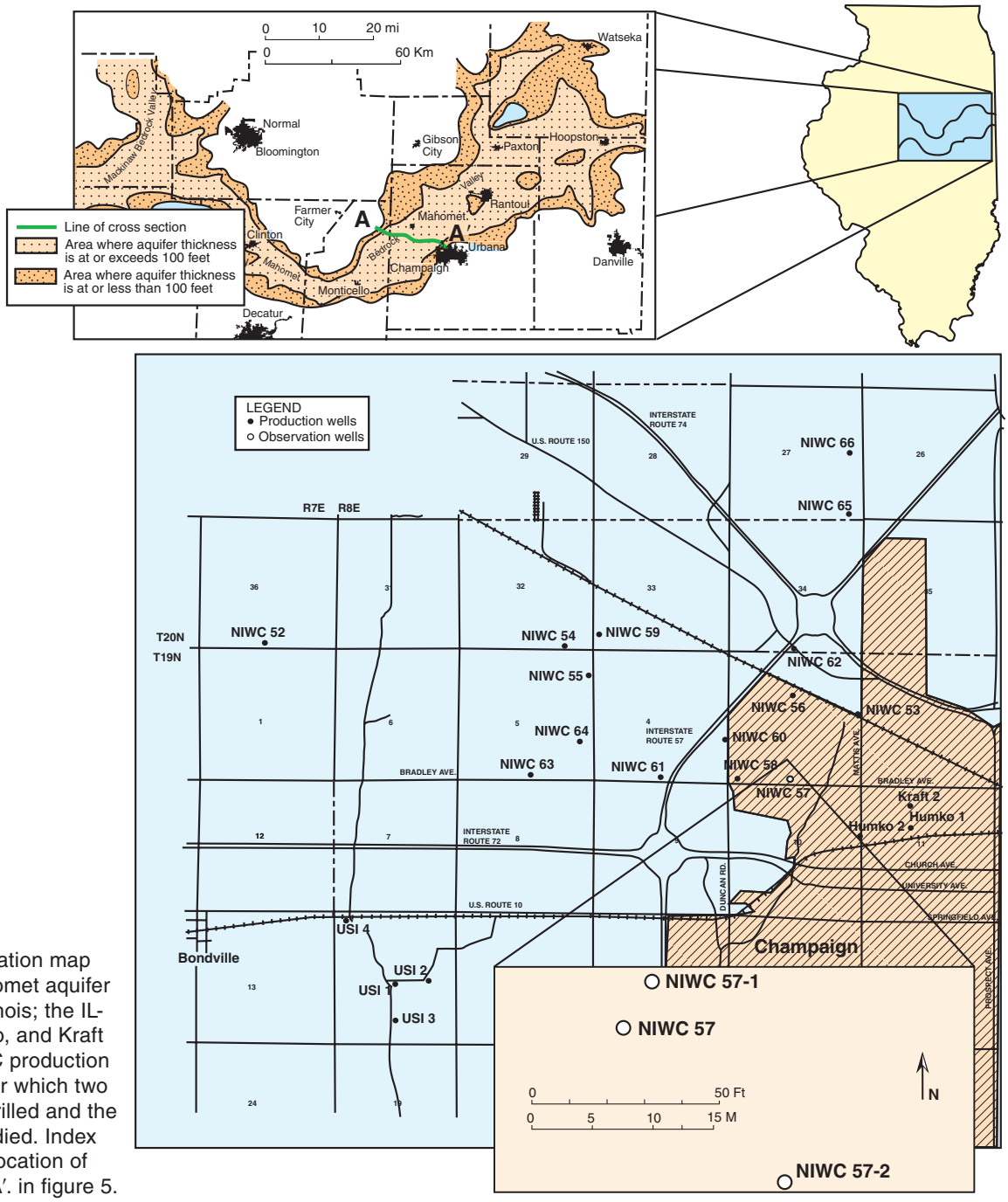

Figure 3 Site location map showing the Mahomet aquifer of east-central Illinois; the IL-AWC, USI, Humko, and Kraft wells; and IL-AWC production well NIWC 57 near which two boreholes were drilled and the core samples studied. Index map also shows location of cross section A–A′. in figure 5.

descriptions of the core samples were made at the site. All samples for particle size, microscopy, X-ray diffraction (XRD), isotopic, and bacterial analyses were taken immediately after the core was extruded from the core barrel. Half of the drill core from both boreholes was collected, placed in core boxes, labeled with borehole numbers and footages, and stored at the Illinois State Geological Survey (ISGS) Geological Samples Library.

In each borehole, a shallow monitoring well was completed in the Glasford aquifer, and a deep well was completed in the Mahomet aquifer (fig. 5). The monitoring wells completed in the Glasford aquifer were designated NIWC 57-1G and NIWC-2G; those completed in the Mahomet aquifer were designated NIWC 57-1M and NIWC 57-2M. The monitoring wells were constructed from 2-inch diameter, threaded joint, schedule 80 polyvinal chloride (PVC) pipe and 2-inch, 10-slot, schedule 80 PVC screens. For the deep wells, PVC pipe was used below the screens to set them at the desired depth. The annulus of each

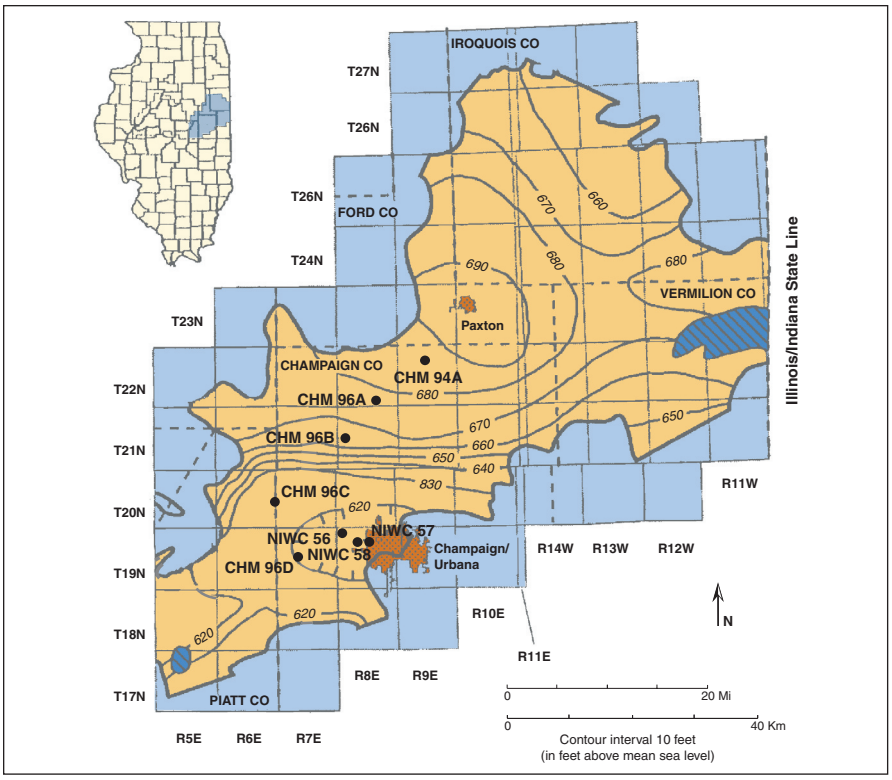

Figure 4 Site location map showing the eastern half of the Mahomet aquifer in Illinois, the Illinois State Water Survey observation well, the IL-AWC production well locations, and contours of the potentiometric surface (modified from Hackley 2002).

borehole was filled mostly with bentonite grout and sand (natural backfill) (fig. 7). Bentonite was used to seal the annulus between the Mahomet and Glasford aquifers as well as above the Glasford aquifer. All of the wells were completed below grade inside steel manholes fitted with bolt-on covers and a rubber seal.

In addition to the samples collected from the two new boreholes, 8 samples of sand and gravel from the Mahomet Sand Member were collected from archived samples from the ISGS Geological Samples Library (NIWC 65 and CHM 96A). NIWC 65 is a production well located about 2 miles north of NIWC 57 (fig. 3) that was drilled in 1996 using the reverse-rotary technique. CHM 96A is a monitoring well located west of Rantoul, Illinois (fig. 4), that was drilled in 1996 by the Illinois State Water Survey using the forward-rotary technique. These archived samples provided additional particle-size and mineralogic information for the investigation.

Description of Core

The drillers operating the rotosonic drilling equipment used vibration and water pressure to extrude core from the core barrel into polyethylene sleeves. Core lengths ranged from 1 to 10 feet. The plastic-encased core was transported to a table and

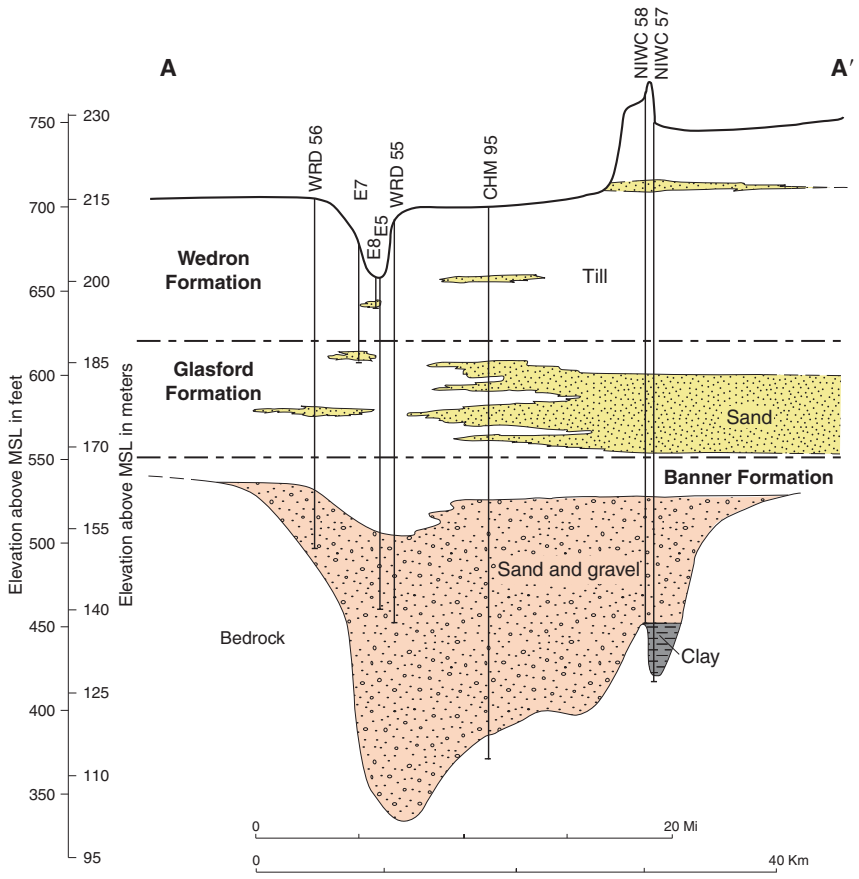

Figure 5 Cross section A–A′ showing the location of Wedron and Glasford aquifers overlying the Mahomet aquifer Banner Formation, which almost completely fills a valley incised into bedrock. Also shown are the locations of IL-AWC production wells NIWC 57 and 58, an Illinois State Water Survey monitoring well, and private wells (modified from Hackley 2002). Cross section line is shown on inset regional map in figure 3.

Figure 6 Drilling operations with rotasonic drill rig immediately adjacent to the well house for NIWC 57. Core recovery was almost 100%, and drilling fluids were not used.

examined and described by ISGS geologists using standard techniques and terminology. Complete descriptions of the cores from boreholes NIWC 57-1 and NIWC 57-2 are in the Appendix.

Particle-Size Analysis

The particle-size distributions of selected samples from the Mahomet aquifer were measured by the ISGS Quaternary materials laboratory using standard-sized sieves. Nineteen samples from borehole NIWC 57-1 were passed through sieves of the following sizes: 2.0000, 1.0000, 0.5000, 0.2500, 0.1770, 0.1250, 0.0880, 0.0625, and 0.0370 mm.

Petrographic Cathodoluminescence and Microscopy

Petrographic studies using polarized light and cathodoluminescence microscopy were completed to examine cements within the sand and gravel samples collected from the Wedron, Glasford, and Mahomet aquifers. Fifty thin sections of sand and gravel from the two rotasonic boreholes (42 samples) and from previously archived samples (8 samples) were prepared by Spectrum Petrographics of Winston, Oregon, using standard techniques. Because the samples consisted of unlithified sand and gravel, samples first were impregnated with a clear, heat-resistant epoxy, cemented to a glass slide, and cut and polished into thin (30-μm) sections. The thin sections were examined using the petrographic and cathodoluminescence equipment at the Geology Department, University of Illinois, Urbana-Champaign. Methods are described in more detail by Fouke and Rakovan (2001).

Petrographic point counts were completed for 32 of the 50 thin sections to determine the mineralogic compositions of the Mahomet and overlying aquifers. Thin sections were placed under a petrographic microscope equiped with an adjustable stage. Approximately 200 points were counted for each thin section, and the mineralogy of each grain intersected was identified as quartz, carbonate minerals, feldspar, chert, or rock fragments.

Cathodoluminescence was used to help reveal diagenetic textures and growth features within the sedimentary rocks not visible using conventional polarized-light petrographic techniques. Cathodoluminescence is achieved by bombarding a polished thin section, under vacuum, with a controlled electron beam emitted from a cathode-ray tube. Some of the energy from the electron beam is absorbed, some is transmitted, and some is reflected as X-rays, secondary electrons, auger electrons, phonons, and photons. The visible light portion of this reflected spectrum constitutes cathodoluminescence (Machel and Burton 1991). The intensity of the luminescence from the thin section depends on the amount and type of impurities present in the crystal lattices of the minerals. For example, Mn^{2+} and Cr^{3+} are "activators" that emit photons in the range of visible light; Ni^{2+}, Fe^{2+}, and Co^{2+} are "quenchers" that emit energy as phonons (heat) instead of visible photons (Machel and Burton 1991). Thus, materials with relatively high concentrations of Fe^{2+}, Ni^{2+}, and Co^{2+} in the crystal lattice have low or no lumines-

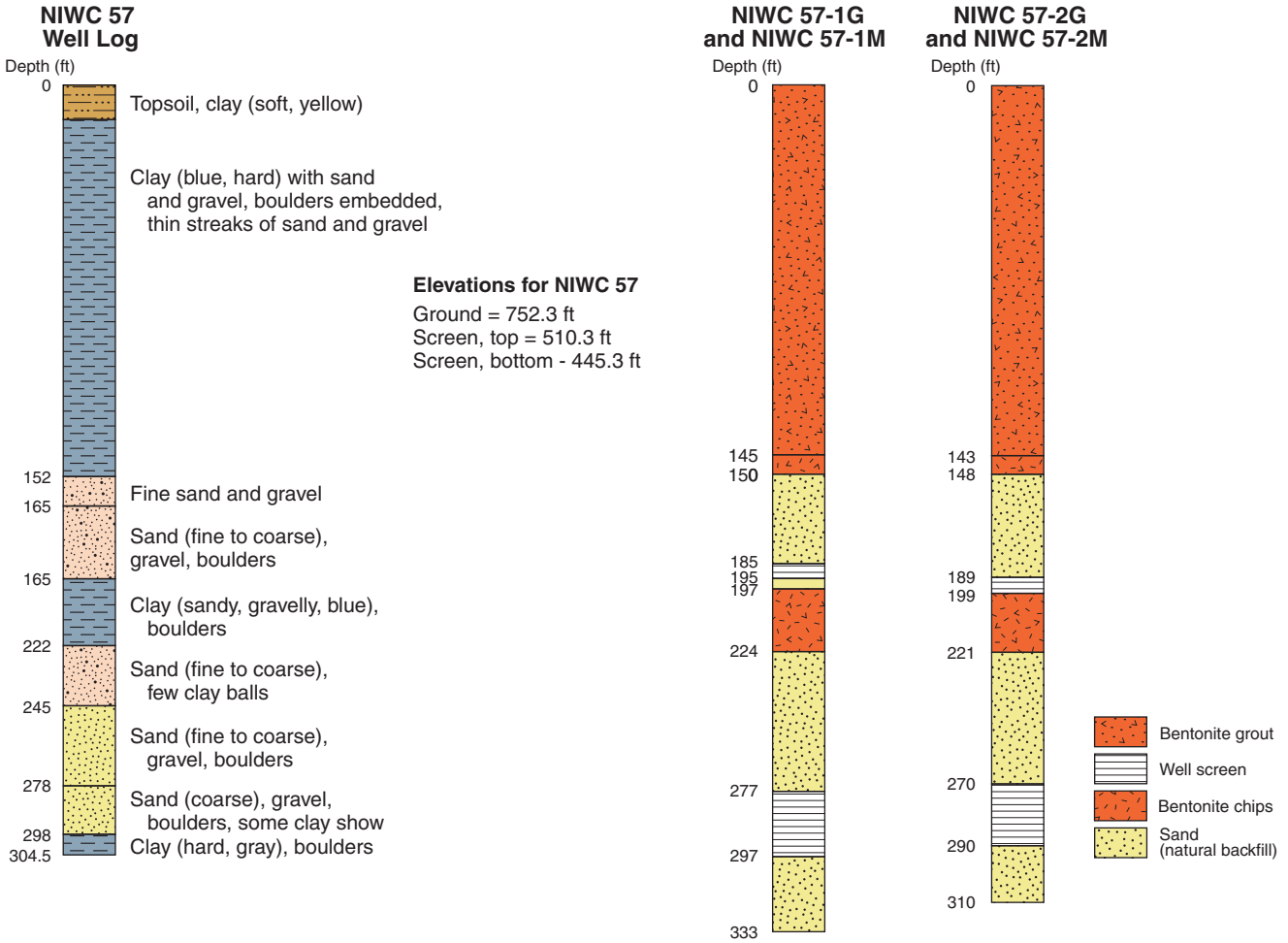

Figure 7 Condensed driller's log for IL-AWC production well NIWC 57 (left) and construction details for monitoring wells installed at the site (right).

cence. Materials with relatively high concentrations of Mn^{2+} and Cr^{3+} in the crystal lattice show relatively bright luminescence.

Scanning Electron Microscopy

Twenty samples collected from cores of the sand and gravel of the Banner and Glasford Formations (from boreholes NIWC 57-1 and NIWC 57-2) were examined using scanning electron microscopy (SEM). These samples included bulk sand and gravel, a sample of the ≤325-mesh (<44-μm) size fraction, and thin sections of lithified sand and gravel held together by blocky calcite cement. An Amray 1830 SEM coupled with a Noran 5500 series II, high-energy dispersive X-ray system and a VISTA imaging system, was used. Samples were examined under a 20-kV electron beam at a distance of 20 mm. Selected points on each sample were analyzed using the high-energy dispersive X-ray system. The elemental spectrum of a mineral phase was collected for 30 s, and the relative abundances of the elements in the spectrum were used to identify the minerals.

Other samples selected for SEM and high-energy dispersive X-ray system analysis included the samples from certain horizons in the Mahomet aquifer from boreholes NIWC 57-1 and NIWC 57-2, and thin sections of cemented sand nodules from near the base of borehole NIWC 57-1 and <325-mesh (<44-μm) size fraction from archival samples of the Mahomet and Glasford aquifers from boreholes NIWC 65 and CHM 96A. NIWC 65 is located about 2 miles from the cluster of high-capacity wells examined in this investigation. CHM 96A is located 13 miles from the well field and would not be subjected to the possible geochemical effects of pumping high-capacity wells (fig. 3). Selected samples were washed through a <325-mesh (<44-μm) screen with deionized water to separate the fine fraction from the sand and gravel. The fine fraction in the wash water was collected, dried at 70°C, and placed in a Nalgene bottle with 99% ethyl alcohol as a dispersant. Several milliliters of the alcohol-sediment mixture were pipetted onto an aluminum SEM stub coated with silver conductive paint. After the alcohol had evaporated, the samples were sputter coated with gold-palladium for 120 s.

Thin sections of sand nodules cemented with calcite were coated with carbon in a carbon evaporation chamber to collect backscattered electron images that yielded maps of the distribution of major elements in the thin sections.

Suspended solids in groundwater pumped from wells NIWC 55, NIWC 57, and NIWC 58 were trapped on 0.50-μm Teflon filters that were 142 mm in diameter. Approximately 130 gallons of water discharged from each of these three wells were passed through the filters over a period of about 5 hours of normal pumping rates at each well (NIWC 55 at 1,100 gpm, NIWC 57 at 1,700 gpm, and NIWC 58 at 2,300 gpm). In addition, suspended solids were collected from monitoring well NIWC 57-1M by pumping and filtering the water through the same type of filter at a rate of about 5 gpm for 1 hour (fig. 8). Relatively large volumes of water had to be passed through the filters to collect enough material because the concentration of suspended solids in the discharging groundwater was very low. The filters were removed, covered with aluminum foil, and allowed to dry in the laboratory. Approximately one quarter of each filter was cut off, prepared for SEM analysis using standard techniques, and examined visually using SEM and the high-energy dispersive X-ray (EDX) system.

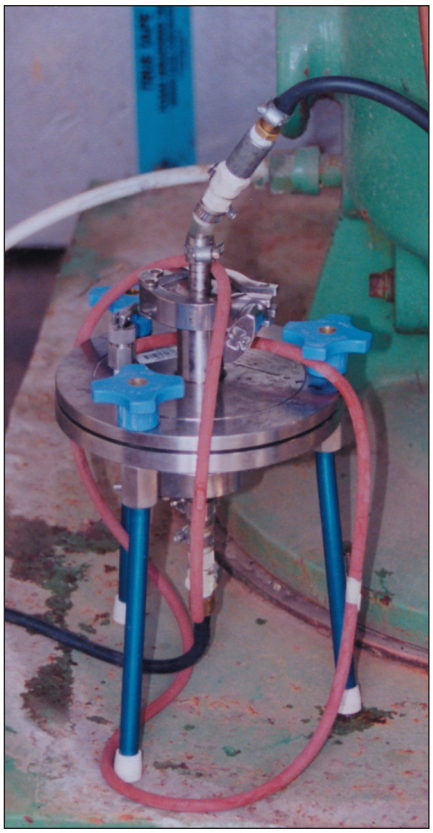

Figure 8 Apparatus used to filter approximately 130 gallons of groundwater through a 0.50-μm Teflon filter. The materials collected on the filter were examined using scanning electron microscopy.

X-ray Diffraction

The mineralogy of 47 samples from cuttings retrieved from boreholes NIWC 57-1, NIWC 57-2, NIWC 65, and CHM 96A was analyzed using standard XRD techniques. Two procedures were used to analyze all of the samples: (1) a smear method for small quantities of <325-mesh (<44-μm) fine-fraction samples and (2) a bulk powder method.

All standard operating procedures for XRD are on file in the office of the Industrial Minerals and Resource Economics Section of the ISGS. Bulk powders were prepared by wet screening them to <35-mesh (<500-μm), grinding 1.3-g samples of the >35-mesh (>500-μm) size fraction with a McCrone Micronizer, drying the samples, and packing them in end-loading sample holders. The samples were then X-rayed. The weight percent of a sample >35 mesh (>500-μm) was determined, and mineral percentages were calculated for all X-ray patterns using established standard operating procedures. Samples with insufficient volume for a bulk powder pack were analyzed by smearing the <325-mesh (<44-μm) samples, which involved brushing them onto glass slides, adding a few drops of dispersant solution, and smearing them with a microspatula. Because of their small volume, the overall composition of the samples was not quantified; the mineralogy of the smears was analyzed in order to fingerprint the samples. X-ray tracings were made using a Scintag diffractometer using Cu-Kα radiation.

Isotopic Analysis

Calcite-cemented nodules and their cements from NIWC 57-1, collected from a depth of 295 feet, and a sample of sand and gravel with dolomite-enriched fines from NIWC 57-2, collected from a depth of 290 feet, were analyzed for ^{14}C and stable carbon isotopes ($\delta^{13}C$). Using a binocular microscope and stainless steel probing tools, small pieces of cement were removed from fragments of the cemented nodule. Four samples were prepared from one of the nodules. The first sample contained only cement, the second sample appeared to be composed primarily of cement and a few small clasts, and the third and fourth samples were composed of a part of the nodule containing a mixture of both cement and clasts. Because of their relatively small size, the first three samples were analyzed for ^{14}C using accelerator mass spectrometry (AMS) technique (Ramsey and Hedges 1997). This special technique uses particle acceleration and ion beam capture to measure the ^{14}C concentration and is well suited for small samples such as the cement from the NIWC 57-1 nodule. The carbonate in the three small samples was converted to CO_2 by reacting with phosphoric acid at 50°C. The CO_2 released was purified and shipped to an AMS laboratory at Oxford University, England, for ^{14}C analysis. There was enough carbon in the larger part of the nodule (using the bulk sample) and in the NIWC 57-2 fines sample to analyze at the ISGS radiocarbon laboratory using the conventional liquid scintillation spectrometry method developed by Noakes et al. (1965, 1967). These samples were prepared by acidifying each sample in a vial attached to a vacuum line and producing CO_2, which was cryogenically purified and converted into benzene following the procedure outlined by Coleman (1976). The concentrations of ^{14}C are reported as percent modern carbon relative to a National Bureau of Standards reference material (oxalic acid no. 1), which is defined as 100% modern carbon. The age is reported in radiocarbon years before present (B.P.); "present" is defined as 1950.

The stable carbon isotopes were measured by taking a split of the CO_2 prepared for ^{14}C analysis and analyzing the gas on a Finnigan Delta-E isotope ratio mass spectrometer. The stable carbon isotope results are expressed in delta notation ($\delta^{13}C$). The $\delta^{13}C$ is a measure of the per mil difference in the ratio of the less abundant isotope (^{13}C) to the most abundant isotope (^{12}C) in the sample (SMPL) relative to the same ratio in a known standard (STND). The following equation presents the definition of $\delta^{13}C$:

$$\delta^{13}C = \left[\frac{(^{13}C/^{12}C)_{SMPL} - {}^{13}C/^{12}C)_{STND}}{(^{13}C/^{12}C)_{STND}}\right] \cdot 10^3$$

The reference standard used for reporting these carbon isotope results was Pee Dee belemnite from the Cretaceous Pee Dee Formation (Clark and Fritz 1997).

Bacterial Analysis

Core samples for bacterial analysis were collected by first carefully removing the exterior of the core with knives and spatulas. The knives and spatulas were soaked in ethanol for at least 1 minute between sample collections. Approximately 50 g of sample from the interior of the core were removed and placed into a clean ziplock bag. The bags were sealed, placed into a second ziplock bag, and immediately placed in an ice-filled cooler. Double-bagged samples were shipped in coolers filled with blue ice to the Illinois Department of Agriculture Animal Disease Laboratory in Centralia, Illinois. Although water was not used in the drilling process, it was used to help remove the core from the core barrel. A sample of that water was collected in sterile bottles.

Ten grams of the material from each sample collected for bacterial analysis and 100 mL of sterile water were placed in a sterilized blender and agitated for 3 minutes. The samples of agitated water and samples of the water used to aid in core extraction were cultured (within 24 hours of collection in the field) using standard methods to isolate and identify bacterial colonies present (Clesceri et al. 1989). Bacterial genera and species were identified using standard physiological techniques, and bacterial indicators were identified. The genera and species present in each sample were identified and listed in order of abundance. All water samples were analyzed for iron-depositing and sulfate-reducing bacteria using the biological activity and reaction test (BART; Droycon Bioconcepts Inc. 1996). This technique involves the culturing of bacteria under anaerobic conditions (Buelow and Walton 1971). All bacterial genera, species, and indicators are reported as colony-forming units (cfu) per 100 mL of water. A portion of each sand and gravel sample processed for bacterial analysis was also examined with a binocular microscope for evidence of biofilms or the deposition of iron oxyhydroxide within the sample.

In addition, water samples collected from wells NIWC 55, NIWC 57, and NIWC 58 were analyzed for bacterial genera and species and iron-depositing and sulfate-reducing bacteria using techniques described by Mehnert et al. (1999) and Panno et al. (1999) and as described for agitated water.

Collection and Analysis of Groundwater Samples from Production and Monitoring Wells

Several groundwater samples were collected during spring 2000 from three production wells and the two monitoring wells located next to well NIWC 57. Water samples from the monitoring wells were collected using a Grundfos Redi-Flo2 centrifugal pump (Grundfos Pumps Corporation). All groundwater samples were collected using standard techniques (Wood 1981). Two sets of samples were collected from the monitoring wells. The first set was collected after well NIWC 57 had been shut down for several months, and the second was collected after NIWC 57 had been pumped for 10 days at a rate of 1,600 to 1,800 gpm. All samples were submitted to ISGS laboratories for chemical, isotopic, and suspended solids analyses.

Groundwater samples were analyzed for major and minor cations and anions and ^{14}C (NIWC 57 only). Samples collected for chemical analysis were filtered through 0.45-μm membranes and stored in high-density polyethylene bottles. Samples to be analyzed for cations were acidified in the field with ultrapure nitric acid to pH <2. All samples were transported in ice-filled coolers to the laboratory and kept refrigerated at approximately 4° C until analyses were completed in approximately 3 to 4 weeks.

Concentrations of cations in water samples were determined with a Thermo-Jarrell Ash Model ICAP 61e inductively coupled argon plasma spectrometer. Instrument operation, interelement interference correction, background correction, and data collection were controlled using ThermoSPEC/AE 6.20 software. Blanks, calibration check standards, and reference standards were run with each sample set. Solution concentrations of anions were determined using a Dionex 211i ion chromatograph with Ionpac AG14 Guard Column, Ionpac AS14 Analytical Column, and Anion Self-regenerating Suppressor-11 (4 mm) following U.S. Environmental Protection Agency Method 300.0 (Pfaff 1993). Analytes were measured with a CDM-3 conductivity detector cell with a DS4 detection stabilizer. The eluent was prepared with 3.5 m*M* sodium carbonate and 1.0 m*M* sodium bicarbonate. Instrument operations and data collection were controlled using PeakNet 5.01 software. A calibration check standard and blank were run with each sample set.

The ^{14}C in the dissolved inorganic carbon in the groundwater was analyzed by acidifying a 5-gallon sample of groundwater and quantitatively collecting the released CO_2 in a vacuum line. The CO_2 produced during the acidification was converted to benzene and was analyzed for its ^{14}C content using liquid scintillation spectrometry as described earlier for the solid carbonate samples.

Results

Based on the geology of the aquifer and historic pumping practices, the loss of specific capacity of the high-

capacity wells could have several causes, including (1) the inorganic precipitation of minerals (e.g., calcite and iron oxyhydroxide) because of changing geochemical conditions near the pumping wells as a result of pumping-induced outgassing of CO_2 and/or changing redox conditions; (2) biofouling by the bacterially mediated precipitation of Fe, SO_4^{2-} reduction, and deposition of slime-forming bacteria; and (3) the physical plugging of the aquifer, gravel pack, or well screens by pumping-induced transport of clay, silt, or fine sand (Catania and Getchell 1997).

Core Samples

Binocular Microscopy Our initial examination of the wet sand and gravel samples collected from the Glasford and Mahomet aquifers in boreholes NIWC 57-1 and NIWC 57-2 was done with a binocular microscope. Microscopic examination revealed clean, rounded sand and gravel particles with no evidence of biofilms or bacterially deposited iron oxyhydroxide. However, we did find a fine-grained, white-colored material that tended to clump the sand grains together. Only gentle probing was needed to disaggregate these clumps. When dry, the material acted as a very weak cement holding sand grains together. Acid (10% HCl) applied to the white material resulted in a vigorous reaction that removed the carbonate fraction and left a fine, brown residue. This reaction suggested that carbonate mineral(s) made up a large fraction of the white material. It was also assumed that separation of the <325 mesh (44-μm) size fraction from the sand and gravel would concentrate the white material that was binding the "clumps" for further examination. This material was assumed to contain at least some of the calcite that was expected to have precipitated within the aquifer near NIWC 57. The composition of this material, based on SEM and XRD analyses, included clay minerals (illite, kaolinite, and chlorite), dolomite, quartz, and feldspar. The total amount of clay minerals in the fines (as determined by XRD) was significantly enriched in core samples in all units and at all depths of borehole NIWC 57-1 compared with NIWC 57-2.

Examination of sand and gravel samples from borehole NIWC 57-1 revealed nodules of strongly cemented sand and gravel at depths from 252 to 297.5 feet. Seven nearly spherical to irregularly shaped nodules ranging from about 1.0 to 2.5 inches in diameter and four smaller ones <0.5 inches in diameter were collected from this borehole (fig. 9). No cemented nodules were found in samples from borehole NIWC 57-2. Cemented sand and gravel nodules have not been described as occurring in the Mahomet aquifer (John Kempton, ISGS, personal communication 1999). Such nodules also were not observed in our background samples from NIWC 65 and CHM 96A, which, however, could be the result of differences in sampling methods. The occurrence of the nodules only in the closest borehole, the previous geochemical modeling of the groundwater (Mehnert et al. 1999), and the likelihood of calcite cement formation on production well screens suggested that the nodules could be physical evidence of cementation occurring in the aquifer near NIWC 57. Consequently, the age and origin of the nodules were considered to be important, and the nodules were examined in detail.

Point Counting Thirty-two thin sections of epoxy-impregnated sand and gravel and the cemented nodules were point counted under a petrographic microscope to quantify their mineralogical composition and to help determine the origin of the nodules. The results of the point counting are given in Appendix table A1. In general, the dominant minerals present in the Glasford and Mahomet aquifer samples were almost identical and included, as combined arithmetic means, quartz (57.9%), carbonate

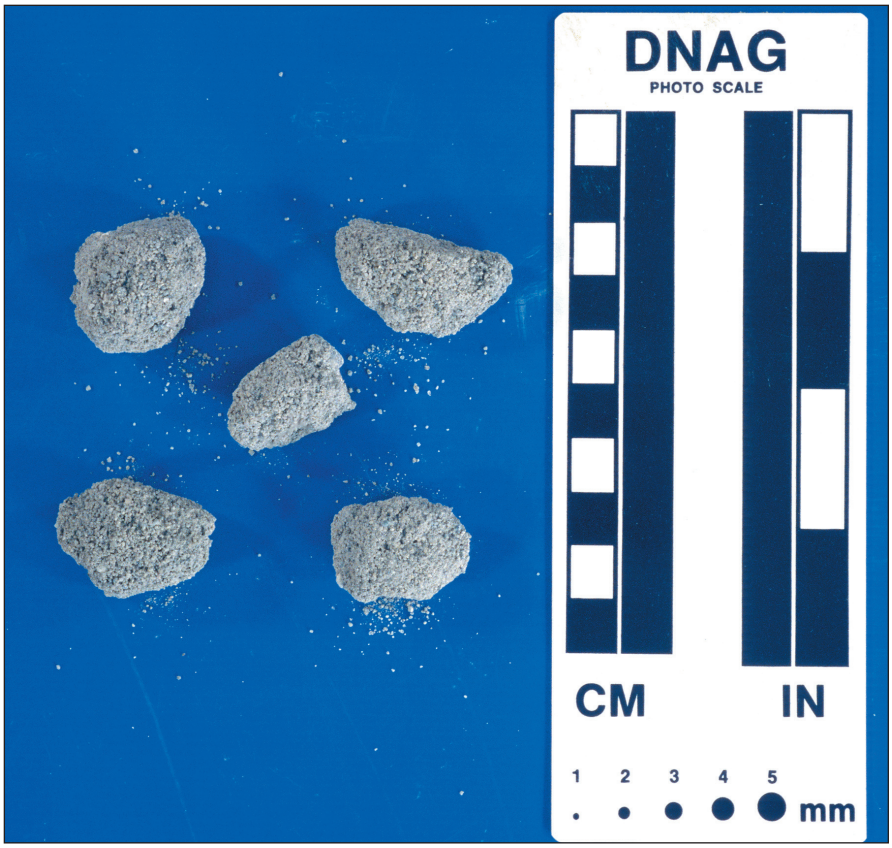

Figure 9 Five of 11 cemented nodules collected from the sand and gravel of the Mahomet aquifer from borehole NIWC 57-1 at depths from 252 to 297.5 feet. The nodules collected ranged from <0.5 inches to 2.5 inches in diameter.

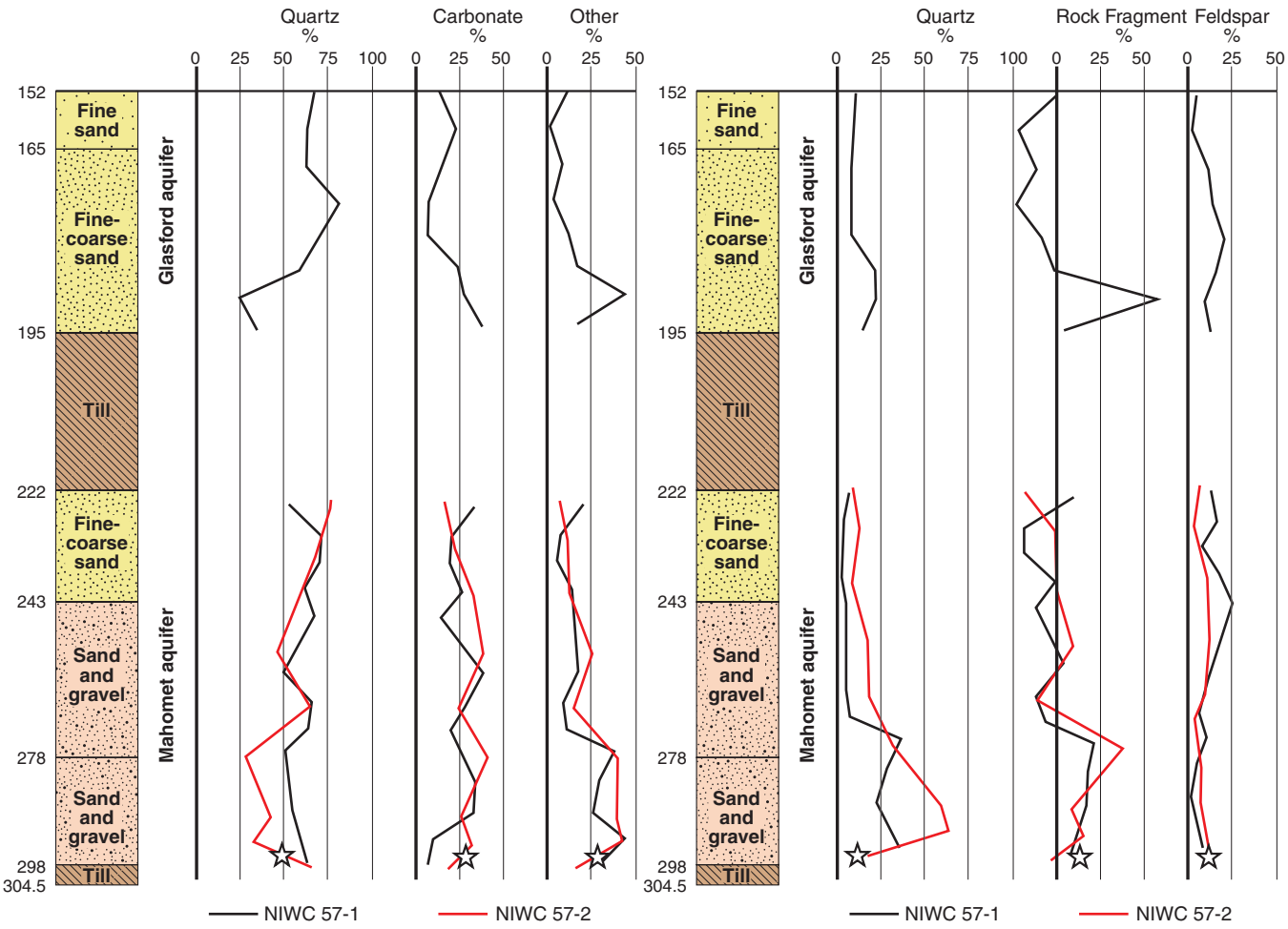

Figure 10 Point count results of Glasford and Mahomet aquifers revealing slight variations in constituent minerals with depth. "Other" is chert, rock fragments, and feldspar combined. The stars at the bottom of the figure represent the mineral composition of a cemented nodule (excluding the calcite cement).

clasts (calcite and dolomite) (22.0%), feldspar (4.4%), chert (5.0%), and rock fragments (10.5%). This composition was consistent with results obtained by Willman and Frye (1970) and Manos (1961), who found that the sand and gravel of the Mahomet aquifer is made up predominantly of quartz, lesser amounts of carbonate minerals, K-feldspar and Ca-Na feldspar, and minor amounts of translucent heavy minerals that include hornblende, garnet, epidote, and hyperenstatite. Others observed that, in general, the dominant carbonate minerals are dolomite in the Glasford aquifer and calcite in the Mahomet aquifer (H. Glass, ISGS, personal communication 1992).

The mineralogical composition of the sand and gravel in the cemented nodules found in the Mahomet aquifer in borehole NIWC 57-1 was found to be identical to the other sand and gravel samples from NIWC 57-1, except for calcite cement (fig. 10). That is, point count results for the nodules (clasts only) were identical to those for the sand and gravel containing nodules.

Petrographic and Cathodoluminescence Microscopy Thin sections of sand and gravel from the Mahomet and Glasford aquifers were examined and compared with each other and with thin sections made from samples of the same units collected from background well NIWC 65 (fig. 11). All samples collected from NIWC 57-1 and NIWC 57-2 contained some sand grains that were partially coated with a thin rim of calcite-rich, silty material that can be described as a drusy/dogtooth-shaped, cathodoluminescent material (fig. 12). For this report, this material is referred to as silt and is assumed to be a size fraction that is present and, at times, mobile within the aquifers. This material appeared to be a dehydrated version of the white material observed as very small clumps under the binocular microscope. Only a thin coating of silt-size material was found on clasts in the samples of the Mahomet aquifer collected during drilling of background well (NIWC 65) using conventional, mud-rotary drilling techniques (figs. 11C and 12). Most of the fine fraction in these samples was likely washed out of the sand and gravel during drilling, sample collection, and subsequent washing of the samples in preparation for permanent storage in the ISGS Geological Samples Library.

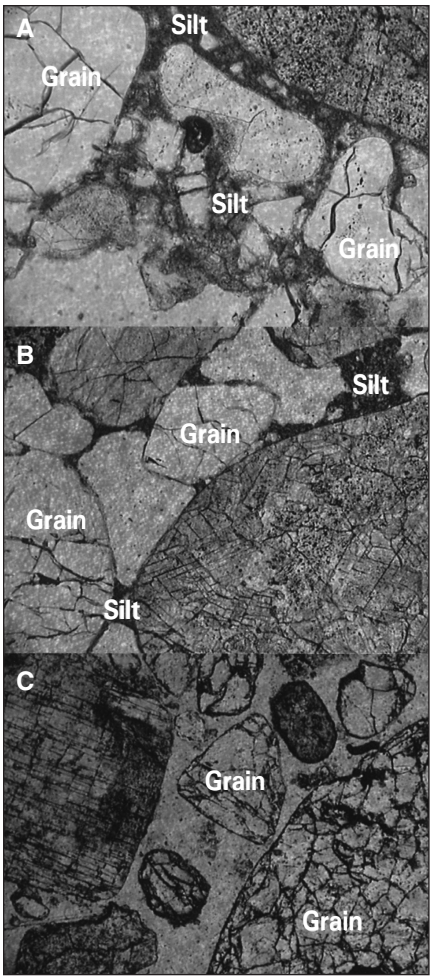

Figure 11 Photomicrographs of a Glasford aquifer sample at 190 feet (A) and Mahomet aquifer sample at 275 feet (B) from borehole NIWC 57-1 showing the fine silt that is pervasive throughout the formations at this site. Background photomicrograph (C) from the Mahomet aquifer in IL-AWC production well NIWC 65 was drilled using the reverse rotary drilling technique with drilling fluids and showed very little silt fraction. Plane polarized light photo at 5×.

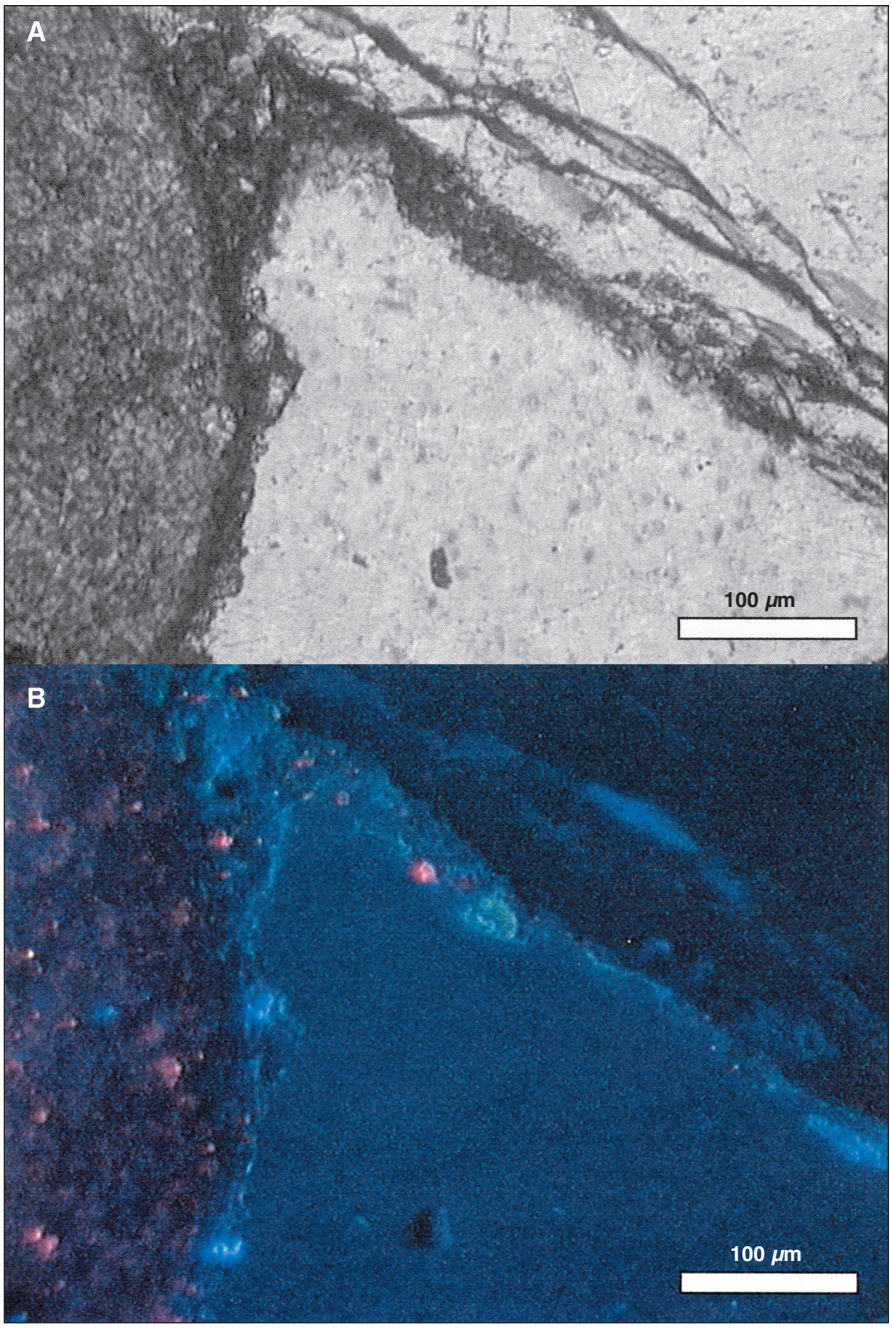

Figure 12 Photomicrographs of Mahomet aquifer sand from Illinois State Water Survey observation well CHM 96A showing a thin (<10-μm) crust of fine material coating the sand and gravel clasts (A). Under cathodoluminescent light (B), the fine material is luminescent.

The cement identified in sand and gravel samples collected from borehole NIWC 57-1 at 252 to 259 feet, 270 feet, and 295 to 297.5 feet was coarsely crystalline or blocky looking and easily distinguished from the thin, drusy/dogtooth-type material observed in other samples (fig. 13).

The amount of calcite cement in the cemented nodules was determined (using point counting of 200 points per thin section) to estimate the in situ porosity of the sand and gravel of the samples. The two samples examined were from 295 to 297.5 feet and contained 60 and 66% clasts, 34 and 30% cement, and 6 and 4% pore spaces, respectively. Thus, the total porosity for the samples was 34 and 40% prior to their cementation.

SEM Analysis Examination of the <325-mesh (<44-μm) size fraction from the Glasford and Mahomet

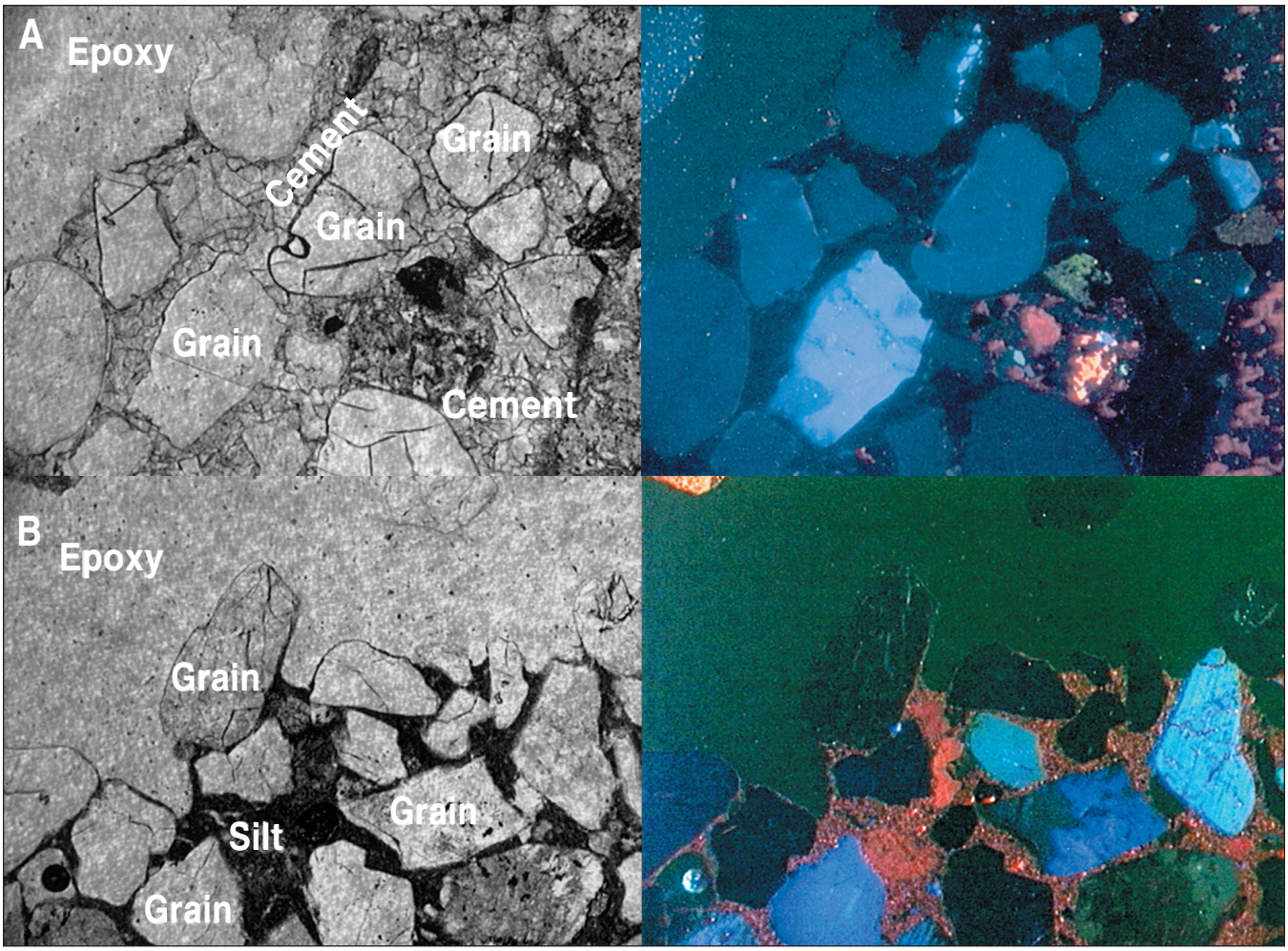

Figure 13 Photomicrographs of the Mahomet aquifer sand sample from borehole NIWC 57-1 (A) and NIWC 57-2 (B); both samples are from depth 295 feet and are shown in plane light (left) and cathodoluminescent light (right). The sand and gravel from borehole NIWC 57-1 is cemented with calcite, whereas the sand and gravel sample from borehole NIWC 57-2 was not cemented and showed the presence of the silt fraction. The calcite cement in A is nonluminescent; the silt in B is luminescent under cathodoluminescent light.

aquifers under SEM was conducted to determine the composition of the potentially mobile fraction of the aquifer and to look for authigenic calcite. Observations revealed a heterogeneous mineralogical composition made of the same minerals found in the petrographic analysis of the sand and gravel, plus clay minerals. Two obvious characteristics of the alcohol-dispersed <44-μm material were that it was composed of silt- and clay-size materials, and the calcite was typically very small, about 1 to 2 μm in diameter (fig. 14). Identification of some of the material, using the high-energy dispersive X-ray system, at scattered locations along transects across the dispersed samples yielded qualitative information on the composition of the mineral fragments. A sample of the fine fraction from sand of the Glasford aquifer taken from a depth of 175 feet in NIWC 57-2 contained quartz, dolomite, and feldspar (fig. 15). A sample of the fine fraction of the Mahomet aquifer taken from a depth of 295 feet in NIWC 57-1 was composed of feldspar, clay minerals, and quartz with abundant, but very small (<1 μm in diameter) pieces of calcite (not visible or identified in the figure) throughout the field of view (fig. 16). An archival sample of the Mahomet aquifer taken from a depth of 355 feet in NIWC 65 contained clay minerals, feldspar, calcite, quartz, and dolomite (fig. 17).

Examination of a thin section of one of the cemented nodules using backscatter electron imagery produced elemental maps that revealed a relatively pure calcite cement. That is, the cement was predominantly calcium carbonate, had no obvious inclusions of other materials, and had few impurities such as magnesium or iron. These results were consistent with petrographic observations that showed a clear, sparry calcite cementing the sand grains (fig. 13A).

XRD Bulk Pack Analyses The XRD patterns of bulk samples of sand and

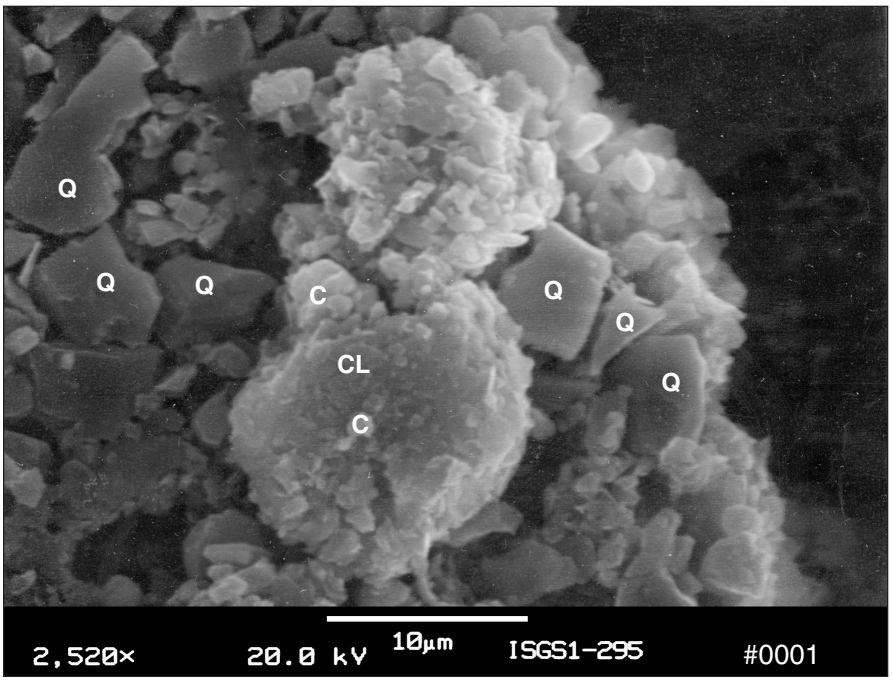

Figure 14 Photomicrograph of a dried clump of white material from NIWC 57-1, 295 feet depth, from the Mahomet aquifer. The clump appears to be dominated by angular quartz (Q) fragments. A relatively large, clay-rich particle (CL) containing small (1 to 2 μm) fragments of calcite (C) can be seen.

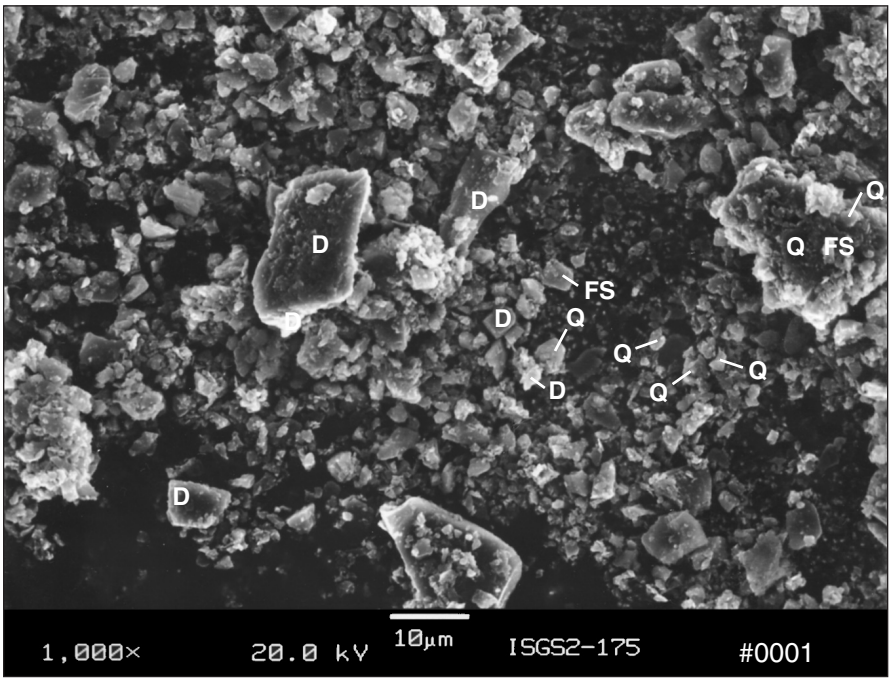

Figure 15 Photomicrograph of the alcohol-dispersed, fine fraction of NIWC 57-1, 175 feet depth, from the Glasford aquifer. The mineralogy is mostly dolomite (D) and quartz (Q) with minor amounts of feldspar (FS).

gravel from boreholes NIWC 57-1 and NIWC 57-2 revealed that the Wedron, Glasford, and Mahomet aquifers are all composed of, in order of decreasing relative amounts, quartz, dolomite, calcite, plagioclase feldspar, K-feldspar, illite, kaolinite, chlorite, and hornblende. The values for mineral percentages determined by XRD (tables 1 to 4) were similar to those determined by point counting.

Calcite appears to be enriched in samples of the Mahomet aquifer from core samples from NIWC 57-1M and NIWC-2M relative to cuttings from ISWS well CHM 96A. The percentage of calcite in samples from well CHM 96A ranged from 4.3 to 5.6% with a mean of 4.9% (table 1). By contrast, the percentages of calcite in core samples from the Mahomet aquifer at NIWC 57-1 and NIWC 57-2 ranged from 5.3 to 12% ($\bar{x}$ = 8.0%) (table 2) and 6.0 to 21% ($\bar{x}$ = 12%) (table 3), respectively. Although qualitative, these compositional differences are supported by the calcite/quartz ratios of the samples from the different boreholes. The calcite/quartz ratios for archival samples ranged from 0.59 to 1.61 ($\bar{x}$ = 0.98) (table 1; combined means not shown). The ratios of samples from boreholes NIWC 57-1M and NIWC-2M ranged from 0.74 to 2.10 ($\bar{x}$ = 1.22) (table 2) and from 0.79 to 3.67 ($\bar{x}$ = 1.96) (table 3), respectively.

Relative to the archival samples, dolomite also appeared to be enriched in samples from boreholes NIWC 57-1 and NIWC 57-2 in both the Glasford and Mahomet aquifers, but it has a more sporadic distribution than calcite. The greatest concentration of dolomite occurred near the base of borehole NIWC 57-2 at 290 feet where it constituted 28% of the total mineralogy (table 3). Dolomite was present as part of a loose, brown coating on the sand and gravel at this depth as determined by XRD of the coating.

XRD of the Fine Fraction The fine fraction (<325 mesh or <44 μm) of the Mahomet and Glasford aquifers from boreholes NIWC 57-1 and NIWC 57-2 contained the same minerals as the coarse fraction, although in different

amounts (table 4). The fine fraction from the Mahomet aquifer (from both boreholes) contained greater amounts of clay minerals and carbonate minerals and less quartz than that from the Glasford aquifer. The most notable difference was in the percentages of clay minerals in the Mahomet and Glasford aquifers of the two new boreholes. Specifically, sand and gravel of the Mahomet aquifer in borehole NIWC 57-1 contained greater concentrations (by a factor of 5 to 10) of the clay minerals illite and kaolinite plus chlorite relative to those of samples from the same aquifer in borehole NIWC 57-2. Illite in the Glasford aquifer in borehole NIWC 57-1 was enriched by about a factor of 2 relative to samples from the same aquifer in borehole NIWC 57-2 (table 4 and fig. 18).

The dolomite-rich coating on sand and gravel samples collected from borehole NIWC 57-2 initially were suspected to be residue from prior test drilling because of its appearance as a fine, clay-like coating on sand and gravel. Although the location of the prior test drilling in the vicinity of NIWC 57 was not well documented, it was suspected that the dolomite-rich fines had been created by drilling through the dolomite-rich gravels of the aquifer. Subsequent well development could have forced these materials farther from the well and into the more permeable zones within the aquifer. However, XRD analysis of the fines did not find the expandable clay minerals from drilling mud that would be expected if the dolomite were an artifact left by test drilling (Randall Hughes, ISGS, personal communications 1999). However, this scenario assumes that an expandable clay-bearing mud was used during drilling of the pilot hole, which was not necessarily the case (Mark Johnson, IL-AWC, personal communication 2000).

XRD of Calcite-cemented Nodule

The XRD data on one of the calcite-cemented nodules collected at a depth of 295 to 297.5 feet showed that calcite in the nodule represented 42% of its total mass (table 2). This result

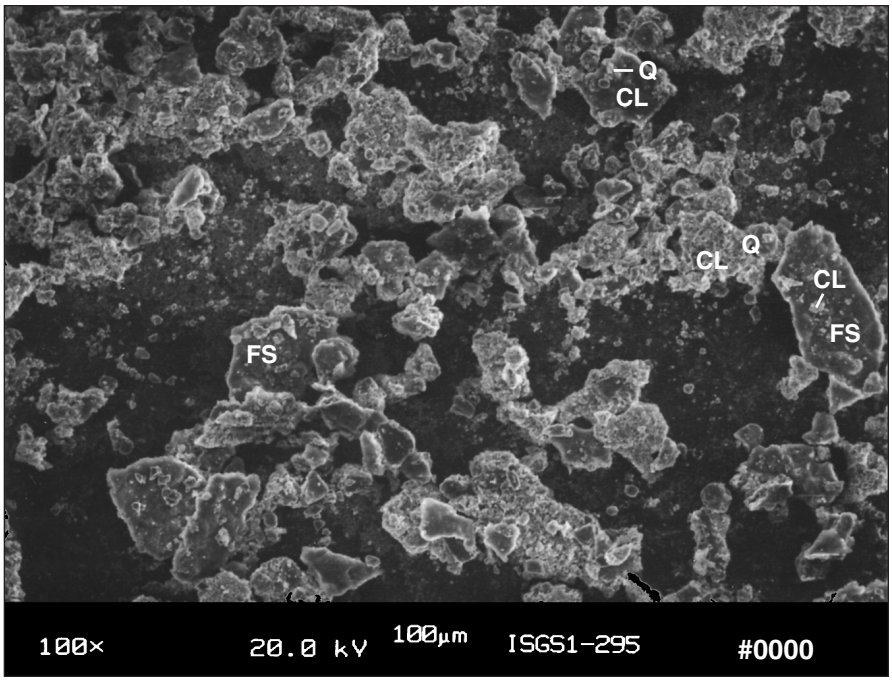

Figure 16 Photomicrograph of the alcohol-dispersed, fine fraction in NIWC 57-1, 295 feet depth, from the Mahomet aquifer. The mineralogy is dominated by clay minerals (CL), feldspar (FS), and quartz (Q), with minute pieces of calcite (<1 μm in diameter) scattered throughout the field of view.

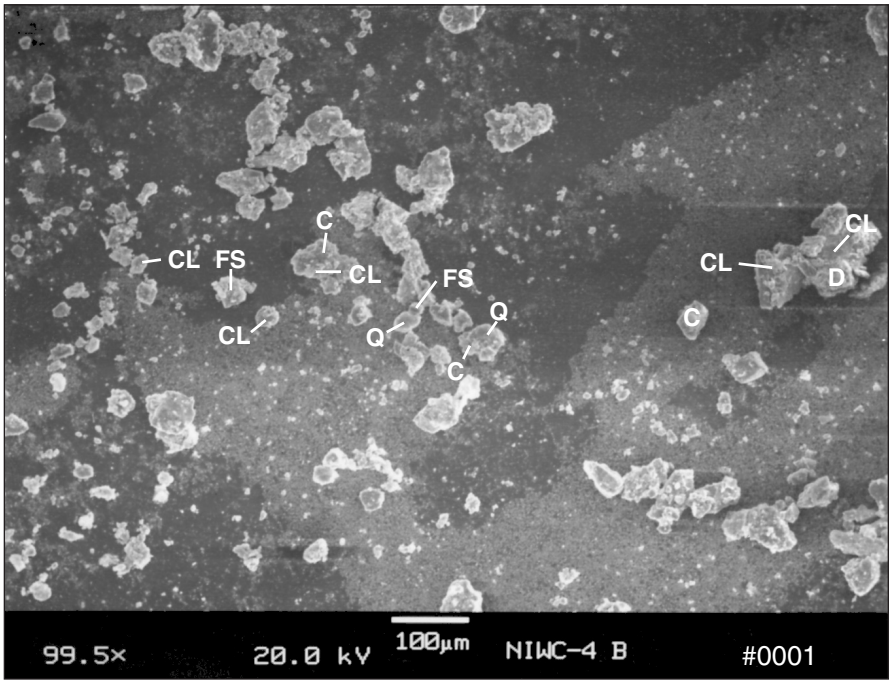

Figure 17 Photomicrograph of the alcohol-dispersed, fine fraction of a reference sample from IL-AWC borehole NIWC 65, at 355 feet depth, from the Mahomet aquifer. The mineralogy is dominated by clay minerals (CL), with lesser amounts of calcite (C), quartz (Q), feldspar (FS), and dolomite (D).

Table 1 Mineralogical composition of samples from background boreholes NIWC 65 and CHM 96A determined by X-ray diffraction for bulk pack and smear samples.

Borehole	Depth (ft)	Unit[1]	%>35M	%I	%H	%K+C	%Q	%Kf	%Pf	%Cc	%D	%Cc+D	%Cc/ %Cc+D	Cc/Q[2]	D/Q[2]	Cc+D/Q	Kf/Pf[2]	Kf/Q[2]	Pf/Q[2]
NIWC 65	290	M	96	4.6	0.3	1.6	66	2.4	5.6	11	9.2	20	0.54	1.61	1.40	0.30	0.30	0.37	0.86
NIWC 65	315	M	72	2.3	0.0	0.7	79	2.7	4.5	7.0	4.1	11	0.63	0.88	0.52	0.14	0.37	0.34	0.57
NIWC 65	335	M	94	2.6	0.3	1.3	69	2.6	7.5	8.8	8.0	17	0.52	1.27	1.17	0.24	0.26	0.38	1.09
NIWC 65	355(smd)	M	99	7.5	0.6	2.7	58	3.9	3.7	7.4	16	23	0.32	1.27	2.75	0.40	0.52	0.68	0.63
Mean			90	4.3	0.3	1.6	68	2.9	5.3	8.4	9.3	18	0.50	1.26	1.46	0.27	0.36	0.44	0.79
Std. Dev.(excluding smd)[1]			11	21	0.2	0.7	7.0	0.6	1.4	1.4	1.4	4.3	5.0	0.11	0.30	0.80	0.09	0.14	0.20
CHM 96	A-253	M	92	5.9	0.0	1.9	63	3.4	7.6	5.6	12	18	0.31	0.88	1.92	0.28	0.31	0.53	1.20
CHM 96	A-293	M	61	3.0	0.4	0.9	74	3.6	5.7	4.4	7.6	12	0.36	0.59	1.03	0.16	0.38	0.48	0.77
CHM 96	A-313	M	64	6.3	0.3	2.3	68	3.1	7.4	4.3	8.5	13	0.33	0.63	1.25	0.19	0.29	0.45	1.10
CHM 96	A-328(RP)	M	82	5.1	0.4	1.7	69	2.7	6.1	5.3	9.3	15	0.36	0.76	1.34	0.21	0.30	0.38	0.88
Mean			75	5.1	0.3	1.7	69	3.2	6.7	4.9	9.4	14	0.34	0.72	1.39	0.21	0.32	0.46	0.99
Std Dev.			13	1.3	0.2	0.5	4.0	0.3	0.8	0.6	3.3	2.0	0.02	0.10	0.30	0.04	0.04	0.05	0.17

[1]smd, smear air-dried (sample too small for bulk pack); RP, bulk pack repeat run; M, Mahomet Sand; %>35M, percent greater than 35 mesh; I, illite; H, hornblende; K+C, kaolinite+chlorite; Q, quartz; Kf, K-feldspar; Pf, plagioclase feldspar; Cc, calcite; D, dolomite; Cc+D/Q as is Cc/Q = 10× %Cc/Q.
[2]All 10× numerator/Q; Kf/Pf = %Kf/(%Kf+Pf).

Table 2 Mineralogical composition of bulk pack and lithified samples from borehole NIWC 57-1.

Borehole	Depth (ft)	Unit[1]	%>35M	%I	%H	%K+C	%Q	%Kf	%Pf	%Cc	%D	%Cc+D	%Cc/ %Cc+D	Cc/Q[2]	D/Q[2]	Cc+D/Q	Kf/Pf[2]	Kf/Q[2]	Pf/Q[2]
NIWC 57	159	G	54	0.9	0.2	0.3	88	2.8	3.4	1.3	3.0	4.2	0.30	0.14	0.34	0.05	0.45	0.32	0.39
NIWC 57	164	G	0.1	2.2	0.6	0.7	64	5.0	8.4	2.7	16	19	0.14	0.43	2.53	0.30	0.37	0.78	1.30
NIWC 57	169.5	G	0.6	0.8	0.0	0.3	75	4.6	4.4	3.2	11	15	0.22	0.42	1.52	0.19	0.51	0.61	0.58
NIWC 57	175	G	5.1	2.3	0.4	0.0	74	3.9	5.5	3.4	10	13	0.25	0.46	1.34	0.18	0.41	0.52	0.75
NIWC 57	179.5	G	34	1.2	0.2	0.4	81	3.9	4.2	2.7	6.5	9.2	0.29	0.33	0.80	0.11	0.48	0.49	0.52
NIWC 57	185	G	50	1.6	0.4	0.4	79	3.6	3.8	2.8	8.7	11	0.24	0.35	1.11	0.15	0.48	0.46	0.49
NIWC 57	190	G	90	1.8	0.0	0.9	64	3.3	5.9	6.2	18	24	0.26	0.96	2.76	0.37	0.36	0.52	0.92
NIWC 57	195	G	81	1.2	0.3	0.4	78	2.7	4.0	4.2	8.9	13	0.32	0.54	1.14	0.17	0.40	0.34	0.51
Mean			39	1.5	0.3	0.4	75.5	3.7	5.0	3.3	10.3	13.6	0.25	0.45	1.44	0.19	0.43	0.50	0.68
Std Dev. (%)			33	0.6	0.2	0.3	8	0.8	1.5	1.3	4.5	5.6	0.05	0.22	0.77	0.10	0.05	0.14	0.28
NIWC 57-1	230	M	77	2.0	0.6	0.7	72	5.2	7.8	5.3	6.7	12	0.44	0.74	0.93	0.17	0.40	0.73	1.09
NIWC 57-1	235	M	26	3.1	1.2	0.8	70	3.5	7.3	6.3	8.2	15	0.43	0.91	1.19	0.21	0.33	0.51	1.05
NIWC 57-1	240	M	36	1.3	0.5	0.6	72	4.6	8.2	5.9	6.6	13	0.47	0.82	0.92	0.17	0.36	0.64	1.14
NIWC 57-1	245	M	77	2.8	0.9	0.8	71	4.1	4.3	7.7	8.8	16	0.47	1.08	1.24	0.23	0.48	0.58	0.62
NIWC 57-1	250	M	60	2.8	0.6	0.9	66	2.9	7.4	10	8.7	19	0.54	1.57	1.31	0.29	0.29	0.44	1.11
NIWC 57-1	255	M	80	4.0	0.8	1.2	63	2.6	5.7	11	12	23	0.49	1.78	1.86	0.36	0.31	0.41	0.90
NIWC 57-1	260	M	88	5.0	0.8	1.8	58	2.5	5.7	12	14	26	0.47	2.10	2.35	0.44	0.31	0.43	0.97
NIWC 57-1	265	M	80	2.7	0.6	1.0	73	3.8	5.5	7.0	6.5	13	0.52	0.95	0.89	0.18	0.41	0.53	0.75
NIWC 57-1	270	M	67	3.5	0.9	1.4	64	2.6	7.3	9.9	10	20	0.49	1.54	1.57	0.31	0.27	0.41	1.14
NIWC 57-1	275	M	98	4.9	0.0	1.8	57	2.5	4.6	9.5	20	30	0.32	1.68	3.53	0.52	0.35	0.44	0.81
NIWC 57-1	280	M	91	5.1	0.4	1.3	62	2.7	7.3	7.2	14	22	0.33	1.16	2.34	0.35	0.27	0.43	1.18
NIWC 57-1	285	M	77	1.9	0.6	0.6	75	3.5	5.8	5.7	6.5	12	0.47	0.76	0.86	0.16	0.37	0.46	0.78
NIWC 57-1	290	M	33	1.3	0.4	1.1	70	3.9	7.4	6.8	9.4	16	0.42	0.98	1.35	0.23	0.35	0.56	1.06
NIWC 57-1	295	M	80	3.5	1.2	1.4	71	3.1	5.8	6.7	7.6	14	0.47	0.94	1.07	0.20	0.35	0.43	0.82
NIWC 57-1	297.5	M	81	3.2	1.0	2.0	67	2.8	7.1	8.4	8.6	17	0.49	1.26	1.29	0.26	0.28	0.42	1.07
NIWC 57-1	270L	M	60	1.7	0.6	1.1	65	3.3	9.2	9.7	9.2	19	0.51	1.49	1.40	0.29	0.26	0.50	1.41
NIWC 57-1	297.5L	M	73	1.7	0.6	1.5	33	0.8	3.8	42	16	59	0.72	12.9	4.96	1.79	0.18	0.25	1.14
Mean (excluding 270L & 297.5L)			70	3.1	0.7	1.2	67	3.4	6.5	8.0	9.8	18	0.46	1.22	1.51	0.27	0.34	0.50	0.97
Std. Dev. (excluding 270L & 297.5L)			21	1.2	0.3	0.4	5.0	0.8	1.2	2.1	3.6	5.0	0.06	0.40	0.70	0.10	0.06	0.09	0.17

[1]G, Glasford Formation sand; M, Mahomet Sand; %>35M, percent greater than 35 mesh; I, illite; H, hornblende; K+C, kaolinite+chlorite; Q, quartz; Kf, K-feldspar; Pf, plagioclase feldspar; Cc, calcite; D, dolomite; Cc+D/Q as is Cc/Q= 10× %Cc/Q.
[2]All 10× numerator/Q; Kf/Pf= %Kf/(%Kf+Pf).

Table 3 Mineralogical composition of samples from borehole NIWC 57-1 determined by X-ray diffraction of bulk pack samples.

Borehole	Depth (ft)	Unit[1]	%>35M	%I	%H	%K+C	%Q	%Kf	%Pf	%Cc	%D	%Cc+D	%Cc/ %Cc+D	Cc/Q[2]	D/Q[2]	Cc+D/Q	Kf/Pf[2]	Kf/Q[2]	Pf/Q[2]
NIWC 57-2	35	W	72	3.3	0.0	0.7	77	3.6	6.4	3.1	6.4	9.5	0.32	0.40	0.84	0.12	0.36	0.46	0.83
NIWC 57-2	155	G	63	0.9	0.0	0.6	77	2.8	5.8	3.7	9.5	13	0.28	0.49	1.23	0.17	0.33	0.37	0.75
NIWC 57-2	165	G	1.0	1.6	0.3	0.3	76	4.7	5.6	2.4	9.5	12	0.20	0.32	1.25	0.16	0.46	0.62	0.74
NIWC 57-2	175	G	0.8	0.0	0.0	0.0	80	4.0	5.8	2.9	7.1	10	0.29	0.37	0.89	0.13	0.41	0.50	0.72
NIWC 57-2	180	G	81	3.1	0.0	0.7	73	3.3	4.3	4.8	11	16	0.30	0.66	1.54	0.22	0.44	0.46	0.59
NIWC 57-2	185	G	75	0.9	0.0	0.0	80	2.5	4.2	4.5	7.8	12	0.37	0.56	0.98	0.15	0.37	0.31	0.52
NIWC 57-2	190	G	87	1.6	0.4	0.9	65	1.9	4.5	7.0	18	25	0.28	1.08	2.82	0.39	0.30	0.29	0.68
Mean			51	1.3	0.1	0.4	75	3.2	5.0	4.2	11	15	0.29	0.58	1.45	0.20	0.38	0.42	0.67
Std Dev. (%)			36	1.0	0.2	0.3	5	0.9	0.7	1.5	3.7	5	0.05	0.25	0.64	0.09	0.06	0.12	0.08
NIWC 57-2	225	M	50	0.0	0.0	0.0	67	3.1	7.1	12	11	23	0.52	1.81	1.66	0.35	0.30	0.46	1.06
NIWC 57-2	235	M	28	1.6	0.6	0.4	76	2.8	6.2	6.0	6.6	13	0.48	0.79	0.87	0.17	0.31	0.37	0.81
NIWC 57-2	245	M	74	2.2	0.4	1.0	57	2.1	5.0	15	17	32	0.47	2.61	2.91	0.55	0.30	0.37	0.88
NIWC 57-2	255	M	77	2.6	0.5	0.6	57	1.6	7.1	14	16	30	0.47	2.49	2.82	0.53	0.18	0.28	1.24
NIWC 57-2	265	M	45	2.2	0.6	0.3	75	3.9	6.7	6.4	5.2	12	0.55	0.85	0.70	0.15	0.37	0.53	0.90
NIWC 57-2	275	M	87	4.1	0.5	2.0	58	2.8	5.5	8.7	19	27	0.32	1.51	3.25	0.48	0.34	0.49	0.95
NIWC 57-2	285	M	87	2.3	0.5	1.5	61	2.9	9.4	7.6	15	22	0.34	1.24	2.38	0.36	0.23	0.47	1.54
NIWC 57-2	290	M	89	3.0	0.4	1.8	49	3.2	1.2	13	28	41	0.32	2.69	5.80	0.85	0.74	0.66	0.24
NIWC 57-2	295	M	68	3.0	0.0	1.2	57	3.2	8.6	21	6.1	27	0.77	3.67	1.07	0.47	0.27	0.56	1.52
Mean			67	2.3	0.4	1.0	62	2.9	6.3	12	14	25	0.47	1.96	2.38	0.43	0.34	0.47	1.01
Std Dev.			20	1.1	0.2	0.7	8.4	0.6	2.2	4.6	7.0	8.8	0.14	0.91	1.50	0.20	0.15	0.11	0.37

[1]W, Wedron; G, Glasford Formation sand; M, Mahomet Sand; %>35M, percent greater than 35 mesh; I, illite; H, hornblende; K+C, kaolinite+chlorite; Q, quartz; Kf, K-feldspar; Pf, plagiclase feldspar; Cc, calcite; D, dolomite; Cc+D/Q as is Cc/Q=10×%Cc/Q.
[2]All 10× numerator/Q; Kf/Pf= %Kf/(%Kf+Pf).

Table 4 Mineralogical composition of samples from boreholes NIWC 57-1 and NIWC 57-2 determined by X-ray diffraction of smear samples.

Borehole	Depth (ft)	Unit[1]	%>35M	%I	%H	%K+C	%Q	%Kf	%Pf	%Cc	%D	%Cc+D	%Cc/ %Cc+D	Cc/Q[2]	D/Q[2]	Cc+D/Q	Kf/Pf[2]	Kf/Q[2]	Pf/Q[2]
NIWC 57-1	175	G	NA	11	0.0	4.7	33	5.1	4.7	19	22	41	0.47	5.74	6.57	1.23	0.52	1.53	1.43
NIWC 57-2	175	G	NA	5.3	0.5	2.3	40	3.2	3.6	14	31	45	0.31	3.56	7.77	1.13	0.47	0.81	0.90
Mean			NA	8.4	0.3	3.5	37	4.1	4.2	17	26	43	0.39	4.65	7.17	1.18	0.49	1.17	1.16
NIWC 57-1	255	M	NA	24	0.5	20	17	1.7	7.2	10	20	30	0.34	5.90	12.0	1.74	0.19	1.00	4.20
NIWC 57-1	295	M	NA	19	1.2	11	29	2.1	6.1	14	18	32	0.45	4.90	6.10	1.10	0.26	0.74	2.10
Mean			NA	21	0.9	15	23	1.9	6.6	12	19	31	0.39	5.40	8.81	1.42	0.23	0.87	3.15
NIWC 57-2	255	M	NA	4.8	0.8	1.9	44	4.5	6.3	16	21	38	0.44	3.72	4.82	0.85	0.42	1.02	1.42
NIWC 57-2	295	M	NA	3.7	0.9	2.0	35	3.5	7.3	15	33	47	0.31	4.12	9.20	1.33	0.32	0.99	2.07
Mean			NA	4.3	0.8	2.0	40	4.0	6.8	16	27	42	0.37	3.92	7.01	1.09	0.37	1.01	1.75

[1]NA, not applicable; G, Glasford Formation; M, Mahomet Sand; %>35M, percent greater than 35 mesh; I, illite; H, hornblende; K+C, kaolinite+chlorite; Q, quartz; Kf, K-feldspar; Pf, plagiclase feldspar; Cc, calcite; D, dolomite, Cc+D/Q as is Cc/Q=10× %Cc/Q; D/Q.
[2]All 10× numerator/Q; Kf/Pf= %Kf/(%Kf+Pf).

was in contrast to the approximately 8.4% calcite concentration in the "uncemented" or "unlithified" sand and gravel from the same sample interval. Thus, approximately 33.6% of the nodule was composed of calcite cement, which is consistent with the results of point counting data previously described. Dolomite was also present in a greater concentration in the nodule, representing 16% of the total mass (compared to an 8.6% concentration for the uncemented sand). Examination of the nodule by petrographic microscopy and SEM revealed that the calcite was concentrated in the cement, and the dolomite was present only as clasts.

Carbon Isotopes of Calcite-cemented Nodule Separation of the calcite cement from a nodule involved samples of different degrees of purity. The samples consisted of (1) all cement, (2) mostly cement with some clasts,

and (3) an unseparated sample. The separated sample of calcite cement yielded ^{14}C AMS results of 0.35 percent modern carbon (pmc); the unseparated sample submitted for AMS dating yielded only 0.03 pmc. Because the unseparated sample was large enough for standard ^{14}C dating techniques, an analysis at the ISGS isotope geochemistry laboratory was conducted. The results were the same as with AMS dating techniques (table 5); the calcite in the cement contained no detectable ^{14}C. The small amount of ^{14}C activity in these samples was attributed to contamination from the evaporation of groundwater on the sand and gravel when the samples were dried. The formation of a film of material on the unrinsed samples could have accounted for the activity observed.

The $\delta^{13}C$ of the calcite cement in the nodule was isotopically heavier than would be expected for calcium carbonate precipitated in equilibrium with the calcium bicarbonate (Ca^{2+}-HCO_3^-)-type groundwater from well NIWC 57 (table 5). As the purity of the cement samples increased, the $\delta^{13}C$ values became increasingly more negative.

Particle-Size Analysis The results of particle-size analyses of the samples of the Mahomet aquifer revealed distinct differences between the gravel pack and the aquifer material (table 6 and fig. 19). The particle-size distributions for representative samples from borehole NIWC 57-1 are shown in figure 19. The coefficient of uniformity is a relative measure of the sorting of a sample (table 6); larger coefficients represent grain-size distributions that are more poorly sorted (or well graded to engineers). The finest-grained and best-sorted materials were collected from the upper portion of the Mahomet aquifer at depths ranging from 234 to 252 feet. The coarsest, more poorly sorted materials came from 270 to 282 feet, toward the bottom of the Mahomet aquifer. The higher values for the coefficient of uniformity are found in the deeper intervals, but these are still finer than the materials from test hole TH 3-56. TH 3-56 was drilled by NIWC in 1956 next to NIWC 58. Well NIWC 58 is located approximately 2,000 feet west of NIWC 57.

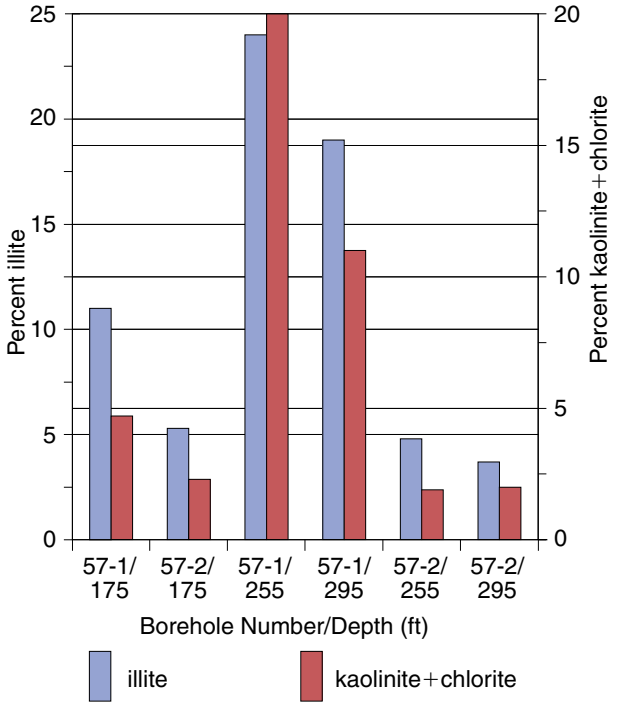

Figure 18 The relative percentages of clay minerals (the <44-μm size fraction) in samples collected from the Mahomet and Glasford (boreholes NIWC 57-1 and NIWC 57-2) aquifers. Clay minerals in the Mahomet aquifer closest to IL-AWC production well NIWC 57 exceed those in wells farther away in the aquifer by a factor of 2 to 10. This result suggests a migration and buildup of clay minerals toward and in the vicinity of municipal well NIWC 57.

Table 5 Isotopic data from calcite-cemented nodules and dissolved inorganic carbon (DIC) in groundwater collected from the Mahomet aquifer near NIWC 57.

Sample description	$\delta^{13}C$ (%)	^{14}C (% modern) $\bar{x} \pm$ SD	^{14}C age (years B.P.)
Cement separated from nodule	–4.6	0.35 ± 0.13	45,600
Partially separated cement containing clasts	–3.2	0.35 ± 0.10	45,700
Bulk nodule (unseparated)	–1.8	0.03 ± 0.10	>49,400
NIWC 60 DIC	ND	33.1 ± 0.31	8,890
NIWC 57-1M DIC	–12.1	26.3 ± 0.40	10,730
NIWC 57 groundwater DIC	–10.0	23.6 ± 0.40	11,620
Bulk nodule (unseparated)	–1.7	0.11 ± 0.06	>49,100
Gravel and fines from NIWC 57-2 (290 feet)	–0.7	0.34 ± 0.07	45,800

Well NIWC 57 is screened from a depth of 242 to 297 feet, but the gravel pack extends 11 feet above and 7 feet below the well screen (fig. 7). The pack has a coefficient of 1.8. The design criteria for this gravel pack and well screen were unknown to us. Driscoll (1986) described a method for designing a gravel pack for a well

The TH 3-56 data are significant because test holes are drilled to collect data for constructing the production wells, including particle-size data needed to design the well screen and gravel pack. No particle-size data were found for a test hole near NIWC 57, so only NIWC 58 data could be examined. The sample from TH 3-56 appeared to be much coarser than any sample collected from NIWC 57-1 (fig. 19). This difference in grain size may be real or may be caused by differences in drilling techniques. Samples from NIWC 57-1 were obtained during rotasonic coring. Samples from TH 3-56 were most likely obtained during forward mud rotary drilling. With mud rotary drilling, finer-grain materials such as silts, clays, and very fine sand are entrained in the drilling fluid and are not collected. Use of this drilling method is expected to skew the particle-size distribution of unlithified sand and gravel samples toward coarser average grain sizes.

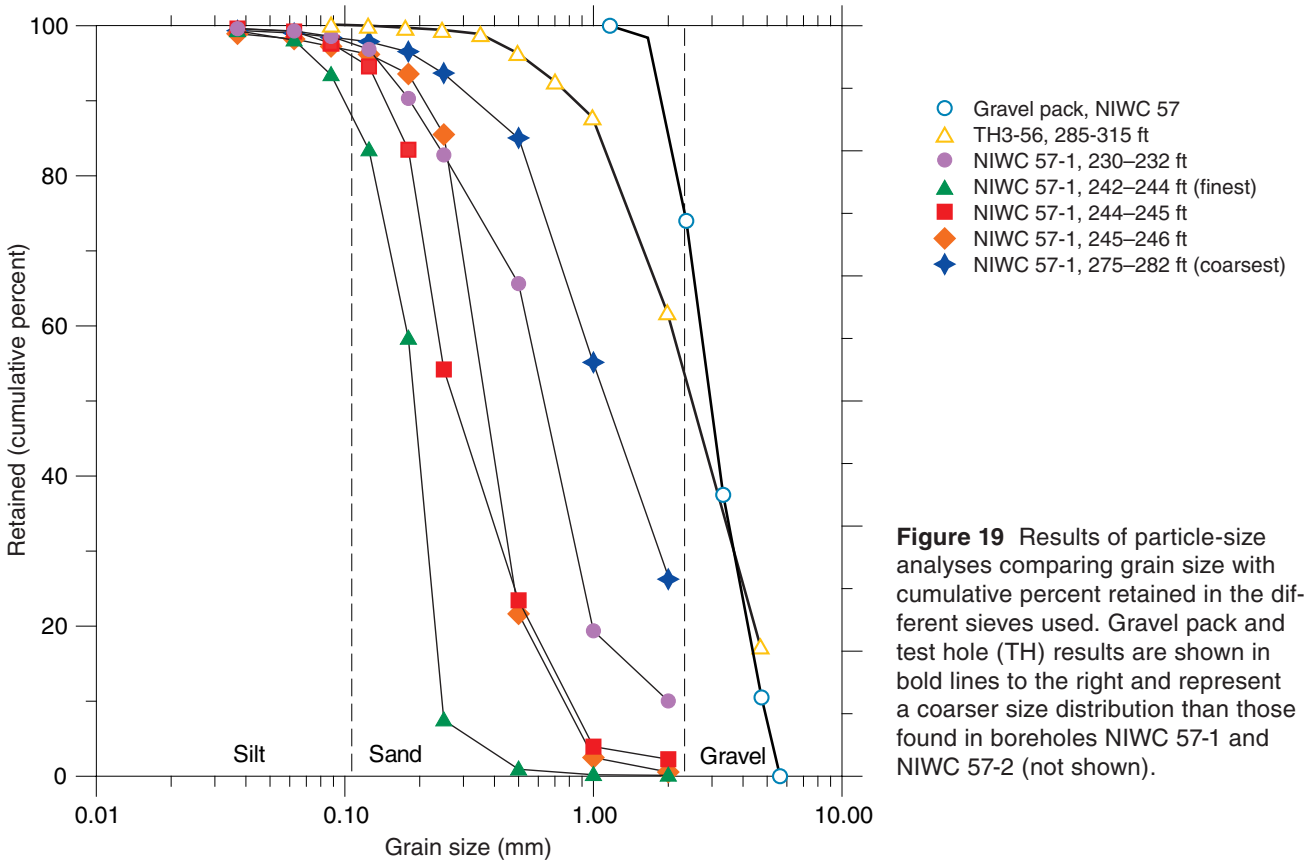

Figure 19 Results of particle-size analyses comparing grain size with cumulative percent retained in the different sieves used. Gravel pack and test hole (TH) results are shown in bold lines to the right and represent a coarser size distribution than those found in boreholes NIWC 57-1 and NIWC 57-2 (not shown).

Table 6 Particle size analyses for drill core samples from borehole NIWC 57-1.

Sample interval (ft)	90% retained size[1] (mm)	40% retained size[2] (mm)	CU[3]
225–230	0.13	0.24	1.8
230–232	0.19	0.75	3.9
232–234	0.20	0.75	3.8
234–239	0.12	0.24	2.0
239–242	0.12	0.22	1.8
242–244	0.10	0.20	2.0
244–245	0.15	0.33	2.2
245–246	0.21	0.41	2.0
246–249	0.19	0.39	2.1
249–252	0.16	0.24	1.5
252–259	0.30	0.85	2.8
259–261	0.28	0.73	2.6
261–262	0.18	0.57	3.2
262–270	0.20	0.73	3.7
270–272	0.12	1.30	11
272–275	0.20	1.30	6.5
275–282	0.32	1.60	5.0
282–285	0.19	0.45	2.4
285–290	0.19	0.37	1.9

[1]The grain size at which 90% of the sample is coarser than the specified grain size and 10% is finer.
[2]The grain size at which 40% of the sample is coarser than the given size and 60% is finer.
[3]The coefficient of uniformity (CU) is defined as the 40% retained size divided by the 90% percent retained size.

such as NIWC 57. Using the method of Driscoll, we found that 70% of the gravel pack should have been coarser than 1.12 to 1.68 mm. Instead, 70% of the gravel pack for NIWC 57 was coarser than 2.4 mm. Thus, based on the particle-size distribution of the aquifer in test hole NIWC 57-1 drilled 15 feet away, the gravel pack for NIWC 57 may have been too coarse for the particle-size distribution of the aquifer. If the gravel pack is too coarse, finer-grained sediment from the aquifer may migrate into the gravel pack. No samples from the gravel pack were available, so it was impossible to determine whether fines (originating in the aquifer) migrated into the gravel pack at NIWC 57 and, if so, whether they contributed significantly to the observed decline in specific capacity of this well.

Bacterial Analysis of Core Samples

Bacterial indicators, genera, and species present within the cores retrieved from boreholes NIWC 57-1 and NIWC 57-2 (tables 7 and 8) included a wide

Table 7 Bacterial analysis of core samples from borehole NIWC 57-1.

Depth (ft)	TA[1] (cfu)	TC (cfu)	FC (cfu)	Ent. (cfu)	Fe-rel (cfu)	SO_4-red (cfu)	Species[2]	Lithology
5	---[3]	---	---	---	---	---	---	
10	0	0	0	0	0	0	None	
15	---	---	---	---	---	---	---	
20	0	0	0	0	0	0	None	
25	---	---	---	---	---	---	---	
30	2,100	200	0	1,700	0	0	Bs, Kp, Sf	
35	---	---	---	---	---	---	---	
40	0	0	0	0	0	0	None	Clay
50	260	100	0	0	0	0	Bs,Kp	(silty and sandy)
60	300	300	0	0	0	0	Kp, Af	Wedron Group
80	0	0	0	0	100	0	Fe-rel	
90	160	100	0	0	0	0	Kp,Bs	
110	0	0	0	0	0	0	None	
122	0	0	0	0	0	0	None	
130	0	0	0	0	0	0	None	
140	0	0	0	0	0	0	None	
145	---	---	---	---	---	---	---	
155	---	---	---	---	---	---	---	
159	3,700	0	0	0	100	0	Bs, Kp, Ps	
165	---	---	---	---	---	---	---	Sand and gravel
170	130	0	0	0	0	0	Bs	(fine to coarse)
180	0	0	0	0	0	0	None	Glasford
185	---	---	---	---	---	---	---	Formation
190	110	0	0	0	0	0	Ps	
195	---	---	---	---	---	---	---	
200	0	0	0	0	0	0	None	Clay
210	0	0	0	0	0	0	None	(sandy and
220	0	0	0	0	0	0	None	gravelly)
225	---	---	---	---	---	---	--	
230	0	0	0	0	0	0	None	
235	---	---	---	---	---	---	---	
240	0	0	0	0	0	0	None	
245	---	---	---	---	---	---	---	
250	400	0	0	0	0	0	Kp, Pa	
255	---	---	---	---	---	---	---	Sand and gravel
260	0	0	0	0	0	0	None	(fine to coarse)
265	---	---	---	---	---	---	---	Banner
270	0	0	0	0	0	0	None	Formation
275	---	---	---	---	---	---	---	
280	0	0	0	0	0	0	None	
285	---	---	---	---	---	---	---	
290	0	0	0	0	0	0	None	
295	---	---	---	---	---	---	---	
300	90	0	0	0	0	0	Bs	
315	0	0	0	0	0	0	None	Clay (hard)
Water	1,600	42	0	2	100	0	Kp, Pa, S, Ss	
Water	28	0	0	0	0	0	Pc, S	

[1]TA, total aerobic bacteria; TC, total coliforms; FC, fecal coliforms; Ent., fecal enterococci; Fe-rel, iron-related; SO_4-red, sulfate-reducing bacteria; cfu, colony-forming units.
[2] Bs, *Bacillus* spp., Kp, *Klebsiella pneumoniae*; Sf, *Staphyloccus faecium*; Pa, *Pseudomonas aeruginosa*; Ps, *Pseudomonas* spp.; Af, *Aspergillus fumigatus*; S, *Staphylococcus* spp.; Ss, *Serratia* spp.
[3]---, no samples.

variety of aerobic and iron-depositing bacteria. No SO_4^{2-}-reducing bacteria were detected in the samples. Bacteria isolated from the cores included soil-related bacteria (*Bacillus* spp., *Serratia* spp., *Pseudomonas* spp., and *Klebsiella pneumoniae*) and fecal streptococci (*Streptococcus faecium*). Tests for iron-depositing bacteria were positive for core samples from the upper part of borehole NIWC 57-1 within the till and the upper part of the Glasford aquifer. Iron-depositing bacteria were detected sporadically throughout borehole NIWC 57-2. In addition, a common blue-green fungus (*Aspergillus fumigatus*) was found within a till sample from NIWC 57-1.

The largest counts of total aerobic bacteria and fecal streptococci were found in cores from the upper sections of both boreholes, particularly the upper 5 feet and within the shallow Wedron aquifer (tables 7 and 8). Relatively large bacterial counts also were detected in the sand and gravel of the Glasford aquifer. There were a few occurrences of bacteria at very low concentrations within the cores taken from the Mahomet aquifer in borehole NIWC 57-1 near the production well. However, iron-depositing bacteria were present in relatively large concentrations (5,000 cfu/100 mL) within a 20-foot section near the base of the Glasford aquifer and at the base of borehole NIWC 57-2 within the Mahomet aquifer (table 8).

Near the base of the Mahomet aquifer, at a depth of 290 feet, a large accumulation of fine-grained dolomite was observed in borehole NIWC 57-2 (table 3). The significance of the accumulation of this material and the occurrence of iron-depositing bacteria with the fine-grained dolomite (table 8) is unclear. No biofilms or evidence of aquifer biofouling at this depth or anywhere else within the Mahomet aquifer interval was observed when using a binocular microscope to examine the core samples, nor did the XRD studies show similar concentrations of calcite or dolomite at this or any other depth in the Glasford or Mahomet aquifers (tables 1 through 4).

A limited volume of water was used during the drilling of boreholes NIWC

57-1 and NIWC 57-2 to lubricate the borehole in the unsaturated zone and to provide pressure to help push core from the core barrel. This water was finished water obtained from the IL-AWC water treatment plant on Mattis Avenue in Champaign. Bacteria present in samples of this water (table 8), collected on two different days during drilling, included *Klebsiella pneumoniae, Pseudomonas aeruginosa, Pseudomonas capacia, Staphylococcus* spp.*, Serratia* spp.*,* and iron-related bacteria. These species typically live in the natural environment in soils, surface waters, and shallow groundwater and could have entered the water used in the drilling through contact with soil that inadvertently fell into or was present in the water tank (table 8). The suite of bacteria present in the drilling water was not reflected in the core samples, indicating there probably was little or no contamination of the selected core samples by the drilling water.

Groundwater Samples

Groundwater samples were collected from NIWC 57 and monitoring wells NIWC 57-1M and NIWC 57-2M to determine whether calcite saturation of the groundwater was affected by the greater drawdown adjacent to well NIWC 57. Monitoring well NIWC 57-2M was found to be partially blocked with the Na-bentonite used to construct the wells. Unfortunately, the bentonite may have affected the chemical composition of the groundwater samples collected from monitoring well NIWC 57-2M (table 9). Bentonite contains approximately 2.5% Na_2O, 1.8% CaO, 65% SiO_2, and 4.4% Fe_2O_3 (Black Hills Bentonite-Technical data, www.bhbentonite.com).

Groundwater Chemistry The chemical composition of groundwater samples from NIWC 57-2M apparently reflects the presence of Na-bentonite within the well. For example, Na^+ was elevated in NIWC 57-2M by about 10 mg/L compared with NIWC 57 and NIWC 57-1M (table 9) and was greater than the Na^+ concentrations found in other production wells and in the Illinois State Water Survey's monitoring wells in the area (table A2). However,

Table 8 Bacterial analysis of core samples from borehole NIWC 57-2.

Depth (ft)	TA[1] (cfu)	TC (cfu)	FC (cfu)	Ent. (cfu)	Fe-rel (cfu)	SO_4-red (cfu)	Species[2]	Lithology
5	7,800	2	0	3,700	5,000	0	Bs, Kp, Ps, Sf	
10	9,000	0	0	0	0	0	Pc	
15	0	0	0	0	0	0	None	
20	0	0	0	0	0	0	None	
25	0	0	0	0	0	0	None	
30	0	0	0	0	0	0	None	
35	0	0	0	0	0	0	None	
40	---[3]	---	---	---	---	---	---	Clay
50	---	---	---	---	---	---	---	(silty and sandy)
60	---	---	---	---	---	---	---	Wedron Group
80	---	---	---	---	---	---	---	
90	---	---	---	---	---	---	---	
110	---	---	---	---	---	---	---	
122	---	---	---	---	---	---	---	
130	---	---	---	---	---	---	---	
140	---	---	---	---	---	---	---	
145	0	0	0	0	0	0	None	
155	0	0	0	0	100	0	Fe-rel	
159	---	---	---	---	---	---	---	
165	0	0	0	0	0	0	None	Sand and gravel
170	---	---	---	---	---	---	---	(fine to coarse)
180	400	0	0	0	0	0	Bs	Glasford
185	740	200	0	0	0	0	Bs, Kp	Formation
190	---	---	---	---	---	---	---	
195	0	0	0	0	5,000	0	Fe-rel	
200	---	---	---	---	---	---	---	Clay
210	---	---	---	---	---	---	---	(sand and
220	---	---	---	---	---	---	---	gravel)
225	0	0	0	0	0	0	None	
230	---	---	---	---	---	---	---	
235	0	0	0	0	0	0	None	
240	---	---	---	---	---	---	---	
245	0	0	0	0	0	0	None	
250	---	---	---	---	---	---	---	
255	0	0	0	0	0	0	None	Sand and gravel
260	---	---	---	---	---	---	---	(fine to coarse)
265	0	0	0	0	0	0	None	Banner
270	---	---	---	---	---	---	---	Formation
275	0	0	0	0	5,000	0	Fe-rel	
280	---	---	---	---	---	---	---	
285	0	0	0	0	5,000	0	Fe-rel	
290	---	---	---	---	---	---	---	
295	0	0	0	0	5,000	0	Fe-rel	
300	---	---	---	---	---	---	---	
315	---	---	---	---	---	---	---	Clay (hard)
Water	1,600	42	0	2	100	0	Kp, Pa, S, Ss	Finished water from the IL-AWC water plant
Water	28	0	0	0	0	0	Pc, S	

[1]TA, total aerobic; TC, total coliforms; FC, fecal coliforms; Ent., fecal enterococci; Fe-rel, iron-related; SO_4-red, sulfate-reducing; cfu, colony-forming units.
[2] Bs, *Bacillus* spp., Kp, *Klebsiella pneumoniae*; Ps, *Pseudomonas* spp.; Sf, *Staphyloccus faecium*; Pc*, Pseudomonas capacia*; Pa, *Pseudomonas aeruginosa*; S, *Staphylococcu*s spp.; Ss, *Serratia* spp.
[3]---, no samples.

Table 9 Chemical composition of water samples from IL-AWC production wells and monitoring (M) wells near NIWC 57.

Parameter[1]	NIWC 57	NIWC 57-1M (NP)[2]	NIWC 57-1M (P)	NIWC 57-1M (P)	NIWC 57-2M (P)	NIWC 57-1G (NP)
Temp.	13.1	15.2	15.4	16.0	15.1	15.3
pH	7.72	7.63	7.76	7.70	7.41	7.40
Eh	63	46	48	51	59	53
Sp. cond.	595	612	563	576	628	715
B	0.90	0.78	0.77	0.79	1.14	1.81
Ba	0.367	0.331	0.328	0.312	0.329	0.268
Ca	56.5	56.5	54.4	52.4	58.0	60.0
Fe	1.41	1.33	1.26	1.25	1.71	3.04
K	< 1	< 1	< 1	2	< 1	< 1
Mg	33.5	33.8	32.7	31.2	33.2	33.0
Mn	0.210	0.019	0.170	0.017	0.220	0.020
Na	52.0	48.7	47.5	46.2	61.4	70.5
Si	5.59	5.31	5.27	5.04	6.22	6.84
Sr	0.640	0.648	0.632	0.607	0.667	0.781
NO_3N	< 0.02	< 0.02	< 0.02	< 0.02	< 0.02	< 0.02
SO_4	< 0.1	< 0.1	< 0.1	< 0.1	< 0.1	< 0.1
F	0.31	0.33	0.31	0.37	0.31	0.40
Cl	1.6	1.6	1.3	1.4	0.9	0.7
T. Alk.	362	362	354	348	382	428
Date	05/09/00	04/14/00	05/02/00	05/09/00	05/09/00	04/14/00

[1]All parameters in milligrams per liter except for temperature (°C), pH (pH units), redox potential (Eh in mV), specific conductance (Sp. cond. in μS/cm), and total alkalinity (T.Alk. in mg/L as $CaCO_3$).
[2]NP, sampled while NIWC 57 was not being pumped; P, sampled during pumping of NIWC 57.

no such problems with bentonite seals were found in well NIWC 57-1M. Because of the uncertainty of the quality of the water sample from NIWC 57-2M relative to the other samples, those data were not used to determine the mass of calcite that might be precipitating between monitoring wells NIWC 57-2M and NIWC 57-1M.

Iron-depositing Bacteria Water samples collected from IL-AWC production wells NIWC 55, NIWC 57, and NIWC 58 were analyzed for indicator, iron-related, and sulfate-reducing bacteria (table 10). Chapelle (1993) stated that ". . . the presence of iron-oxidizing bacteria in aquifer sediments is indicated by their common presence in water wells." The rotasonic drilling technique yielded core samples with a minimum of bacterial contamination. The presence of iron-depositing bacteria near the base of the Mahomet aquifer in borehole NIWC 57-2 suggested that Chapelle was correct in his assumption that these bacteria are ". . . a common component of the subsurface microflora." Aerobic bacteria were found in groundwater collected from wells NIWC 57 and NIWC 58, but not in well NIWC 55. *Bacillus* and *Pseudomonas* spp. are ubiquitous in soil and wells and have been identified in shallow aerobic aquifers (Chapelle 1993). Although these bacteria could have been introduced during drilling or well construction, their persistence and their biofilm production strongly suggest that O_2 is somehow getting into the well and well screen. Iron-related and sulfate-reducing bacteria were detected in groundwater samples from all three production wells sampled.

Suspended Solids

The suspended solids collected on 0.50-μm filters when sampling the water from NIWC 55, NIWC 57, and NIWC 58 yielded important clues to the biological activities and environmental conditions within the production wells. The SEM examination showed the suspended solids trapped on the filters to be a mixture of detrital mineral fragments, iron oxide and hydroxide tubercles, twisted filaments of iron-depositing bacteria, and authigenic calcite crystals. The

Table 10 Bacterial indicators and fecal, sulfate-reducing, and iron-related bacteria present in water samples collected from three production wells in the IL-AWC western well field.

Well	TA[1] (cfu)	TC (cfu)	FC (cfu)	FS (cfu)	Iron-related bacteria (cfu)	Sulfate-reducing bacteria (cfu)	Bacterial species
NIWC 55	0	0	0	0	100	100	None isolated
NIWC 57	9	0	0	0	100	100	*Bacillus* spp. *Pseudomonas* spp.
NIWC 58	2	0	0	0	100	100	*Bacillus* spp. *Pseudomonas* spp.

[1]TA, total aerobic; TC, total coliforms; FC, fecal coliforms; FS, fecal streptococci; cfu, colony-forming units.

size of the mineral fragments and amount of bacterial material present on the filters collected at each of the three wells were different, and the differences appeared to be related to the rate at which each well was being pumped. Qualitatively, the filter used at well NIWC 55 contained relatively few mineral and bacterial fragments, and these fragments were rarely over 10 μm in length or diameter. The filter used at well NIWC 57 contained abundant bacterially generated materials and larger mineral fragments that were typically up to 20 μm in diameter. The filter from well NIWC 58 contained the largest (up to 100 μm across) and most abundant mineral fragments and bacterially generated fragments (fig. 20). The materials found on the filters, the well construction, and the potential sources of oxygen in the vicinity of the wells are discussed.

Bacteria The SEM showed the presence of bacteria-related deposits on the filters used at wells NIWC 55, NIWC 57, and NIWC 58. The filters for NIWC 57 and NIWC 58, originally white, were stained a solid to patchy reddish orange and held stalks and tubercles composed of carbon, iron, calcium, and silicon formed by the iron-depositing bacteria (fig. 20). The filter from NIWC 55 was a grayish buff color with no reddish patches; it contained some sparsely distributed tubercles (fig. 20). Little et al. (1997)

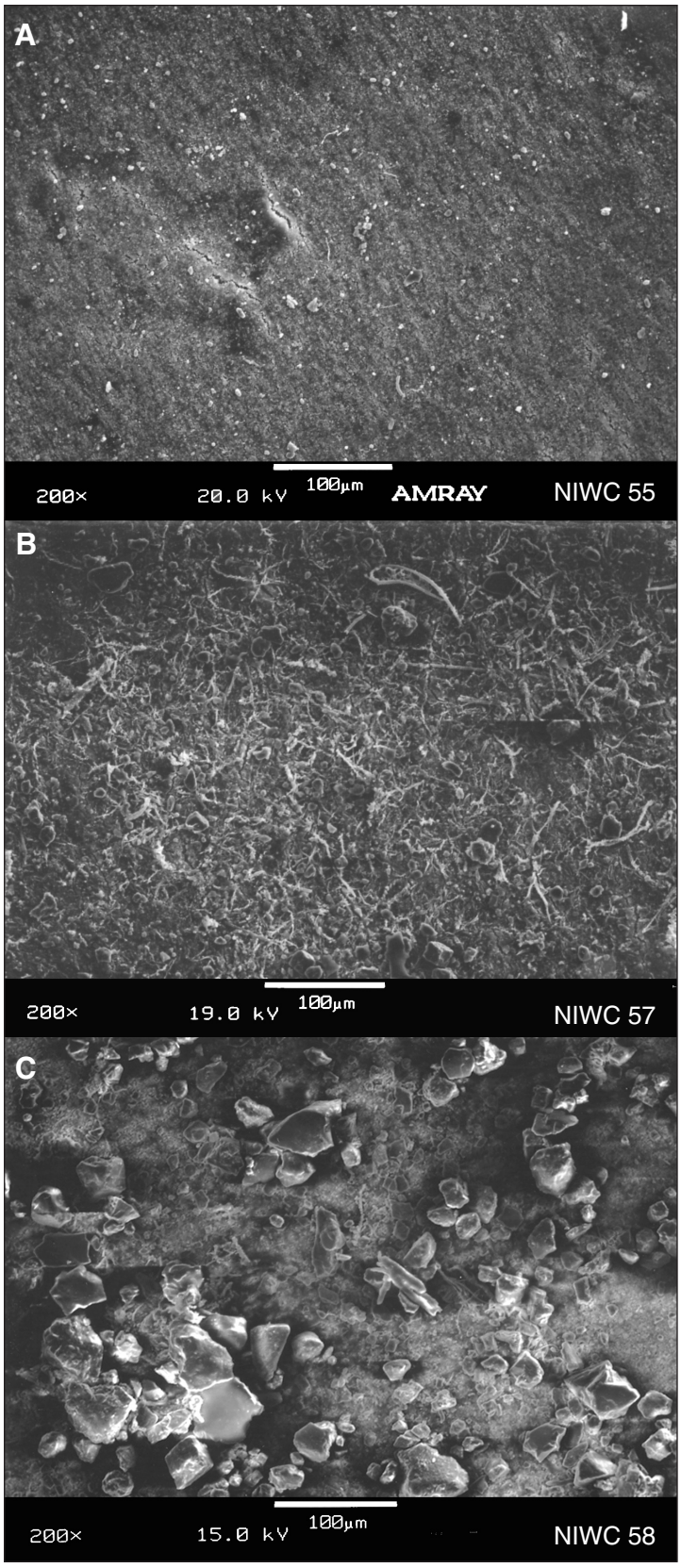

Figure 20 Photomicrographs of 0.50-μm filters through which approximately 130 gallons of groundwater from the discharge stream of three production wells was filtered. Magnification is 200×. Captured suspended solids progressively increase in abundance, size, and diversity as pumping rates increase. A, the filter used at well NIWC 55, which was pumped at a rate of about 1,100 gpm, showed only specks of a white material (calcite) and small strands (bacterially generated strands and tubercles of iron oxides and hydroxides). B, larger, more abundant strands and tubercles and detrital mineral fragments appeared on the filter used at well NIWC 57, which was pumped at a rate of about 1,700 gpm. C, the largest material was found on the filter used at well NIWC 58, which was pumped at a rate of about 2,300 gpm.

noted that "iron-depositing bacteria produce orange-red tubercles [composed] of iron oxides and hydroxides by oxidizing ferrous ions from the bulk medium or the substratum." The tubercles were hollow and provided an armored shelter for iron-depositing bacteria against environmental assaults (e.g., disinfectants).

Bacilli and cocci (rod- and sphere-shaped, respectively) bacteria were observed on the surfaces of the filters and intermixed with fragments of detached biofilms (fig. 21). Biogenic filaments composed predominantly of iron oxide were scattered over the filters (figs. 21 to 25) and were entwined around and engulfing detrital mineral fragments (figs. 26 and 27). The abundance and size of the bacterial fragments, at least from the three wells sampled, appeared to depend on the pumping rate of the wells. The largest and most abundant biogenic fragments were collected from NIWC 58, which was being pumped at about 2,300 gpm. The smallest and fewest were collected from NIWC 55, which was being pumped at about 1,100 gpm.

Mineral Fragments The mineral fragments caught on the filters included dolomite, calcite, quartz, feldspar, and clay minerals. The size range of these fragments also appeared to be related to the well pumping rates (fig. 20). Specifically, the largest mineral fragments (typically about 40 μm in diameter) were collected on the filter used at well NIWC 58, which had a pumping rate of about 2,300 gpm, whereas the smallest fragments (typically about 5 μm in diameter) were collected on the filter used at well NIWC 55 that had a pumping rate of about 1,100 gpm. Intermediate size fragments (typically about 10 μm in diameter) were collected on the filter used at well NIWC 57 that had a pumping rate intermediate between NIWC 58 and NIWC 55 (fig. 20). Thus, the groundwater flowing into the well annulus during pumping operations apparently entrained fine mineral fragments from the aquifer and gravel pack; the greater the pumping rate, the larger were the entrained mineral fragments.

Clay minerals are much more abundant in samples from the Mahomet aquifer from well NIWC 57-1, drilled just 15 feet from the production well, than from well NIWC 57-2, drilled 60 feet from the production well (fig. 18). This result suggests that clay minerals are being transported toward the production well during pumping operations. Mineral fragments that were not trapped within the aquifer were either trapped with the other materials in the biofilm-based deposits at the well screen or were transported up the well with the water.

The filter from well NIWC 55 contained few detrital minerals. Most of the mineral matter on the filter was composed of euhedral calcite crystals that were about 5 μm in diameter (fig. 28). The size, morphology, and monomineralic nature of these crystals suggest that they are not of detrital origin, but precipitated directly from solution. The calcite probably precipitated within the pores of the aquifer, in the gravel pack, and/or in the well bore during pumping and as a result of pumping-induced outgassing of CO_2 from the groundwater. Crystals such as these may also be found in the materials examined on the filters used at the other two production wells. However, it was very difficult to distinguish between authigenic and detrital calcite crystals in the materials collected on the filters at the other production wells. The abundance of other materials trapped on the filters obscured the presence of the smaller, authigenic calcite crystals.

Although most of the calcite masses were relatively small (about 5 μm in diameter) and euhedral, one rectangular-shaped fragment found on the filter from well NIWC 55 was 70 μm by 40 μm by 30 μm and showed signs of dissolution (pitting) as well as reprecipitation (euhedral calcite crystals about 1 μm across) on other parts of the fragment. This fragment may reflect the presence of a dynamic equilibrium in the calcium-bicarbonate system in the vicinity of the production wells, possibly because of the effects of pumping and/or the effects of well remediation activities.

Discussion

Results revealed evidence of several processes that may be contributing to the decreased specific capacity of well NIWC 57 and possibly the other production wells in the western well field that have shown declines in specific capacity. Those processes include (1) a gravel pack that was too coarse to keep aquifer materials from migrating to the well screen, (2) biofilm formation on the well screen and possibly within the gravel pack, (3) calcite precipitation within the aquifer and gravel pack, and (4) the transport of clay- and silt-size detrital minerals in the aquifer toward the well during pumping. If precipitated calcite and transported detrital mineral grains become entrapped within the biofilms on the screen or within the gravel pack, the loss of specific capacity might increase. These processes and the potential interactions among them are discussed.

Calcite Precipitation from Groundwater

Groundwater Chemistry Mehnert et al. (1999) determined that CO_2 outgassing probably occurred in the vicinity of high-capacity production wells in the IL-AWC western well field. It is well known that reduced pressure and agitation results in CO_2 outgassing from groundwater as it flows from an aquifer. Hydrostatic pressure reduction produced in the vicinity of a pumping well decreases the pressure on the groundwater, causing outgassing of CO_2. The outgassing increases the groundwater pH within or close to the well, causing the water to become oversaturated with carbonate minerals (especially calcite). As a consequence, crystals of calcite and/or other carbonate minerals may precipitate from the groundwater (e.g., Hubbard and Herman 1991).

The smaller concentrations of total dissolved solids and Ca^{2+}, the greater pH values, and the lower partial pressure CO_2 (pCO_2) in groundwater samples from the western well field (fig. 29), compared with values in the background monitoring wells, support the possibility of calcite

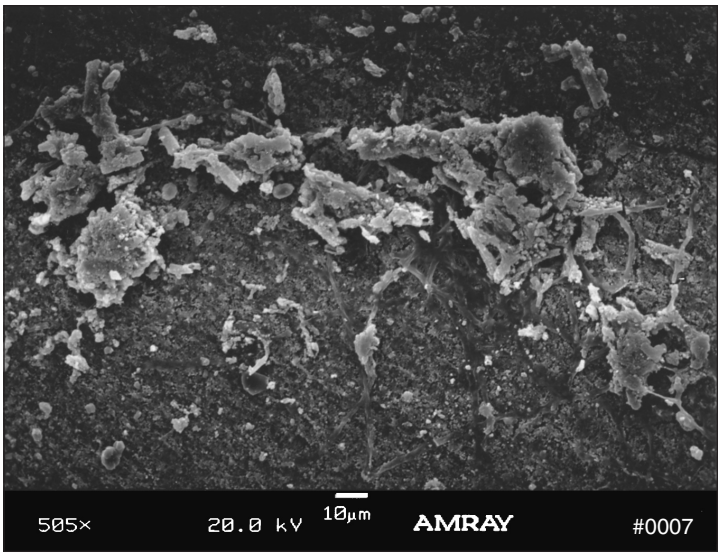

Figure 21 Photomicrograph of the fragments of a biofilm dislodged from a surface within well NIWC 55 during pumping operations. The view shows the underside of the biofilm; bacilli and cocci are present on the largest fragment in the upper right quadrant of the photomicrograph; calcite crystals are visible as scattered 5-μm diameter specks. Magnification is 505×.

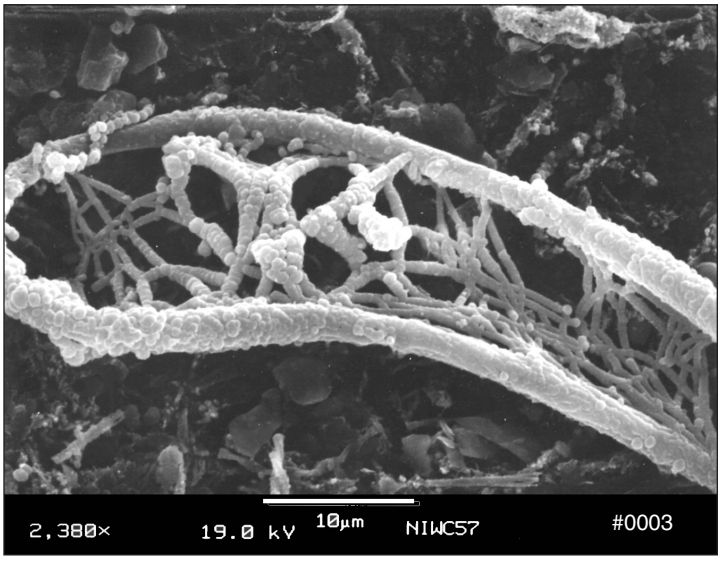

Figure 22 Photomicrograph of a fish-shaped tubercle trapped on the filter from well NIWC 57. High-energy dispersive X-ray backscatter analysis revealed that the encrustation on the tubercles was made up predominantly of carbon, iron, and oxygen. Smaller mineral fragments are visible in the background, and a twisted filament is visible near the bottom center of the photomicrograph. Magnification is 2,380×.

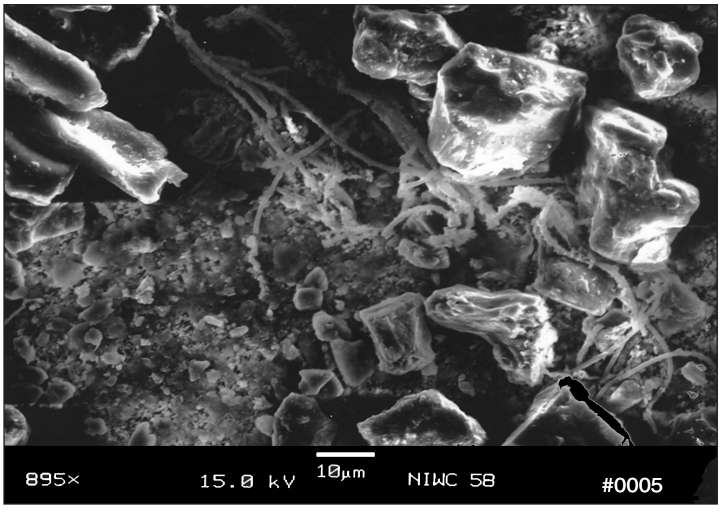

Figure 23 Photomicrograph of a large tubercle (top left), filaments (center), and detrital minerals collected from well NIWC 58. Magnification is 895×.

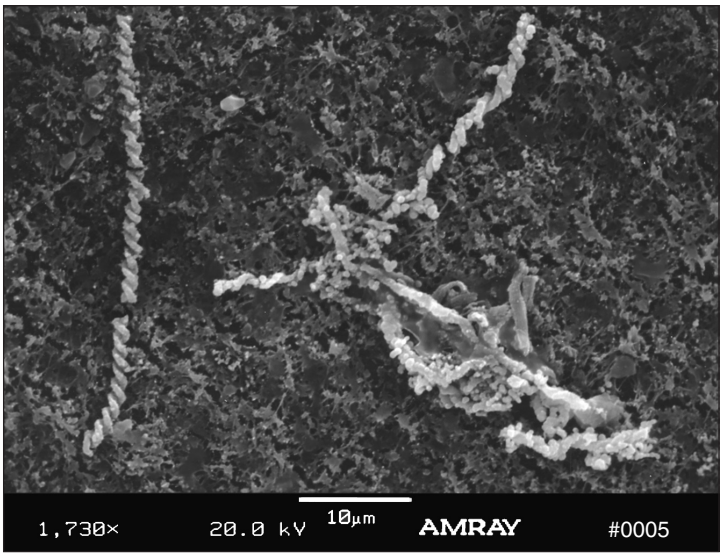

Figure 24 Photomicrograph of twisted stalks produced by iron-depositing bacteria during their sessile (attachment and growth) phase collected from well NIWC 55. The more massive material in the lower right corner appears to be a fragment of biofilm. Magnification is 1,730×.

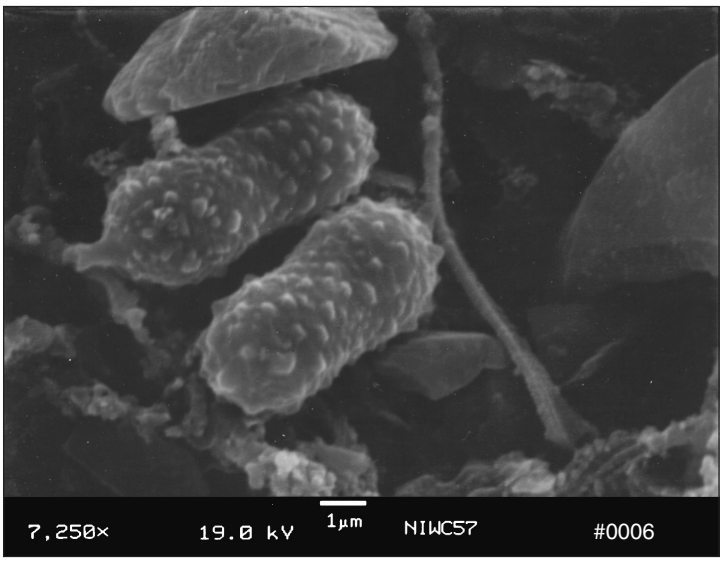

Figure 25 Photomicrograph of what appears to be the motile form of an iron-depositing bacteria lying among the debris field on the filter from well NIWC 57. Magnification is 7,250×

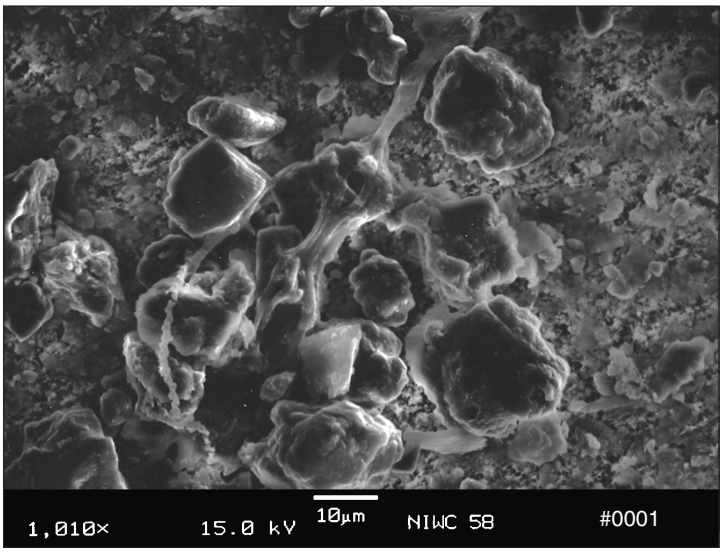

Figure 26 Photomicrograph of long filaments of iron-depositing bacteria that have enveloped detrital mineral fragments in well NIWC 58. Magnification is 1,010×.

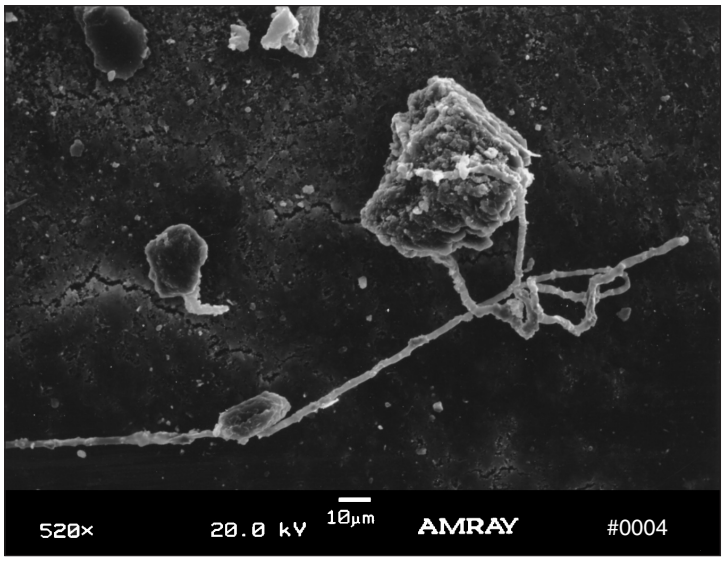

Figure 27 Photomicrograph of the filament of an iron-depositing bacteria entwined around a relatively large calcite crystal from well NIWC 55. Magnification is 520×.

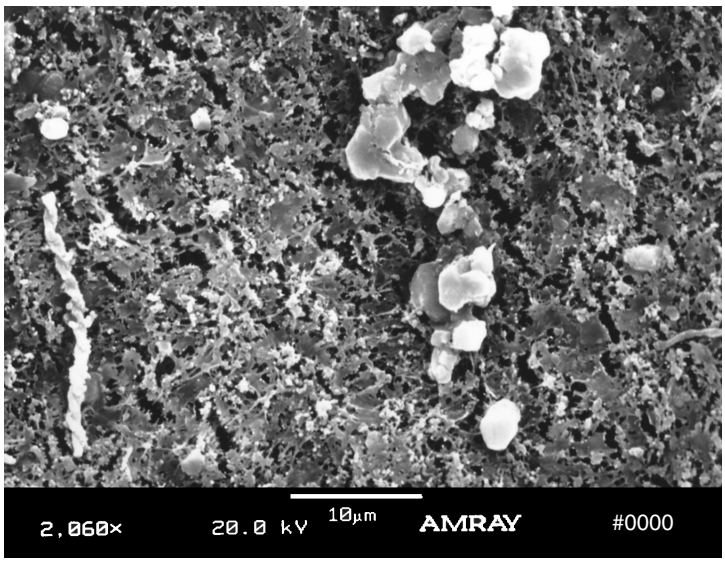

Figure 28 Photomicrograph of a cluster of calcite crystals in the shape of a backwards question mark from well NIWC 55. The twisted, rope-like stalk on the left was produced by an iron-depositing bacteria (probably *Gallionella ferruginea*). The fibrous material in the background is the filter. Magnification is 2,060×.

precipitation adjacent to the production wells. The chemical composition of the groundwater at NIWC 57 indicates that the groundwater is oversaturated with calcite (fig. 30). Calcite, therefore, is probably precipitating near the high-capacity wells (including well NIWC 57) and may also be precipitating within the aquifer, gravel pack, and/or at the well screens.

In general, results from this current investigation were consistent with the findings of Mehnert et al. (1999). We hypothesized that pumping the wells at rates of about 1,000 gpm lowered hydrostatic pressure within the aquifer enough to cause outgassing of CO_2 from groundwater and a concomitant precipitation of calcite. A decrease in the total dissolved solids (TDS) concentration in groundwater samples from the western well field (fig. 30) was assumed to be, at least in part, the result of the precipitation of calcite, perhaps in very close proximity to the production wells. Considering other chemical characteristics of the background wells, compared with those of the production wells, the explanation for calcite precipitation may be more complicated than originally hypothesized. Part of the difference in TDS could be explained by the differences in SO_4^{2-} concentrations (table A2) and SO_4^{2-} reduction. The SO_4^{2-} reduction in groundwater within the aquifer between the background wells and the western well field would involve the formation of bicarbonate through the reaction of SO_4^{2-} with organic matter, represented by CH_2O, as follows:

$$2CH_2O + SO_4^{2-} \rightleftharpoons H_2S + 2HCO_3^-.$$

The formation of HCO_3^- ions could result in the precipitation of calcite within the aquifer because of oversaturation. Consequently, the reaction

$$2Ca^{2+} + 2HCO_3^- \rightleftharpoons 2CaCO_3 + H_2O$$

would cause the precipitation of calcite within the aquifer and could

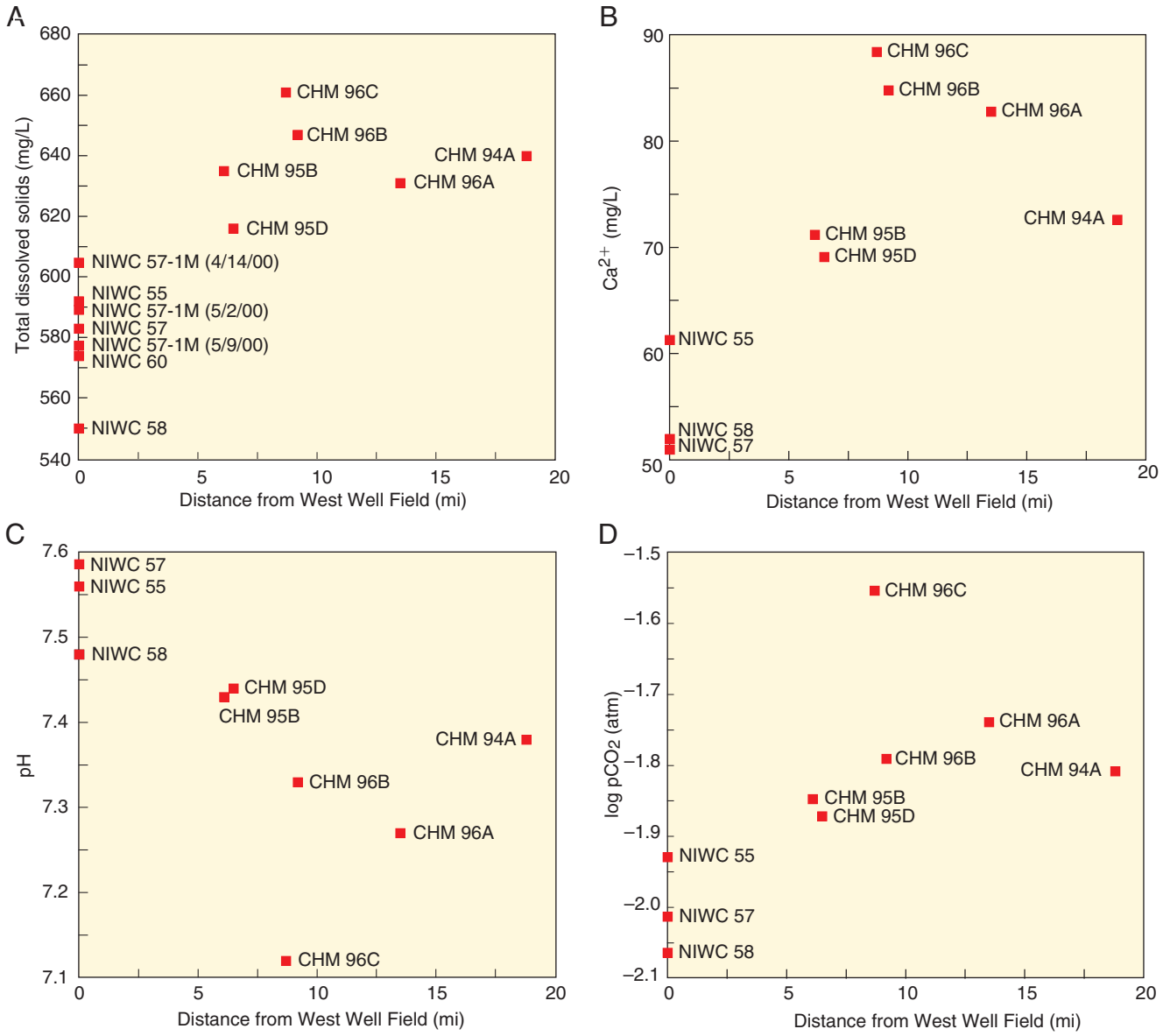

Figure 29 Total dissolved solids, Ca^{2+}, pH, and partial pressure of CO_2 (pCO_2) in groundwater samples from 3 IL-AWC production wells in the western well field and 6 Illinois State Water Survey (ISWS) observation wells in the Mahomet aquifer (data from Mehnert et al. 1999). CHM, lightly pumped observation wells drilled by ISWS; NIWC, production wells of the IL-AWC.

explain the loss of Ca^{2+} and TDS along the hydraulic gradient of the Mahomet aquifer (toward the well field from the background wells). The relationship of Ca^{2+} to SO_4^{2-} (fig. 31) reveals two trends: (1) the loss of Ca^{2+} and SO_4^{2-} due to SO_4^{2-} reduction and precipitation of calcite and (2) the loss of Ca^{2+} within the well field due to outgassing of CO_2 (as predicted by Mehnert et al. 1999). Thus, the loss of Ca^{2+} and TDS in proximity of the western well field is likely a combination of these two reactions.

To test further the hypothesis of outgassing-induced precipitation of calcite near the production wells, the data obtained from the chemical analyses of water samples collected from background wells and production wells NIWC 55, NIWC 57, and NIWC 58 (tables 9 and A2) were used to model the geochemistry of the groundwater. The REACT model from The Geochemist's Workbench® (Bethke 1996) was used in this effort. Outgassing was modeled by decreasing the CO_2 in the groundwater (shown as fugacity CO_2) over the ranges of values observed from archival sample CHM 95D and production well sample NIWC 57 (fig. 32A). The equilibrium model predicted an increase in pH of about 0.12 pH units, whereas the equilibrium pH values showed a change of 0.15 pH units (fig. 32A). The change in the field pH of the groundwater for the 6 miles between ISWS well CHM 95D (table A2) and well NIWC 57 was between 0.1 and 0.2 pH units. The model predicted that, for the given loss in the log fugacity

CO_2 of 0.16, TDS concentration should have decreased about 60 mg/L, which was close to what was measured (fig. 32B). Associated with a loss of TDS, the model also predicts calcite precipitation of approximately 30 mg/L (fig. 32C). In addition, the CO_2 outgassing equilibrium model predicted a total carbon in water loss of approximately 10.5 mg/L between CHM 95D and NIWC 57 (fig. 32D). However, equilibrium concentrations between the two wells show only about 6 mg of difference in their total carbon contents (fig. 32d). The equilibrium geochemical modeling predicted very similar changes in chemical parameters that were observed for equilibrium conditions and items that were actually measured. Because the modeling accurately predicted a loss of TDS and precipitation of minerals, and we observed decreases in the concentrations of TDS, Ca^{2+}, HCO_3^- and other constituents [SiO_2 and Fe (table A2)] between the monitoring wells and the 3 production wells, it is likely that some calcite and perhaps other minerals were precipitating in close proximity to the production wells.

Physical Evidence The apparent enrichment of calcite in the sand and gravel of the Mahomet aquifer near well NIWC 57 relative to reference samples, as determined by XRD (percent of calcite in tables 1, 2, and 3), is interpreted as physical evidence of the precipitation of calcite within the Mahomet aquifer that was observed in the core samples. Because the reference samples of the Mahomet aquifer were collected using forward rotary drilling techniques, the fine fraction may have been underrepresented in these samples. Alternatively, a comparison of the fine fractions (calcite/quartz ratios) from smeared XRD samples should provide a less biased comparison between borehole samples from near well NIWC 57 and background boreholes. That is, the remaining fine fraction should retain its original mineralogic composition and reflect the addition of any authigenic calcite that might have precipitated within the aquifer, whereas the bulk pack samples would not. Smear samples from boreholes NIWC 57-1 and NIWC 57-2 show average calcite/quartz ratio values of 5.40 and 3.92, respectively (table 4). A single value from a reference borehole had a calcite/quartz ratio value of 1.27 (table 1). Thus, these limited observations from the calcite data support the enrichment of calcite in the vicinity of well NIWC 57.

Although the calcite-cemented nodules appeared to be strong evidence of cementation in the sand and gravel aquifer near well NIWC 57, ^{14}C dates of the calcite cement showed that these features were cemented tens of thousands of radiocarbon years before the installation of well NIWC 57. Specifically, the samples yielded only 0.35 pmc (percent modern carbon) for the two samples of cement separated from the nodule and 0.03 pmc for the bulk sample (table 5). If the calcite cement had been recently precipitated, it should have had a ^{14}C activity similar to that of the dissolved inorganic carbon (23 to 26 pmc) measured in groundwater samples from NIWC 57 and NIWC 57-1M. The calcite cement samples may not have been pure and may have contained some ancient clasts. Thus, the lowest

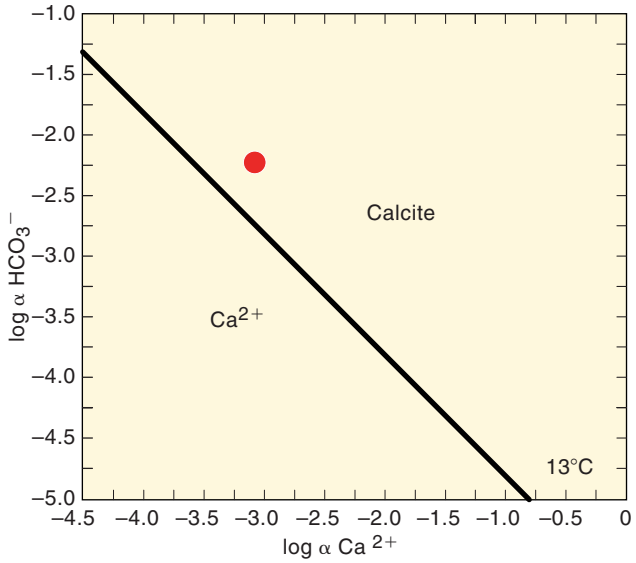

Figure 30 Activity diagram for HCO_3^- and Ca^{2+} showing the location of groundwater from well NIWC 57 (red dot). The location of the groundwater sample shows that the groundwater from the Mahomet aquifer at this location is oversaturated with respect to calcite.

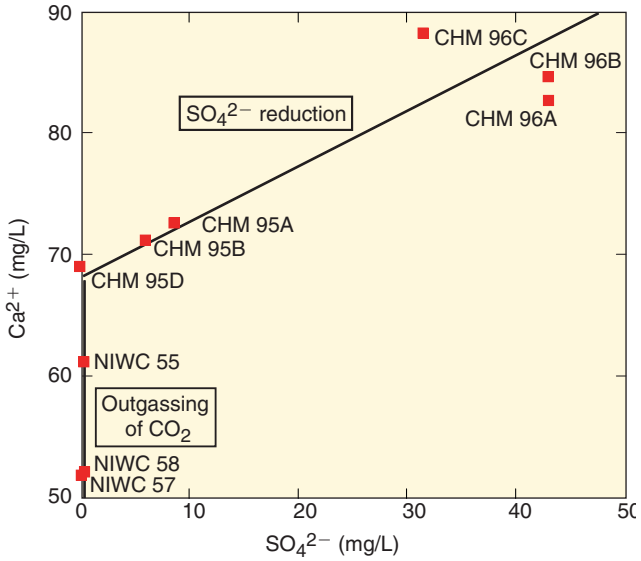

Figure 31 Comparison of Ca^{2+} to SO_4^{2-} revealing that background observation wells in the vicinity of the recharge area of the Mahomet aquifer (northern Champaign County) are losing Ca^{2+} and SO_4^{2-} to SO_4^{2-} reduction and concomitant precipitation of calcite as groundwater flows downgradient toward the western well field. In the vicinity of the production wells, calcium is probably being precipitated as a result of outgassing of CO_2.

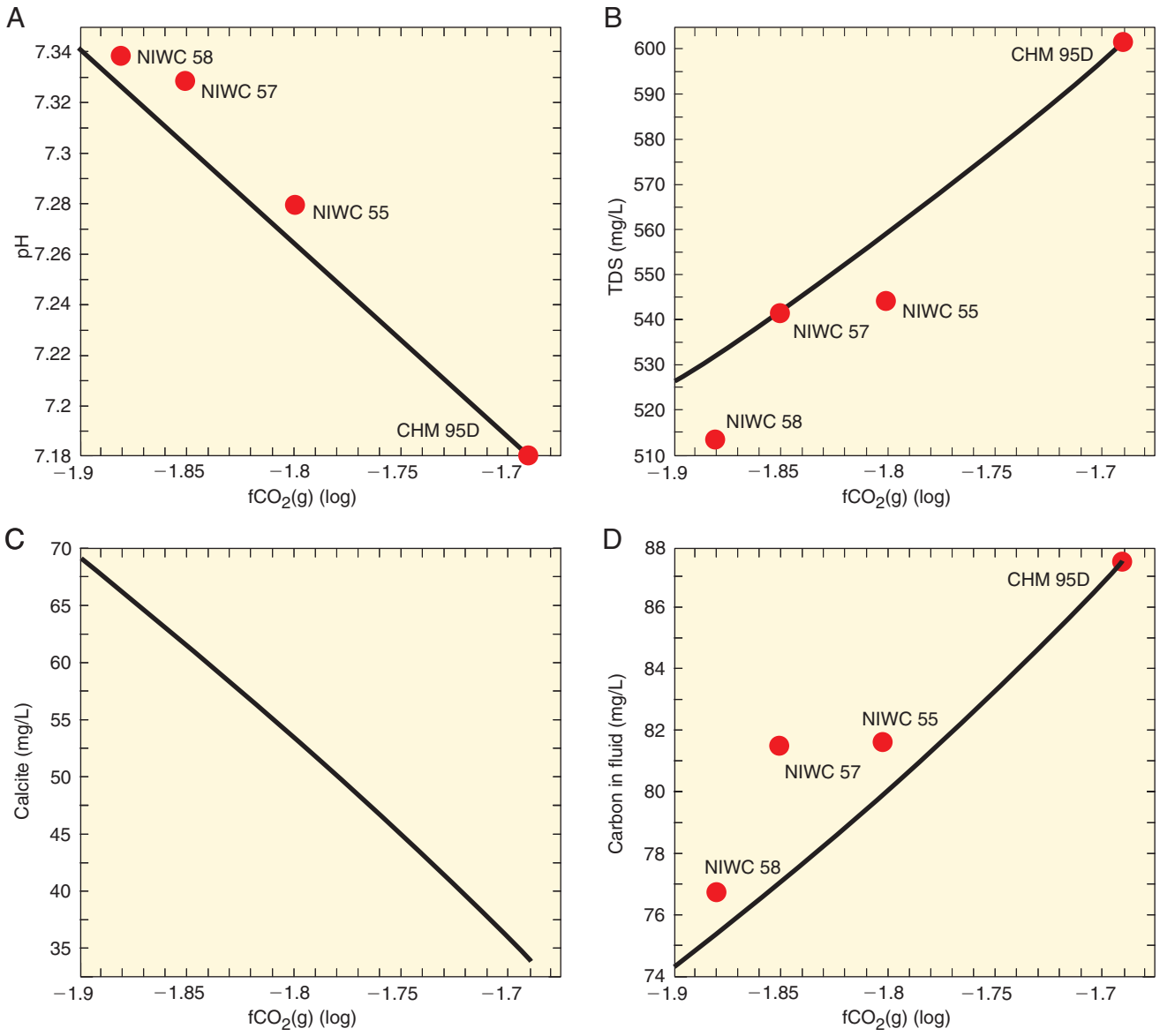

Figure 32 Geochemical modeling results and observed results using groundwater data from observation well CHM 95D. For this model, dolomite, strontianite, and witherite were not allowed to precipitate, and equilibrium values for groundwater samples are shown. The observed loss of CO_2 fugacity (fCO_2) from reference wells to western well field wells corresponds with these observed results: (A) pH increased 0.1 to 0.16 pH units (the model predicted an increase of 0.08 to 0.15 pH units); (B) a loss of 56 to 86 mg/L total dissolved solids (prediction, 42 to 68 mg of TDS/L); (C) precipitation of about 30 mg of calcite/L; and (D) a loss of 5.5 to 10.7 mg/L carbon (prediction, 7.5 to 12 mg/L), strongly suggesting the occurrence of outgassing and calcite precipitation within the Mahomet aquifer in proximity to the western well field. "NIWC" indicate production wells of the IL-AWC; "CHM" indicate lightly pumped observation wells drilled by Illinois State Water Survey. The diagrams were generated using The Geochemist's Workbench® (Bethke 1996).

^{14}C activity expected for the cement if it were recently precipitated would be approximately 8 pmc for the bulk sample, assuming 35% porosity. The much lower ^{14}C activity of the cement indicates that it was precipitated sometime between 1.6 million years B.P. (the beginning of the Pleistocene Epoch) and tens of thousands of radiocarbon years B.P., and not as a result of pumping activities in the western well field.

The SEM images from the Teflon filters provided more conclusive evidence for precipitation of calcite. The calcite euhedral crystals filtered from the water discharging from well NIWC 55 were clear evidence that calcite was precipitating within the aquifer and/or gravel pack of the production wells. These crystals were probably most visible in the filtered material from well NIWC 55 because of the paucity of other detrital materials and bacterial matter relative to the other two production wells sampled.

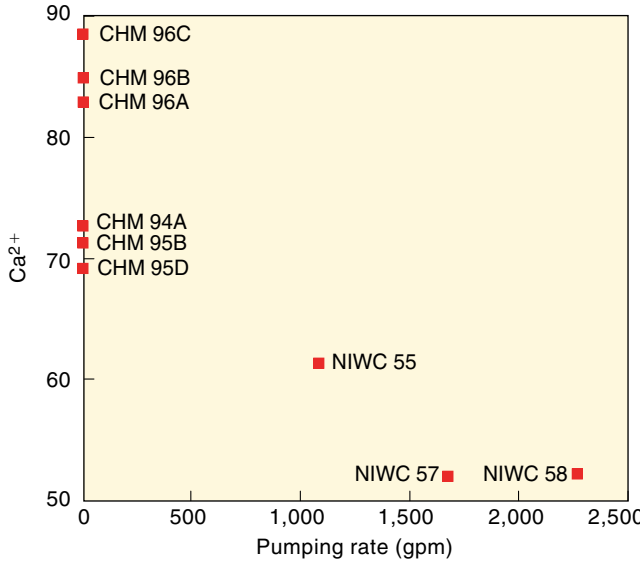

Figure 33 Effect of pumping rate on concentration of Ca^{2+} in groundwater samples collected from three production wells in the western field and six observation wells elsewhere in the Mahomet aquifer (data from Mehnert et al. 1999). CHM, lightly pumped observation wells drilled by the Illinois State Water Survey; NIWC, production wells of the IL-AWC. Greater Ca^{2+} concentrations in wells CHM 96A, CHM 96B, and CHM 96C are, in part, related to greater SO_4^{2-} concentrations in these wells (table A2).

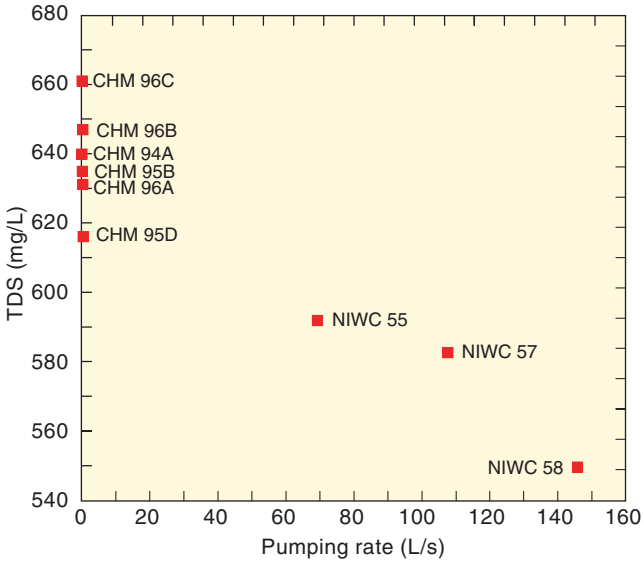

Figure 34 Variation in total dissolved solids (TDS) with an increase in pumping rate is thought to reflect the precipitation of calcite and other minerals within the aquifer surrounding the three IL-AWC production wells relative to six observation wells located elsewhere in the Mahomet aquifer (data from Mehnert et al. 1999). CHM, lightly pumped observation wells drilled by ISWS; NIWC, production wells of the IL-AWC.

The relatively large calcite fragment found on the filter from NIWC 55 shows evidence of dissolution and reprecipitation and suggests that some of these crystals have been present in the aquifer and/or gravel pack longer than the time required to travel up the borehole from the well screens (approximately 1 minute or less).

Because the calcite saturation indices of groundwater samples from the three production wells were only about 0.25 (Mehnert et al. 1999), the kinetics of calcite precipitation would be sluggish (Appelo and Postma 1994). However, the agitation of the groundwater close to the production wells caused by the higher velocities and lower pressure within the gravel pack and adjacent aquifer could facilitate the release of CO_2 and help overcome the kinetics problem. For example, Herman and Lorah (1988) used geochemical modeling to predict the precipitation of calcite along a karst stream. They found that calcite precipitated at waterfalls at a rate much greater than that predicted by their stream model. Even though the flow regime of the groundwater near the well is not altogether comparable with that of a waterfall, the increase in the energy of the flow systems in both cases causes agitation and CO_2 outgassing from the water. Carbon dioxide outgassing and concomitant encrustation of water well screens are common problems in many wells (Mogg 1971, Bruce 1976, Johnson Division 1982) and was suggested by Mehnert et al. (1999) as a possible reason for the loss of specific capacity of wells in the NIWC western well field. Calcite encrustation of well screens has been cited many times in the literature, but only the Johnson Division (1982) source mentioned the precipitation of carbonate minerals within the aquifer itself. That situation involved the encrustation of a well in fractured sandstone in Lansing, Michigan. Blasting of the well resulted in samples of sandstone that revealed encrustation extending about 0.5 inches into the aquifer.

In addition to their chemical effects, pumps induce physical effects on groundwater that may be of concern. The water interacts with the pump or blades of a submersible-centrifugal pump. Such interaction can initiate outgassing and can create partial vacuums in lines that result in significant outgassing of volatile constituents in the water. Geochemical data from the analysis of water samples collected from the Illinois State Water Survey and production wells (table A2) showed that the concentrations of Ca^{2+} and TDS in the groundwater decreased as the rate of pumping increased (figs. 33 and 34). The Ca^{2+} concentrations in groundwater samples collected from the wells CHM 96, CHM 95, and CHM 94 (fig. 4) reflect the broad range of the Ca^{2+} content in the Mahomet aquifer in Champaign County.

Transport of the Fine Fraction of Minerals

Core Samples Agglomeration of the fine fraction (<325 mesh or <44 μm) within the samples from the Mahomet and Glasford aquifers was apparent under binocular and petro-

graphic microscopy. As stated earlier, the mineral composition of the fine fraction included clay minerals (illite, kaolinite, and chlorite), dolomite, quartz, and feldspar. Because clay minerals in the fines were enriched in the samples collected from borehole NIWC 57-1 compared with those in samples collected from NIWC 57-2 and because of the abundance of fine-grained mineral fragments collected on the filters, as shown by SEM analyses (figs. 14 to 17), we concluded that groundwater flowing toward the pumping well was transporting very fine-grained minerals toward the well screens. These clay minerals could play a role in the reduction of specific capacity of well NIWC 57 (and other production wells) by combining with iron-rich biofilms on the well screen and within the gravel pack to partially reduce the available porosity and reduce the hydraulic conductivity in the immediate vicinity of the well.

The cessation of pumping probably resulted in at least temporary deposition of these fine-grained materials (including clay minerals, viruses, and bacteria particles in the size range of 20 μm to 5 μm) in the vicinity of the production well. The transport of fine-grained materials through porous media is well known (Domenico and Schwartz 1990). McDowell-Boyer et al. (1986) found that the accumulation of a small volume of fine particles was capable of significantly reducing the permeability of a porous medium by occluding the pore spaces.

As stated earlier, the gravel pack of well NIWC 57 may have been too coarse for the particle size distribution of the adjacent aquifer. If this is the case, fines from the aquifer could have migrated into the gravel pack and become trapped in pore spaces. Unfortunately, it was not possible to determine from the available data if this actually happened at well NIWC 57.

Bacteria and Biofilm Formation

According to Rittman (1993), a reduction in porosity within the aquifer could occur as a result of the accumulation of biological materials through their growth, decomposition, decay, and detachment. Because biofilm-forming bacteria were detected in groundwater samples collected from well NIWC 57 (Mehnert et al. 1999), biofilm accumulation could have reduced the porosity within the Mahomet aquifer near the production wells and in the gravel pack and well screen of the wells.

In general, symptoms of the biofilm formation on well screens may include a gradual reduction in the volume of groundwater discharged from the well over a given period, an increase in the drawdown of the well for the same pumping rate (unrelated to changes in the piezometric surface), cloudiness or coloring of the water, and/or objectionable taste and odor in the water. The increase in drawdown or decrease in specific capacity results from the reduction of hydraulic conductivity of the gravel pack and possibly the aquifer adjacent to the well, which results in a decreased rate of flow for groundwater moving from the aquifer through the gravel pack and into the well. The formation and effect of biofilms on well screens was summarized by Alford and Cullimore (1999) as follows:

> Biofilms form on and near a well screen, and begin to coalesce into a slimy glutinous mass. As the glutinous mass grows, it reduces the size of the openings of a well screen and begins to interfere with groundwater entering the screen. As more material accumulates within the mass, it increasingly restricts the flow of groundwater. "Sudden plugging" (complete occlusion of the well screen) may occur when the well is at 20 to 60% of its original specific capacity.

The paucity of bacteria within the Mahomet aquifer and the lack of visible biofilms or precipitation of iron oxyhydroxide within the aquifer samples suggested that bacteria do significantly reduce hydraulic conductivity within the aquifer itself. However, it is likely that iron-depositing bacteria are indigenous to the Mahomet aquifer (e.g., Chapelle 1993), and wells within the aquifer have the potential for iron-depositing bacteria to colonize the well screens.

The bacterially generated deposits of iron oxyhydroxide filtered from groundwater during pumping of well NIWC 57 are examples of what is probably being deposited within the gravel pack and on the well screens of other production wells that have exhibited significant reductions in specific capacity. Iron-related bacteria also were observed within the aquifers and associated deposits overlying the Mahomet aquifer.

Wedron Aquifer The concentration of bacteria within the shallow Wedron aquifer at 30 to 40 feet (graphic logs for NIWC 57-1 and NIWC 57-2, Appendix) was relatively large in borehole NIWC 57-1, but not in NIWC 57-2 (tables 7 and 8). The bacteria present consisted of *Staphylococcus faecium*, *Klebsiella pneumoniae,* and *Bacillus* spp. The presence of fecal streptococci within this shallow aquifer intersected by NIWC 57-1 suggested that recharge rain and snowmelt had been contaminated by soil and animal waste. However, the contamination does not appear to be aquifer-wide. In borehole NIWC 57-2, bacterial contamination was found within the glacial till underlying the shallow aquifer that was similar to that found in NIWC 57-1, but without fecal streptococci. This result was not surprising given that fecal streptococci do not live long outside of the host animal (Geldreich 1996). The *Aspergillus fumigatus* found in NIWC 57-1 is commonly found on damp organic materials and is ubiquitous at land surface (Freeman 1985). The occurrence of this fungus in the till was likely the result of the presence of organic debris (e.g., wood fragments) trapped within the glacial till since its deposition.

Glasford Aquifer Bacteria present in the Glasford aquifer included *Pseudomonas* spp., *Klebsiella pneumoniae,* and *Bacillus* spp. Concentrations were greatest in borehole NIWC 57-1, suggesting that these bacteria could have been introduced during the drill-

ing of well NIWC 57 (e.g., by the use of contaminated drilling fluids that flowed into the aquifer). Relatively high concentrations of bacteria and of organic material within the drill core were correlated. For example, organic-rich layers and pieces of wood were found in the NIWC 57-1 drill core at 168.5 feet within the Glasford aquifer where total aerobic bacteria concentrations ranged from 130 to 3,700 cfu (table 7). The bacteria at this depth could have been introduced during drilling operations or could have been present since deposition of the unit.

Mahomet Aquifer Bacteria were detected in the Mahomet aquifer at a depth of 250 feet and 300 feet in borehole NIWC 57-1 (table 7). The isolated nature of these bacteria suggested that they might have been introduced during our drilling and sampling efforts or were isolated occurrences. Borehole NIWC 57-2 has a 20-foot section that contained over 5,000 cfu of iron-reducing bacteria (table 8). This location was also the site of what appeared to be a gray film on the sand and gravel of the drill core during sampling. The "film" was later determined to be an accumulation of dolomite-enriched fines. The origin of the fines is not known and was beyond the scope of this investigation.

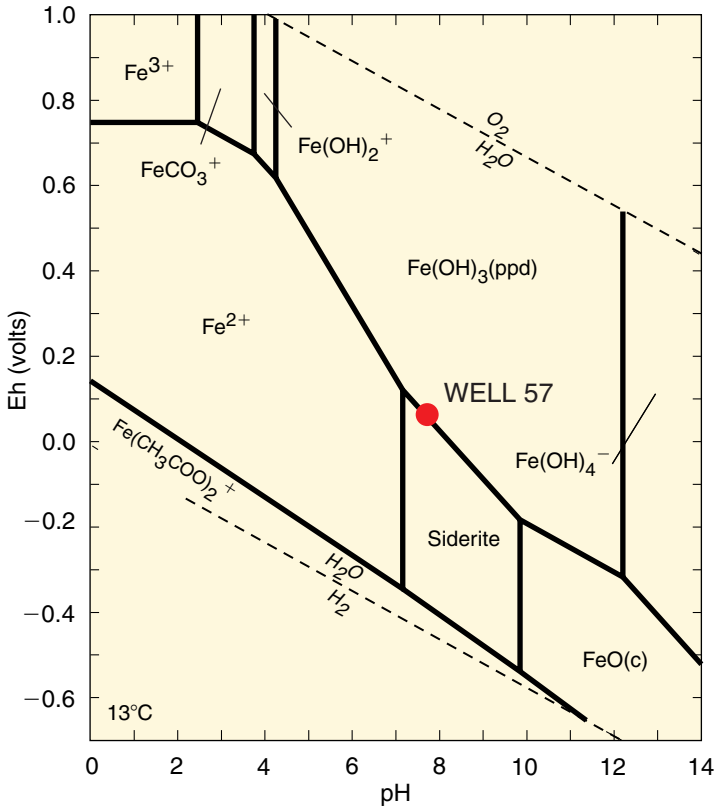

Figure 35 Redox potential (Eh)-pH activity diagram showing the stability fields for some dissolved and solid forms of iron. The Eh-pH of the groundwater sample collected from well NIWC 57 plots near the intersection of the ferrous iron, siderite, and iron oxyhydroxide stability fields. (ppd), precipitated; (c), crystalline. The diagram was generated using The Geochemist's Workbench® (Bethke 1996).

Given the groundwater chemistry and conditions in the vicinity of the production well, the precipitation of iron oxyhydroxide from the groundwater near the production wells is likely. Iron concentrations in groundwater collected from production wells (present as Fe^{2+}) ranged from 0.91 to 1.31 mg/L (table A2; Mehnert et al. 1999). Figure 35 shows the solid and dissolved forms of iron under various pH and redox potential (Eh) conditions. For the groundwater sample collected from well NIWC 57, values fell on the boundary between iron oxyhydroxide ($Fe(OH)_3$) and siderite ($FeCO_3$). The sample was also close to the boundary for ferrous iron (Fe^{2+}). A small shift in Eh, which can be caused by an influx of O_2 or a shift in pH from the outgassing of CO_2, can cause precipitation of solids. Thus, the geochemistry of the groundwater sample from well NIWC 57 shows that stable iron oxyhydroxide and siderite could have formed. Other evidence indicates that iron-rich solids apparently have precipitated on the well screens, albeit through biologically mediated reactions.

Suspended Solids The analyses of groundwater samples and the collection and examination of suspended solids filtered from three production wells (NIWC 55, NIWC 57, and NIWC 58) provided the best physical evidence for the composition of the materials that encrusted the well screens. The iron-enriched tubercles and cells found on the filters (figs. 23 to 28) suggested the presence of iron-depositing bacteria at or near the well screens and perhaps within the gravel pack. The reddish orange color of the filters from wells NIWC 57 and NIWC 58 and the abundance of bacteria filaments and spores on the filters from the three production wells sampled suggested that there was active, biologically mediated precipitation of iron oxyhydroxide within the wells. The possible bacteria responsible for clogging the well screens included the filamentous *Leptothrix, Crenothrix, Sphaerothilus,* and *Gallionella* spp., which are all common iron-depositing bacteria that derive energy from the oxidation of ferrous iron (Geldreich 1996, Atlas and Bartha 1997). The twisted stalks (fig. 24) and sheaths (fig. 25) are characteristic of *Gallionella* and *Leptothrix*, respectively (Banfield et al. 2000).

Other lines of evidence supported the hypothesis that the biologically mediated precipitation of iron oxyhydroxide was taking place at the well screen. First, a downhole video camera used during rehabilitation efforts at well NIWC 57 revealed that a dark-colored coating covered the well screen. The coating had to be broken free from the well screen using small

explosive charges set against the coating. Second, surging during rehabilitation efforts brought up water colored dark brown to reddish brown (G. Juriga, IL-AWC production supervisor, personal communication 2000), which also is indicative of the activity of iron-depositing bacteria. NIWC 58 was rehabilitated in 1990, and a short report on a downhole-camera video of the well describes the well screen as "heavily incrusted" and that "red scale" was removed from the well during the operation.

Ideal growth conditions for iron-depositing bacteria include the presence of Fe^{2+} (an energy source), O_2 (an electron acceptor), and pH 6 to 7.5 (Ghiorse and Wilson 1988). Because of the need for the simultaneous occurrence of reduced iron and the presence of O_2 (at redox transition zones), the conditions found at a well screen are most favorable for the growth of *Gallionella ferruginea* and other iron-depositing bacteria. *Gallionella ferruginea* is an obligate aerobe that survives by oxidizing dissolved ferrous iron to ferric iron (Chapelle 1993).

Bacteria such as *Gallionella ferruginea* have a two-phase life cycle. The first is a motile phase during which the cells move around (fig. 25) and grow exponentially. During the second phase, resulting from changing environmental conditions, the bacterium produces abundant stalks and attaches to surfaces (Hallbeck and Pedersen 1987). Because of its environmental needs, the bacteria must live where aerobic water mixes with anaerobic water such as on well screens. The iron-depositing *Gallionella ferruginea* produces a sheath that commonly is responsible for the clogging of well screens (Chapelle 1993).

Because of the reducing conditions that predominate in this part of the Mahomet aquifer and the lack of large concentrations of ions that could serve as sources of oxygen (e.g., NO_3^-) in the groundwater, it is not clear where the bacteria obtain their oxygen. Specifically, iron-depositing bacteria obtain energy to grow by converting Fe^{2+} to Fe^{3+} through the reaction

$$4Fe^{2+} + 4H^+ + O_2 \rightarrow 4Fe^{3+} + 2H_2O.$$

The presence of iron-depositing bacteria and the apparent buildup of biogenic well scale on the screens from two production wells indicate that the bacteria are obtaining oxygen from some source. Air could travel through vents from the surface to well casings. The drawdown and agitation of the water during pumping could provide the opportunity for air to be transported into the groundwater in the wells. When the production wells shut off, an anti-siphon valve opens at the well head and water flows rapidly back into the well, which could entrain atmospheric O_2. When the wells are not in production, which can be several months per year, atmospheric O_2 may diffuse into the water column within the wells and provide O_2 for iron-depositing bacteria to grow on the inside and outside of the well screens and possibly within the gravel pack. Any particular well may be turned on and off several times during the year. Borch et al. (1993) state that cyclical pumping and prolonged idleness can increase biofilm volume and plugging.

Nonvolatile organic carbon was present in all three of the production wells sampled and may have acted as a food source for bacterial growth (Appelo and Postma 1994). Concentrations of dissolved organic carbon in NIWC 55, NIWC 57, and NIWC 58 are 2.0, 3.5, and 2.7 mg/L, respectively (Mehnert et al. 1999; table A2).

The study results suggest that there is a pumping-rate–related accumulation of biofilms of iron-depositing bacteria, detrital minerals, and authigenic calcite crystals on the well screen and possibly within the gravel pack. This accumulation could explain the observed progressive decrease in specific capacity of the production wells. The SEM evidence suggested that the mineral matter was agglomerated by the bacteria on and around the well screen. Costerton (1987) found that biofilm-forming colonies of bacteria in subaqueous environments initially attach to a surface such as a well screen and form their gelatinous biofilm (exopolysaccharide glycocalyxes). This gelatinous surface, with time, is capable of trapping detrital materials that flow past it. Costerton (1987) found that some biofilms can be up to 97% clay and detritus. In our present investigation, pumping rates appeared to be related to the particle size and quantity of mineral and bacterial matter trapped on the filters; that is, the greater the pumping rate of the wells, the more bacteria and mineral matter were collected on filter media through which equal quantities of groundwater had passed. Because of the paucity of O_2 sources within the aquifer, we suspect that the amount of bacteria present in the three production wells examined is related to the amount of agitation and air mixed with the water during pumping and during well shutdowns. Furthermore, the influx of nonvolatile organic carbon on which the bacteria could be feeding may have played a role in their growth. Mineral matter transported by high pumping rates and the agglomeration of the transported materials by bacteria and their biofilms are probably the primary reasons for the loss of specific capacity of the production wells. We emphasize that our suggestions of possible source(s) of oxygen for the growth of these bacteria are speculative. Further exploration of this issue by experimental means was beyond the scope of our investigation.

Chemical Treatment of IL-AWC Wells

It is important to examine the types of chemicals that are used for well rehabilitation. Depending on the nature of the problem encountered at the well screens, chemical treatment may mitigate or exacerbate the problem. For example, according to IL-AWC records, a blend of chemicals was used to rehabilitate well NIWC 57, including Calgon (sodium hexametaphosphate), soda ash (sodium carbonate), high-test hypochlorite or calcium hypochlorite, and Santomerse (alkyl aryl sulfonate). Although high-test hypochlorite may help inhibit bacterial growth, Calgon could potentially leave behind phosphate in the well, which could act as food for the bacteria. Thus, products containing phosphate are not recommended for rehabilitating wells (Layne Western, personal commu-

nication 1999; George Alford, Alford Inc., personal communication 2000). Considering that the precipitation of carbonate minerals may also have occurred at the well screens, adding soda ash, which contains carbonate and sodium, may exacerbate the problem of carbonate mineral precipitation by adding carbonate ions. Thus, some of the chemicals added may have had a detrimental effect on the problems of well-screen scale buildup.

Conclusions

For over 30 years, most of the IL-AWC production wells screened in the Mahomet aquifer have experienced progressive loss of specific capacity. A preliminary study of three of the wells suggested that encrustation of calcite at the well screens could be related to the loss. Our study tested this hypothesis and other possible scenarios. Core samples from two boreholes drilled 15 and 60 feet from production well NIWC 57 were collected using minimally disruptive rotasonic drilling techniques. Carbon-14 dating of calcite cement nodules found in the borehole closest to NIWC 57 showed that the nodules formed more than 45,000 years ago and were unrelated to well operations.

Thin section and XRD revealed fines and clay enrichment of samples obtained from the borehole adjacent to NIWC 57. We theorized that the abundance of fines and clay minerals were drawn toward the well during pumping operations.

Bacterial analysis of core samples from wells NIWC 57-1 and NIWC 57-2 revealed the presence of aerobic and iron-depositing bacteria within samples from the aquifers. Soil bacteria were found in samples from two of the wells, and iron-related and sulfate-reducing bacteria were found in all three wells. The SEM analysis of materials caught on filters from the three production wells showed the presence of bacteria-related iron deposits and bacterial biofilms. These materials were directly related to well pumping rates. The presence of euhedral crystals of calcite suggests that there may be calcite precipitation near the wells. Chemical analyses showed decreases in TDS and other constituants for groundwater samples within the well field compared with results for monitoring wells further away. Geochemical equilibrium modeling accurately predicted the observed changes in pH, TDS, Ca^{2+}, and carbon concentrations for the production wells.

Geochemical, XRD, SEM, and bacterial analyses indicated that the progressive loss of specific capacity of well NIWC 57 (and probably other wells in the IL-AWC western well field) directly resulted from iron oxyhydroxides due to bacterial activity and the migration and co-accumulation of suspended matter (including authigenic calcite from CO_2 outgassing and fine, detrital mineral fragments) on well screens and probably in the oversized gravel pack surrounding the well screens.

Recommendations for Additional Research

Water company owners could take a number of actions to further investigate the causes for the loss of specific capacity of their production wells. Inspection of the well screens with a downhole camera would quickly indicate whether the screens were being encrusted.

The collection and analysis of any encrustation on the well screens (by techniques described herein) could provide invaluable information as to the nature of the problem. This information also could be used to identify appropriate, commercially available remediation techniques. In addition, water companies could use available information in their records

1. To determine whether the pumping rate is directly related to the loss of specific capacity, as suggested by the results of this investigation, and data from records from the IL-AWC and other water companies with high-capacity wells in confined aquifers
2. To identify the optimum pumping rates to minimize loss of specific capacity, if it is confirmed that the pumping rate is directly related to specific capacity loss
3. To determine how oxygen is reaching the well screens (e.g., as a function of well construction and/or the effects of shutting off the well for extended periods), by examining records of changes in specific capacity and down time and differences in the construction for production wells
4. To determine which well-construction techniques minimize exposure to atmospheric oxygen, and/or adjust pumping schedules to minimize down time for wells if oxygen is reaching the well screens because of well construction and/or down time.

Collecting these types of information would help operators understand the causes for decreases in specific capacity and help them determine the steps to be taken to help resolve the problem.

Acknowledgments

This research was supported, in part, by the Illinois-American Water Company. We thank Mark Johnson who served as project manager, Brian Good, and others at the Illinois-American Water Company for allowing us access to their property and wells. We thank Ellen Storment of the U.S. Department of Agriculture, Animal Disease Laboratory, for conducting the analysis of bacteria samples and assisting in the interpretation of the data. Randall Hughes, Philip DeMaris, and Herbert Glass identified the mineralogy of drill core samples by XRD and assisted with interpretation of the data. Ardith Hansel, Philip DeMaris, Christopher Stohr, Jack Liu, Sallie Greenberg, and Pius Weibel helped us log and sample the core. We also thank, from the Illinois State Water Survey, Steve Burch for assisting with the response test and Jim Angel for providing atmospheric pressure data. This report was greatly improved by the critical reviews of Jon Goodwin and Beverly Herzog and their insightful suggestions. Photographs are by S.V. Panno.

References

Alford, G., and R. Cullimore, 1999, The application of heat and chemicals in the control of biofouling events in wells: New York, Lewis Publishers, 181 p.

Appelo, C.A.J., and D. Postma, 1994, Geochemistry, groundwater and pollution: Rotterdam, A.A. Balkema Publishers, 536 p.

Atlas, R.M., and R. Bartha, 1997, Microbial ecology—Fundamentals and applications: Reading, Massachusetts, Addison Wesley Longman, Inc., 694 p.

Banfield, J.F., S.A. Welch, H. Zhang, T.T. Ebert, and R.L. Penn, 2000, Aggregation-based crystal growth and microstructure development in natural iron oxyhydroxide biomineralization products: Science, v. 289, p. 751–754.

Barrow, J.C., 1994, The resonant sonic drilling method—An innovative technology for environmental restoration programs: Ground Water Monitoring Review, v. 14, p. 153–160.

Bethke, C.M., 1996, Geochemical reaction modeling—Concepts and applications: New York, Oxford University Press, 397 p.

Borch, M.A., S.A. Smith, and L.N. Noble, 1993, Evaluation and restoration of water supply wells: Denver, Colorado, American Water Works Association Research Foundation and American Water Works Association, 272 p.

Bruce, R., 1976, Encrustation: Water Well Journal, no. 8, p. 27.

Buelow, R.W., and G. Walton, 1971, Bacteriological quality vs. residual chlorine: Journal of American Water Works Association, v. 62, p. 28–35.

Catania, C.L., and F.J. Getchell, 1997, Second chance for wells: Water Technology, v. 20, p. 86–88.

Chapelle, F.H., 1993, Ground-water microbiology and geochemistry: New York, John Wiley and Sons, Inc., 424 p.

Clark, I.D., and P. Fritz, 1997, Environmental isotopes in hydrogeology: New York, Lewis Publishers, 328 p.

Clesceri, L.S., A.E. Greenburg, and R.R. Trussel, 1989, Standard methods for the examination of water and wastewater (17th ed.): Washington D.C., American Public Health Association, Part 9000, p. 9-1 to 9-280.

Coleman, D.D., 1976, Isotopic characterization of Illinois natural gas: Urbana-Champaign, Illinois, University of Illinois, Ph.D. dissertation, p. 175.

Costerton, J.W., 1987, Electron microscope studies of biofilm, *in* E.R. Cullimore, ed.: Proceedings of the International Symposium on Biofouled Aquifers—Prevention and Restoration: Bethesda, Maryland, American Water Resources Association, November 1986, p. 169.

Domenico, P.A., and F.W. Schwartz, 1990, Physical and chemical hydrogeology: New York, John Wiley and Sons, Inc., 824 p.

Driscoll, F.G., 1986, Groundwater and wells (2nd ed.): St. Paul, Minnesota, Johnson Division, 1089 p.

Droycon Bioconcepts Inc., 1996, Users quality control manual in support of the BART Biodetection Technologies: Regina, Saskatchewan, Canada, Droycon Bioconcepts Inc.

Fouke, B.W., and J. Rakovan, 2001, An integrated cathodoluminescence video-capture microsampling system: Journal of Sedimentary Research, v. 71, no. 3, p. 509–513.

Freeman, B.A., 1985, Burrows textbook of microbiology (22nd ed.): Philadelphia, Pennsylvania, W.B. Saunders Co., 1038 p.

Geldreich, E.E., 1996, Microbial quality of water supply in distribution systems: New York, Lewis Publishers, 504 p.

Ghiorse, W.C., and J.L. Wilson, 1988, Microbial ecology of the terrestrial subsurface: Advances in Applied Microbiology, v. 33, p. 107–172.

Hackley, K.C., 2002, A chemical and isotopic investigation of the groundwater in the Mahomet Bedrock Valley aquifer— Age, recharge and geochemical evolution of the groundwater: Urbana-Champaign, University of Illinois, Department of Geology, Ph.D. dissertation, 152 p.

Hallbeck, E.-L., and K. Pedersen, 1987, The biology of *Gallionella, in* E.R. Cullimore, ed.: Proceedings of the International Symposium on Biofouled Aquifers—Prevention and Restoration: Atlanta, Georgia, American Water Resources Association, November 1986, p. 87–95.

Herman, J.S., and M.M. Lorah, 1988, Calcite precipitation rates in the field—Measurement and prediction for a travertine-depositing stream: Geochimica et Cosmochimica Acta, v. 52, p. 2347–2355.

Horberg, L, 1953, Pleistocene deposits below the Wisconsin drift in northeastern Illinois: Illinois State Geological Survey, Report of Investigations 165, 61 p.

Hubbard, Jr., D.A., and J.S. Herman, 1991, Travertine-marl—The "doughnut-hole" of karst, *in* E.H Kastning and K.M. Kastning, eds.: Proceedings of the Appalachian Karst Symposium, Radford, Virginia, March 23–26, p. 59–64.

Johnson Division, 1982, Ground water and wells—A reference book for the water-well industry: St. Paul, Minnesota, Johnson Division, UOP Inc., 440 p.

Kempton, J.P., W.H. Johnson, P.C. Heigold, and K. Cartwright, 1991, Mahomet bedrock valley in east-central Illinois; Topography, glacial drift stratigraphy and hydrogeology, *in* W.N. Melhorn and J.P. Kempton, eds., Geology and hydrogeology of the Teays-Mahomet Bedrock Valley system: Boulder, Colorado, Geological Society of America, Special Paper 258, p. 91–124.

Kempton, J.P., W.J. Morse, and A.P. Visocky, 1982, Hydrogeologic evaluation of sand and gravel aquifers for municipal groundwater sup-

plies in east-central Illinois: Illinois State Geological Survey and Illinois State Water Survey, Cooperative Groundwater Report 8, 59 p.

Little, B.J., P.A. Wagner, and Z. Lewandowski, 1997, Spatial relationships between bacteria and mineral surfaces, *in* J.F. Banfield and K.H. Nealson, eds., Geomicrobiology— Interactions between microbes and minerals: Washington, D.C., Mineralogical Society of America, p. 123–159.

Machel, H.G., and E.A. Burton, 1991, Factors governing cathodoluminescence in calcite and dolomite, and their implications for studies of carbonate diagenesis, *in* C.E. Barker and O.C. Kopp, eds., Luminescence microscopy— Quantitative and qualitative aspects: Tulsa, Oklahoma, SEPM, p. 37–57.

Manos, C., 1961, Petrography of the Teays-Mahomet Valley deposits: Journal of Sedimentary Petrology, v. 31, p. 456–466.

McDowell-Boyer, L.M., J.R. Hunt, and N. Sitar, 1986, Particle transport through porous media: Water Resources Research, v. 22. p. 1901–1921.

Mehnert, E., K.C. Hackley, D.R. Larson, and S.V. Panno, 1999, The role of hydraulic, chemical, and biological factors in the decline of specific capacity in the western Champaign well field: A preliminary investigation: Illinois State Geological Survey, Open File Series 1999-5, 48 p.

Melhorn, W.N., and J.P. Kempton, eds., 1991a, Geology and hydrogeology of the Teays-Mahomet Bedrock Valley system: Boulder, Colorado, Geological Society of America, Special Paper 258, 128 p.

Melhorn, W.N., and J.P. Kempton, 1991b, The Teays system— A summary, *in* W.N. Melhorn and J.P. Kempton, eds., Geology and Hydrogeology of the Teays-Mahomet Bedrock Valley System: Boulder, Colorado, Geological Society of America, Special Paper 258, p. 125–128.

Mogg, J.L., 1971, What experience teaches us about incrustation: The Johnson Drillers Journal, May–June, p. 3–4.

Noakes J.E., S.M. Kim, and L.K. Akers, 1967, Recent improvements in benzene chemistry for radiocarbon dating: Geochimica et Cosmo Chimica Acta 13, p. 1094–1096.

Noakes J.E., S.M. Kim, and J.J. Stipp, 1965, Chemical and counting advances in liquid scintillation radiocarbon dating, *in* 6th International Conference on Radiocarbon and Tritium Dating Proceedings, Conference-650652: Washington, D.C., U.S. Atomic Energy Commission, p. 68–98.

Panno, S.V., K.C. Hackley, K. Cartwright, and C.-L. Liu, 1994, Hydrochemistry of the Mahomet Bedrock Valley aquifer, east-central Illinois—Indicators of recharge and ground-water flow: Groundwater, v. 32, p. 591–604.

Panno, S.V., W.R. Kelly, K.C. Hackley, and H.H. Hwang, 1999, Sources of nitrate contamination in karst springs using isotopic, chemical, and bacterial indicators—Preliminary results, *in* Proceedings of the Ninth Annual Conference–Research on Agricultural Chemicals in Illinois Groundwater, Makanda, Illinois, April 1999, p. 91–103.

Pfaff, J.D., 1993, Method 300.0— Determination of inorganic anions in water by ion chromatography, Revision 2.1: Cincinnati, Ohio, U.S. Environmental Protection Agency, 30 p.

Ramsey, C.B., and R.E.M. Hedges, 1997, Hybrid ion sources— Radiocarbon measurements from microgram to milligram: Nuclear Instruments and Methods in Physics Research, v. 123, p. 539–551.

Rittmann, B.E, 1993, The significance of biofilms in porous media: Water Resources Research, v. 29, p. 2195–2202.

Visocky, A.P., and R.J. Schicht, 1969, Groundwater resources of the buried Mahomet Bedrock Valley: Illinois State Water Survey, Report of Investigations 62, 52 p.

Willman, H.B., and J.C. Frye, 1970, Pleistocene stratigraphy of Illinois: Illinois State Geological Survey, Bulletin 94, 204 p.

Wood, W.W., 1981, Chapter D2— Guidelines for collection and field analysis of ground-water samples for selected unstable constituents—Techniques of water-resources investigations of the U.S. Geological Survey, Reston, Virginia, U.S. Geological Survey, Book 1, Chapter D2, 24 p.

Appendix

Detailed Descriptive Log for Borehole NIWC 57-1

Illinois State Geological Survey
NIWC 57-1

Location: Champaign County, SW ¼, SW ¼, SE ¼, Section 3, T19N, R08E
Elevation: 750 ft (msl)
Total depth: 333 ft
Date started: 7/12/99
Drilling method: Rotasonic by Boart Longyear
Location: North side of well house
Core descriptions: David R. Larson and Ardith K. Hansel
Geophysical logs: Natural gamma run inside 2-inch schedule 80 PVC to depth of only 135 ft
Comments: Water level in drill stem at depth 35 ft was 16.2 ft below land surface (elevation = 733.8 ft)

Depth (ft)	Thickness (ft)	Description
0.0–3.3	3.3	Silt, dark brown (10YR 3/3), moderately clayey, noncalcareous; topsoil
3.3–5.0	1.7	Silt, dark yellowish brown (10YR 3/6), loose to blocky texture, noncalcareous; occasional dark brown streaks that are moist
		Wedron Group
5.0–10.0	5.0	Clay, light olive-brown (2.5Y 5/4), very silty to clayey silt, sandy with pebbles; slightly stiff, moderately sticky, slightly calcareous; some olive-brown (2.5Y 4/4) mottles and inclusions
10.0–11.0	1.0	Clay, as above, with some dark gray (2.5Y 4/1) mottles
11.0–27.5	16.5	Clay, dark gray (2.5Y 4/1), moderately silty, slightly to moderately sandy and pebbly with occasional cobbles, slightly to moderately calcareous
27.5–27.9	0.4	Sand, very fine to very coarse, mostly medium to coarse, slightly to moderately well sorted; gravelly sand at 27.0 ft
27.9–28.2	0.3	Clay, as at 10.7–27.0 ft
28.2–28.5	0.3	Sand, as at 27.0–27.9 ft
28.5–34.0	5.5	Clay, as at 11.0–27.5 ft
34.0–40.0	6.0	Sand and gravel, olive-brown to olive-gray, very fine sand to coarse gravel, mostly very coarse sand to medium gravel, poorly sorted, tends to coarsen downward; abundant subangular to subrounded quartz, shale, and carbonate grains with igneous rock fragments; slightly silty and clayey
40.0– 41.0	1.0	Sand and gravel, very fine sand to fine gravel, mostly fine to medium sand with sparse fine gravel, moderately well sorted; slightly silty; abundant subangular to subrounded shale and quartz grains with igneous rock fragments
41.0–41.9	0.9	Sand and gravel, very fine sand to coarse gravel with a few cobbles, poorly sorted; silty
41.9–76.9	35.0	Clay, dark gray (2.5Y 4/1), slightly to moderately silty, slightly to moderately sandy with very fine to very coarse sand, sparse coarse to very coarse sand; slightly to moderately pebbly with fine gravel; slightly calcareous; stiff, dense, very compact, moderately cohesive
76.9–92.0	15.1	Clay, dark grayish brown (10YR 4/2), very silty, slightly to moderately sandy and pebbly; slightly calcareous; massive, compact, dense; mottles of very dark gray (10YR 3/1) clay in upper 0.9 ft

Depth (ft)	Thickness (ft)	Description
92.0–97.0	5.0	Clay, very dark grayish brown (10YR 3/2), very silty, slightly to moderately sandy and pebbly with very fine sand to medium gravel; moderately calcareous; massive, compact, dense; very dark gray (10YR 3/1) mottles in upper 0.9 ft
97.0–99.5	2.5	Clay, dark grayish brown (10YR 4/2), very silty, slightly to moderately sandy with very fine to very coarse sand, moderately pebbly with fine to medium gravel; slightly to moderately calcareous; massive, compact, dense; occasional thin lenses of very fine to fine sand, well sorted, silty, and clayey
99.5–100.0	0.5	Clay, very dark gray (N3/) to black (N2.5/), silty
100.0–100.5	0.5	Igneous rock
100.5–109.4	8.9	Clay as at 97.0–99.5 ft; thickest sand lense (0.2 inch) is at 102.2 ft
109.4–110.3	0.9	Silt, dark grayish brown (10YR 4/2), slightly sandy with very fine to fine sand, slightly clayey; noncohesive, soft; slightly to moderately calcareous
110.3–121.5	11.2	Clay as above 97.0–99.4 ft; color gradually changes to very dark grayish brown (10YR 3/2) with depth
		Glasford Formation
121.5–126.1	4.6	Clay, very dark grayish brown (2.5Y 3/2), very silty to clayey silt; soft, slightly cohesive; moderately calcareous; a few carbonate dropstones; laminated; also some darker, organic laminations; slightly calcareous, lighter grayish brown laminations of silt and silty sand
126.1–126.6	0.5	Sand, dark gray (2.5Y 4/1), very fine to fine, well sorted; slightly silty; mostly subrounded grains; laminations of silt and sandy silt
126.6–140.0	13.4	Clay, dark gray (5Y 4/1) to very dark gray (5Y 3/1), very silty to clayey silt, slightly to moderately sandy with very fine to very coarse sand, slightly to moderately pebbly with fine gravel and occasional coarse gravel to cobbles; stiff, compact; slightly calcareous, becomes somewhat more calcareous with depth; very dark gray (5Y 3/1) undulating upper boundary
140.0–150.0	10.0	Clay, as at 126.6–140.0 ft, but somewhat softer, slightly more sandy, and less pebbly and calcareous
150.0–158.0	8.0	Sand, very fine to medium, mostly fine, well sorted; mostly subrounded to rounded quartz grains with some shale and igneous rock fragments; very slightly calcareous; coarsens downward to sand and gravel below
158.0–161.0	3.0	Sand and gravel, very fine sand to medium gravel, mostly coarse sand to fine gravel, poorly sorted to slightly well sorted; coarse fraction has abundant carbonate grains; slightly silty and clayey at 158.0–159.0 ft; slightly to moderately calcareous; shell fragments present
161.0–162.0	1.0	Sand, grayish brown overall, very silty to sandy silt; very fine to fine with some medium, well-sorted, mostly rounded quartz grains; laminated with thin layers and lenses of gray (5Y 5/1) to dark gray (5Y 4/1), moderately to very calcareous silt
162.0–163.0	1.0	Silt, gray (5Y 5/1) to dark gray (5Y 4/1), noncohesive, soft; moderately to very calcareous
163.0–179.0	16.0	Sand, very fine to fine, mostly fine, well sorted; mostly rounded quartz grains with igneous rock fragments and black shale; slightly calcareous; 0.2 ft thick, black organic-rich layer with wood fibers at 168.5 ft; 0.3-ft-thick layer of gray silt at 168.0 ft; sparse fine gravel at 169.0–171.0 ft
179.0–180.0	1.0	Sand and gravel, very fine sand to medium gravel, mostly fine to coarse sand with rare medium gravel, poorly sorted to slightly well sorted; abundant rounded quartz grains with subangular to subrounded shale and carbonate grains common
180.0–188.0	8.0	Sand and gravel, very fine sand to medium gravel, mostly very fine to medium sand, some coarse to very coarse sand, and rare fine to medium gravel, moderately well sorted to well sorted; abundant subrounded to rounded quartz grains with shale, igneous rock fragments, and carbonates common; coarsens downward with coarse sand to medium gravel more prevalent, slightly to moderately well sorted to poorly sorted near 188.3 ft

Depth (ft)	Thickness (ft)	Description
188.0–190.0	2.0	Sand and gravel, very fine sand to coarse gravel, mostly coarse sand to fine gravel; very clayey to very sandy and pebbly clay; moderately calcareous
190.0–191.0	1.0	Sand, olive-brown overall, very fine to fine, well sorted; mostly rounded quartz grains
191.0–197.0	6.0	Sand and gravel as above 188.0–190.0 ft, but very fine to medium sand more common below 196.6 ft
		Banner Formation
197.0–201.0	4.0	Silt, gray (2.5Y 5/1), slightly clayey, soft, noncohesive; slightly to moderately calcareous, occasional black organic flecks; 0.3 ft layer of very dark grayish brown (2.5Y 3/2), calcareous, very clayey silt to silty clay at 199.0 ft; laminated below 199.0 ft with silt and clayey silt/silty clay
201.0–205.0	4.0	Clay, dark gray (2.5Y 4/1), very silty to clayey silt; slightly to moderately sandy with very fine to very coarse sand, slightly to moderately pebbly with fine to medium gravel that is mostly carbonate and shale; dense, compact, noncohesive; calcareous
205.0–224.0	19.0	Clay, dark grayish brown (2.5Y 4/2) to very dark grayish brown (2.5Y 3/2), very silty to clayey silt; slightly sandy with very fine to very coarse sand, slightly pebbly with fine to medium gravel; dense, compact, noncohesive, blocky to platy texture; slightly to moderately calcareous; occasional thin layers of sand, very fine to very coarse, mostly medium to coarse, slightly well sorted; abundant rounded quartz grains; thin saturated silty clay layers at 216.0 ft and 217.0 ft
		Mahomet Sand Member
224.0–225.0	1.0	Sand, olive-gray overall, very fine to very coarse sand with occasional fine gravel, mostly fine to medium sand, moderately well sorted; mostly subrounded to rounded quartz grains with shale grains; some very thin layers of silt at 224.9–225.0 ft
225.0–226.2	1.2	Sand, olive-brown overall, very fine to very coarse sand with rare fine gravel, mostly fine to medium sand, moderately well sorted to well sorted; mostly subrounded to rounded quartz grains with shale and carbonate grains and some igneous rock fragments; slightly calcareous
226.2–230.0	3.8	Sand and gravel, olive-brown overall, very fine sand to fine gravel with occasional medium to coarse gravel and sparse cobbles, mostly medium to coarse sand, slightly to moderately well sorted; mostly shale, carbonates, and quartz grains; slightly calcareous
230.0–252.0	22.0	Sand, as at 225.0–226.2 ft, but somewhat lighter olive-brown; moderately calcareous with occasional clumps of very calcareous, very fine to fine silty sand that when dry breaks apart into angular, blocky pieces; rare medium gravel to cobbles; several thin silty sand layers at 245.0–246.0 ft
252.0–263.0	11.0	Sand and gravel, olive-brown to olive-gray overall, very fine sand to fine gravel with sparse medium to coarse gravel, mostly fine to very coarse sand, poorly sorted; fines mostly subrounded to rounded quartz and carbonates with shale, rest mostly sub-angular carbonates, shale, and quartz with igneous rock fragments; occasional thin silty and clayey layers that make "clay balls"; several nodules of cemented sand and gravel 0.5 inch or less in diameter at 252.0, 255.0 ft, and 259.0 ft
263.0–268.0	5.0	Sand, very fine sand to coarse, mostly fine to medium; well sorted; sparse coarse gravel in sand matrix; mostly subrounded to rounded quartz grains with shale and carbonates
268.0–271.0	3.0	Sand and gravel, very fine sand to coarse gravel, mostly medium to coarse sand with about 10% gravel, poorly sorted; fines mostly subrounded to rounded quartz and abundant black grains (small nodule of cemented sand and gravel noted in thin section made from the 270-ft sample)
271.0–275.0	4.0	Sand and gravel, as at 268.0–271.0 ft with about 40% gravel; grades to unit below
275.0–285.0	10.0	Sand and gravel, as at 268.0–271.0 ft with about 20% gravel to cobbles; coarse fraction mostly shale, chert, igneous rock fragments, and quartz; fines downward to sand below

Depth (ft)	Thickness (ft)	Description
285.0–286.0	1.0	Sand, very fine to very coarse, mostly medium to coarse, slightly to moderately well sorted; rare fine gravel in sand matrix
286.0–287.5	1.5	Sand and gravel, very fine sand to fine gravel, mostly fine to coarse sand with about 10% gravel, slightly to moderately well sorted; slightly calcareous
287.5–293.0	5.5	Sand, gray to olive-gray overall, very fine to coarse, mostly fine to medium, well sorted; abundant rounded to subrounded quartz grains; slightly calcareous
293.0–294.0	1.0	Sand and gravel, very fine sand to coarse gravel and cobbles, poorly sorted; slightly calcareous
294.0–298.0	4.0	Sand and gravel, very fine sand to coarse gravel and cobbles, poorly sorted; about 30% gravel with 10% coarse gravel and cobbles; four 1.0-inch-diameter nodules of cemented sand and gravel at 295.0 ft, 3 nodules of cemented sand and gravel 1.0–2.5 inches in diameter at 297.5 ft
298.0–310.0	12.0	Clay, very dark gray (5Y 3/1) to dark olive-gray (5Y 3/2) or very dark grayish brown (2.5Y 3/2); very silty to clayey silt; slightly to moderately sandy with very fine to very coarse sand, slightly pebbly with fine to medium gravel; massive, compact, dense; moderately calcareous; coal, sandstone, carbonate, and quartz clasts; some laminations below 308.0 ft
310.0–316.0	6.0	Silt, very dark grayish brown (2.5Y 3/2); moderately clayey; compact, dense, slightly cohesive; thin laminations apparent throughout; moderately calcareous; slightly to moderately micaceous below 315.0 ft
316.0–320.0	4.0	Silt, dark gray (5Y 4/1), moderately clayey, laminated with very dark gray (5Y 3/1) very silty clay; compact, dense; slightly to moderately cohesive; slightly calcareous; with some laminations of gray (2.5Y 6/1) to light gray (2.5Y 7/1) and dark grayish brown (2.5Y 4/2); lighter color laminations are noncalcareous
320.0–321.6	1.6	Silt, very dark brown (10YR 2/2), slightly to moderately clayey, slightly sandy with very fine sand, slightly pebbly with fine to medium gravel (dropstones?); crumbly and loose to slightly cohesive
321.6–323.9	2.3	Clay, black (5Y 2.5/1 to 5Y 2.5/2), very silty, slightly to moderately sandy with very fine to fine sand; massive, dense, compact; noncohesive; very slightly calcareous
323.9–326.0	2.1	Clay, dark olive-gray (5Y 3/2) with mottles of very dark brown (10YR 2/2) and dark greenish gray (5GY 4/1); very silty; dense, compact; noncohesive; breaks with blocky texture
326.0–328.0	2.0	Sand, black (5Y 2.5/2), very fine to medium, mostly fine, well sorted; moderately silty; mostly subrounded to rounded quartz? grains
328.0–329.0	1.0	Clay, black (5Y 2.5/2), very silty to clayey silt; slightly to moderately sandy with very fine to very coarse sand; slightly to moderately pebbly with fine to coarse gravel; dense, compact; noncohesive, breaks with blocky texture; noncalcareous
329.0–329.5	0.5	Sand, dark olive-gray (5Y 3/2), very fine to medium, mostly fine, well sorted; moderately silty; mostly subrounded to rounded quartz? grains
329.5–331.0	1.5	Clay, black (5Y 2.5/2), as at 328.0–329.0 ft but with clasts of black shale
		Pennsylvanian bedrock
331.0–333.0	2.0	Shale, very dark gray (5Y 3/1) to 331.5, black (5Y 2.5/1) below 331.5 ft; dense, compact; friable; noncohesive; noncalcareous; coal at 333 ft

Total depth = 333 ft

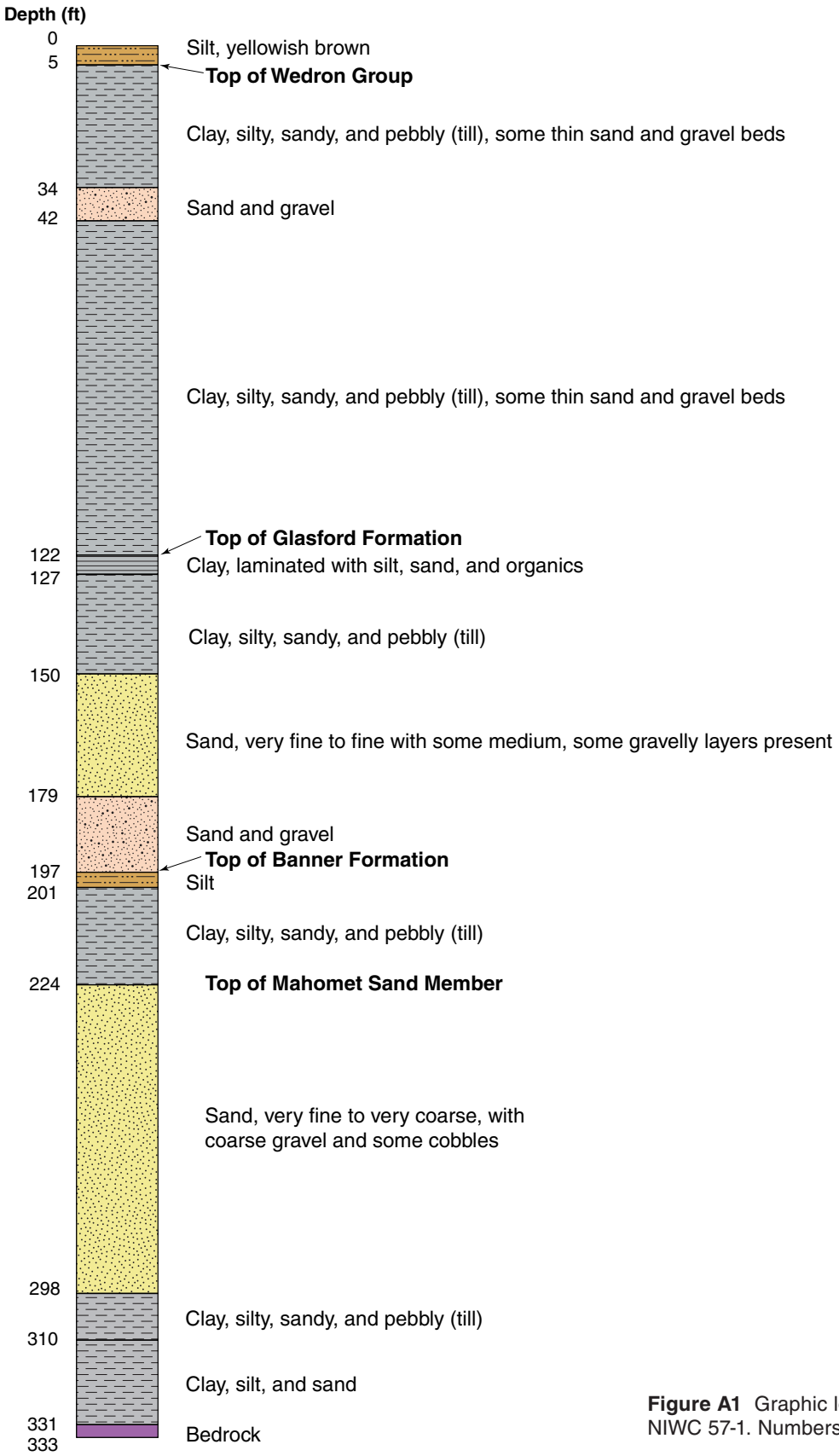

Figure A1 Graphic log for borehole NIWC 57-1. Numbers are rounded.

Detailed Descriptive Log for Borehole NIWC 57-2

Illinois State Geological Survey
NIWC 57-2

Location: Champaign County, SW ¼, SW ¼, SE ¼, Section 3, T19N, R08E
Elevation: 747 ft (msl)
Total depth: 310 ft
Date started: 7/20/99
Drilling method: Rotasonic by Boart Longyear
Location: 60 ft southeast of well house
Core descriptions: David R. Larson and Christopher J. Stohr
Geophysical logs: Natural gamma run inside 2-inch schedule 80 PVC to depth of only 140 ft

Depth (ft)	Thickness (ft)	Description
0.0–1.9	1.9	Silt, dark brown (10YR 3/3), slightly to moderately clayey, slightly sandy with very fine to fine sand, very slightly pebbly with rare to occasional fine to medium gravel; crumbly with blocky texture; noncohesive to very slightly cohesive; very slightly calcareous
1.9–5.0	3.1	Silt, dark brown (7.5YR 3/3), with yellowish brown (10YR 5/6) mottles; as at 0.0–1.9 ft
5.0–9.9	4.9	Silt, light olive-brown (2.5Y 5/4), slightly to moderately clayey, slightly to moderately sandy with very fine to very coarse sand, slightly pebbly with fine to medium gravel; compact, slightly cohesive, somewhat stiff; breaks with blocky texture; a few oxidation mottles
9.9–10.0	0.1	Sand, light olive-brown (2.5Y 5/6), very fine to medium, mostly fine, well sorted; predominantly subrounded to rounded quartz grains; saturated
		Wedron Group
10.0–11.0	1.0	Silt, light olive-brown (2.5Y 5/4), as at 9.9–10.0 ft
11.0–22.0	11.0	Silt, dark gray (10YR 4/1) with mottles of light olive-brown (2.5Y 5/4), slightly to moderately clayey; slightly to moderately sandy with very fine to very coarse sand, mostly very fine to fine sand; slightly pebbly with mostly fine to medium gravel and rare coarse gravel, usually flat, tabular, subangular to subrounded shale; stiff, compact; slightly to moderately cohesive; slightly to moderately calcareous, moderately calcareous below 20 ft
22.0–31.0	9.0	Silt, dark gray (5Y 4/1), moderately clayey, slightly to moderately sandy with very fine to very coarse sand, mostly very fine to fine sand; slightly pebbly with mostly fine to medium gravel and rare coarse gravel, usually flat, tabular, subangular to subrounded shale; somewhat stiffer and more compact than silt above; moderately cohesive; moderately calcareous
31.0–35.0	4.0	Sand, gray overall, very fine to coarse, mostly fine with medium, well sorted occasional fine gravel that is mostly shale pebbles; coarsening downward to very fine to very coarse sand, slightly to moderately well sorted; shale pebbles somewhat more abundant
35.0–39.0	4.0	Sand and gravel, gray overall, very fine sand to coarse gravel, mostly fine to coarse sand, rare coarse gravel, poorly sorted to slightly well sorted, becoming poorly sorted at 39 ft; mostly quartz with shale, igneous rock fragments, and carbonate grains
39.0–39.5	0.5	Sand, very fine to medium
39.5–45.0	5.5	Silt, grayish brown (2.5Y 5/2) mottled with gray (2.5Y 5/1), becomes darker with depth to dark grayish brown (2.5Y 4/2); slightly to moderately sandy with very fine to very coarse sand; slightly pebbly with fine to coarse gravel; cohesive, compact; moderately calcareous
45.0–74.0	29.0	Silt, as at 39.5–45.0 ft but dark gray (5Y 4/1)

Depth (ft)	Thickness (ft)	Description
74.0–74.5	0.5	Sand, very fine to medium, well sorted; mostly subrounded to rounded quartz grains; calcareous
74.5–79.0	4.5	Silt, dark gray (5Y 4/1) as at 45.0–74.0 ft
79.0–82.0	3.0	Silt, dark grayish brown (2.5Y 4/2) to olive-brown (2.5Y 4/3); moderately clayey, slightly to moderately sandy with very fine to very coarse sand, moderately pebbly with fine to coarse gravel; dense, compact, slightly cohesive, moderately calcareous
82.0–85.0	3.0	Silt, dark gray (5Y 4/1), slightly to moderately clayey, slightly to moderately sandy with very fine to very coarse sand, moderately pebbly with fine to coarse gravel; dense, compact, slightly crumbly to slightly cohesive; moderately to very calcareous
85.0–105.0	20.0	Silt, dark grayish brown (10YR 4/2) to brown (10YR 4/3), slightly clayey, slightly sandy with very fine to very coarse sand, slightly to moderately pebbly with fine to coarse gravel; dense, compact, blocky texture; moderately calcareous; thin seams of very fine to fine, well sorted, silty, sand at 102 ft and 104 ft; mostly rounded quartz grains
105.0–108.0	3.0	Silt, very dark grayish brown (2.5Y 3/2), slightly to moderately clayey, slightly sandy with very fine to very coarse sand, slightly pebbly with fine gravel; stiff, compact, dense; slightly cohesive to crumbly; slightly calcareous
108.0–110.0	2.0	Silt, very dark grayish brown (2.5Y 3/2), moderately clayey, slightly sandy very fine to very coarse sand, slightly to moderately pebbly with fine to coarse gravel and occasional cobbles; stiff, compact, dense; slightly to moderately cohesive; slightly calcareous; breaks with vague laminations
		Glasford Formation
110.0–112.0	2.0	Silt, dark gray (2.5Y 4/1), slightly to moderately clayey, laminated; slightly pebbly with medium to coarse gravel (dropstones?); moderately sticky; slightly to moderately compact and dense; slightly to moderately cohesive; slightly to moderately calcareous
112.0–119.0	7.0	Silt as at 110.0–112.0 ft without dropstones
119.0–122.0	3.0	Silt, dark greenish gray (5GY 4/1), moderately clayey, slightly to moderately sandy with very fine to very coarse sand, slightly pebbly with fine gravel; compact, dense, slightly cohesive; moderately calcareous; sharp contact with sand below
122.0–123.0	1.0	Sand, very dark grayish brown (2.5Y 3/2), very fine to medium, mostly fine, well sorted; predominantly rounded quartz grains
123.0–125.0	2.0	Silt, gray (2.5Y 5/1) or (10YR 5/1) with dark yellowish brown (10YR 4/4) mottles; moderately clayey, moderately sandy with very fine to very coarse but mostly very fine to fine sand; slightly to moderately pebbly with fine to coarse gravel; dense, compact, breaks with blocky texture; crumbly; moderately to very calcareous
125.0–138.0	13.0	Silt as at 123.0–125.0 ft but without dark yellowish brown (10YR 4/4) mottles; somewhat more crumbly texture; less calcareous
138.0–143.0	5.0	Sand, gray (2.5Y 5/1), very fine to fine, well sorted; moderately to very silty to sandy silt in part; noncohesive, moderately calcareous
143.0–143.4	0.4	Silt, grayish brown (2.5Y 5/2), very sandy with very fine to fine sand to very silty sand; noncohesive; moderately calcareous
143.4–145.0	1.6	Sand, grayish brown (2.5Y 5/2), very fine to medium, mostly fine, well sorted; mostly subrounded to rounded quartz grains; slightly to moderately silty; moderately to very calcareous
145.0–157.0	12.0	Sand as at 143.4–145.0 ft but very slightly to slightly calcareous
157.0–175.0	18.0	Sand, grayish brown (2.5Y 5/2), very fine to fine, well sorted; mostly rounded quartz grains; slightly to moderately silty; very crumbly, moderately calcareous, 1-inch diameter sand nodules at 175 ft
175.0–177.0	2.0	Sand, grayish brown (2.5Y 5/2), very fine to medium, mostly fine, well sorted; mostly subrounded to rounded quartz grains; slightly to moderately silty; noncalcareous to slightly calcareous
177.0–180.0	3.0	Sand as at 175.0–177.0 ft with dark gray (2.5Y 4/1), moderately calcareous mottles

Depth (ft)	Thickness (ft)	Description
180.0–181.0	1.0	Sand and gravel, very fine sand to coarse gravel and cobbles, mostly very fine to very coarse sand with about 15% fine gravel, occasional medium gravel, and sparse coarse gravel, cobbles at contact with silt below, poorly sorted; fine fraction mostly subangular to rounded quartz with carbonates and shale; coarse fraction has abundant carbonates and shale
181.0–184.0	3.0	Silt, gray (10YR 5/1), very slightly clayey; compact, stiff, not very dense, crumbly to slightly cohesive; slightly calcareous; vaguely laminated; some dropstones of fine to coarse gravel
184.0–184.5	0.5	Silt, gray (2.5Y 5/1), slightly clayey, slightly sandy with very fine to very coarse sand, slightly to moderately pebbly with fine to medium gravel; dense, compact, stiff; crumbly; moderately to very calcareous
184.5–188.0	3.5	Sand and gravel, grayish brown (2.5Y 5/2), very fine sand to coarse gravel and occasional cobbles, mostly fine to very coarse sand with about 40% gravel, poorly sorted; fines mostly subrounded to rounded quartz with subangular to subrounded quartz, carbonate and shale; coarse fraction mostly carbonates and shale with quartz and igneous rock fragments
188.0–193.0	5.0	Sand and gravel, grayish brown (2.5Y 5/2), very fine sand to coarse gravel and cobbles, mostly medium to very coarse sand with about 50% gravel, poorly sorted; fines mostly subrounded to rounded quartz with subangular to subrounded quartz, carbonate, and shale; coarse fraction mostly carbonates, and shale with quartz and igneous rock fragments
193.0–195.0	2.0	Gravel and sand, grayish brown (2.5Y 5/2), very fine sand to coarse gravel and cobbles, mostly coarse gravel and cobbles, poorly sorted; fines mostly subrounded to rounded quartz with subangular to subrounded quartz, carbonates, and shale; coarse fraction mostly carbonates and shale with quartz and igneous rock fragments
		Banner Formation
195.0–198.0	3.0	Silt, very dark gray (5Y 3/1) with some small yellowish brown mottles, moderately clayey; slightly to moderately sandy with very fine sand, slightly to moderately pebbly with fine to coarse gravel; compact, dense, moderately crumbly; moderately to very calcareous
198.0–203.0	5.0	Silt, very dark gray (5Y 3/1) as at 195.0–198.0 ft, but very compact and dense; breaks with blocky texture, vague laminations apparent; thin, saturated, sandy layer at 201 ft
203.0–205.0	2.0	Silt, dark grayish brown (2.5Y 4/2); slightly sandy with very fine to very coarse sand; slightly pebbly with fine gravel; compact, dense, noncohesive; very calcareous; crumbly, breaks with blocky texture, vague laminations apparent
205.0–212.0	7.0	Silt, as at 203.0–205.0 ft, but dark gray (2.5Y4/1) and somewhat less calcareous overall
212.0–217.5	5.5	Silt, dark grayish brown (2.5Y 4/2) as at 203.0–205.0 ft
217.5–217.7	0.2	Silt, light gray (2.5Y 7/1), abundant angular coarse gravel; very loose, noncohesive; very calcareous
217.7–221.0	3.3	Silt, as at 212.0–217.5 ft
		Mahomet Sand Member
221.0–223.0	2.0	Sand, dark grayish brown (2.5Y 4/2), very fine sand to fine, well sorted; mostly subrounded to rounded quartz grains; very silty; moderately calcareous
223.0–225.0	2.0	Sand, gray (2.5Y 5/1), very fine to medium, mostly fine to medium, moderately well sorted to well sorted; abundant subrounded to rounded quartz grains; moderately calcareous
225.0–230.0	5.0	Sand, gray (2.5Y 5/1), very fine to very coarse, mostly fine to coarse, moderately sorted; some thin silty, clayey, moderately to very calcareous layers with occasional fine gravel
230.0–234.0	4.0	Sand, gray (2.5Y 6/1), very fine to fine with sparse fine gravel, well sorted; mostly rounded quartz with some shale grains; silty, moderately to very calcareous

Depth (ft)	Thickness (ft)	Description
234.0–236.0	2.0	Sand, gray (2.5Y 6/1), very fine to coarse, mostly fine, well sorted; mostly rounded quartz with subangular to subrounded quartz, carbonate, and shale; slightly calcareous
236.0–239.0	3.0	Sand as at 230.0–234.0 ft
239.0–245.0	6.0	Sand as at 234.0–236.0 ft
245.0–247.0	2.0	Sand as at 230.0–234.0 ft, but very slightly to slightly calcareous
247.0–249.0	2.0	Sand as at 234.0–236.0 ft
249.0–257.0	8.0	Sand and gravel, very fine sand to sparse fine gravel, poorly sorted; fines are mostly rounded quartz grains; gravel mostly rounded shale
257.0–260.0	3.0	Sand as above 230.0–234.0 ft
260.0–268.0	8.0	Sand and gravel, very fine sand to rare fine gravel, mostly fine to medium sand, moderately well to well sorted; abundant subrounded to rounded quartz with carbonates and shale
268.0–287.0	19.0	Sand and gravel, gray (2.5Y 5/1), very fine sand to coarse gravel, mostly fine sand to fine gravel with about 40% gravel, poorly sorted; slightly to moderately silty, slightly clayey; moderately calcareous; coarsens downward somewhat becoming less silty, clayey, and calcareous
287.0–290.0	3.0	Sand and gravel, gray (2.5Y 5/1), very fine sand to coarse gravel, mostly fine sand to fine gravel with about 40% gravel, poorly sorted; moderately silty and clayey; moderately to very calcareous; gravel has light gray coating that appears to be bentonite, most prominent at 289.0–290.0 ft
290.0–294.0	4.0	Sand, gray (2.5Y 5/1), very fine to very coarse, mostly fine to medium, slightly to moderately well sorted; fines mostly subrounded to rounded quartz; coarse fraction mostly shale and carbonates with quartz; very calcareous
294.0–295.0	1.0	Rock, white (2.5Y 8/1), hard, surrounded by rock fragments of coarse gravel to cobble size; dolomite
295.0–298.0	3.0	Sand as above 290.0–294.0 ft
298.0–301.0	3.0	Clay, dark olive-gray (5Y 3/2) very silty to clayey silt; dense, compact; slightly sticky, slightly to moderately cohesive; slightly calcareous; occasional thin layers of clay, very silty, slightly to moderately sandy with very fine to very coarse sand, and slightly pebbly with fine to coarse gravel
301.0–306.0	5.0	Clay, dark olive-gray (5Y 3/2), slightly to moderately silty, slightly sandy with very fine to very coarse sand, moderately to very pebbly with fine to coarse gravel supported in silty clay matrix; slightly calcareous; breaks with a platy structure; occasional less pebbly layers
306.0–306.2	0.2	Clay, olive (5Y 4/4), slightly to moderately silty, slightly sandy with very fine to very coarse sand, very slightly to slightly pebbly with fine to coarse gravel; very slightly calcareous
306.2–310.0	3.8	Clay, very dark gray (5Y 3/1), slightly to moderately silty, slightly sandy with very fine to very coarse sand, very slightly to slightly pebbly with fine to coarse gravel; slightly to moderately calcareous; breaks with a platy structure

Total depth = 310 ft

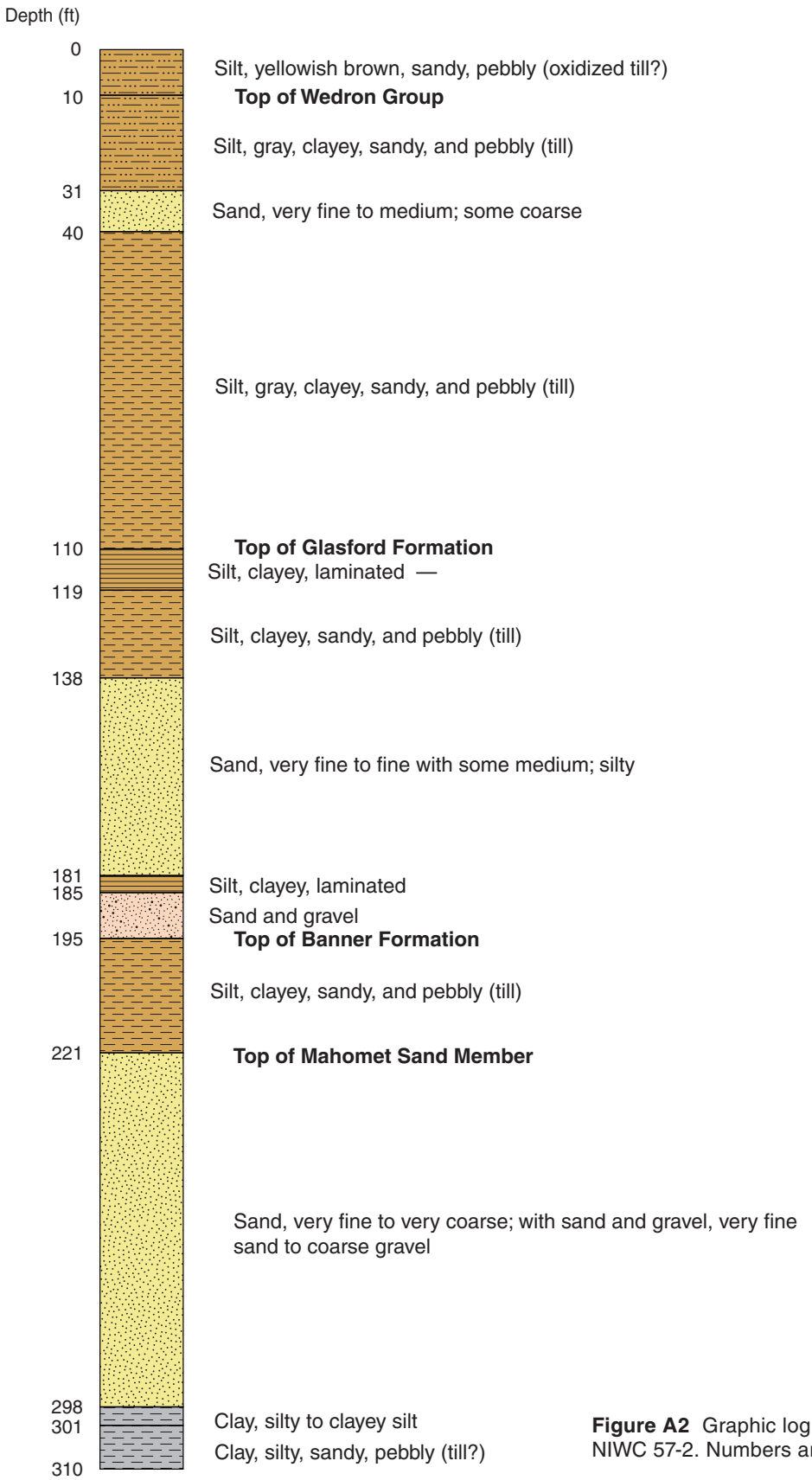

Figure A2 Graphic log for borehole NIWC 57-2. Numbers are rounded.

Table A1 Point count results of major clasts and other clasts from boreholes NIWC 57-1 and NIWC 57-2.

Borehole	Depth (feet)	Quartz (%)	Carbonate (%)	Feldspar (%)	Chert (%)	Rock fragments (%)
NIWC 57-1						
Glasford aquifer						
	159	69.2	16.1	2.8	1.9	10.0
	164	71.0	25.0	1.5	1.0	1.5
	169.5	71.0	18.5	5.0	0.0	5.5
	175	84.3	8.6	5.6	0.0	1.5
	179.5	75.0	9.5	8.5	0.0	7.0
	185	58.0	22.6	5.3	5.8	8.4
	190	27.4	27.4	3.5	7.0	34.8
	195	40.3	41.3	4.5	2.5	11.4
	Mean	62.0	21.1	4.6	2.3	10.0
NIWC 57-2						
Mahomet aquifer						
	230	47.1	29.6	5.8	3.4	14.1
	235	70.2	19.2	7.2	1.0	2.4
	240	72.6	19.9	4.0	1.0	2.5
	245	58.3	24.3	7.8	0.5	9.2
	250	65.9	16.3	10.6	1.9	5.3
	260	42.6	36.8	6.9	2.9	10.8
	265	64.6	24.8	3.9	2.4	4.4
	270	68.0	18.6	3.1	4.1	6.2
	275	36.6	23.4	3.9	17.1	19.0
	280	39.9	29.8	1.9	11.1	17.3
	285	43.8	28.8	1.0	9.1	17.3
	290	71.4	11.4	2.1	3.6	11.4
	297.5	64.0	4.5	3.5	15.0	13.0
	Mean	57.3	22.1	4.7	5.6	10.2
NIWC 57-1						
Cemented nodule						
	297.5	45	29	4	5	17
NIWC 57-1						
Mahomet aquifer						
	225	76.1	13.7	3.4	3.9	2.9
	235	63.6	15.7	2.3	5.1	13.4
	245	54.8	28.4	4.8	2.9	9.1
	255	41.8	31.3	5.0	7.5	14.4
	265	61.4	21.7	4.3	7.7	4.8
	275	24.2	36.2	1.9	12.6	25.1
	285	38.0	22.0	2.4	24.4	13.2
	290	27.6	27.6	2.5	25.6	16.6
	295	64.4	17.3	4.5	6.4	7.4
	Mean	50.2	29	3.5	10.7	11.9

Geochemical and Isotopic Data

Table A2 Geochemical and isotopic data for wells screened in the Mahomet aquifer.

Sample	Date sampled	Owner	Well screen depth (m)	Elevation (m)	Pumping rate (L/s)	Temp. (°C)	pH	Eh[1] (mV)	Sp. cond. (μS/cm)	Tot. alk. as $CaCO_3$ (mg/L)
CHM 94A	10/26/98	ISWS	117	250	0.24	14.1	7.4	71	664	374
CHM 95B	10/27/98	ISWS	85.3	239	0.21	13.8	7.4	40	665	379
CHM 95D	10/27/98	ISWS	86.2	213	0.27	14.0	7.4	–28	645	372
CHM 96A	10/26/98	ISWS	94.5	220	0.34	13.8	7.3	107	670	342
CHM 96B	10/26/98	ISWS	89.9	215	0.31	13.9	7.3	92	676	349
CHM 96C	10/27/98	ISWS	88.4	213	0.28	13.8	7.1	76	699	372
NIWC 55	9/10/98	NIWC	91.4	224	63	13.0	7.6	49	637	360
NIWC 57	9/10/98	NIWC	92.6	229	100	13.2	7.6	37	603	356
NIWC 58	9/10/98	NIWC	99.4	234	150	13.1	7.5	56	648	335

Sample	Na^+ (mg/L)	K^+ (mg/L	Ca^{2+} (mg/L	Mg^{2+} (mg/L	SiO_2 (mg/L	HCO_3^- (mg/L	NO_3^- (mg/L	NH_3^+ (mg/L	SO_4^{2-} (mg/L	Cl^- (mg/L
CHM 94A	48.9	2	72.6	28.3	19.1	456	<1.6	ND	8.7	0.8
CHM 95B	36.1	2	71.2	36.1	18.5	462	<1.6	ND	6.0	1.0
CHM 95D	35.9	2	69.1	33.9	16.9	454	<1.6	ND	<0.3	1.7
CHM 96A	32.8	1	82.8	31.6	19.8	417	<1.6	ND	42.9	0.6
CHM 96B	29.1	2	84.8	33.3	20.5	426	<1.6	ND	42.8	0.9
CHM 96C	26.9	<1	88.4	34.7	22.7	454	<1.6	ND	31.4	1.0
NIWC 55	34.4	3	61.3	34.5	13.1	439	<0.8	0.71	0.21	1.8
NIWC 57	47.3	<1	52.0	29.9	13.5	434	<0.8	1.53	<0.3	1.5
NIWC 58	39.4	<1	52.2	29.9	13.3	408	0.01	1.34	0.22	2.1
Detection limits	1.34	0.629	0.004	0.003	0.024	NA	0.005	0.010	0.010	0.010

Sample	Fe	Mn	Log pCO_2 (atm)	TDS (mg/L)	SI_{CAL}	SI_{ARAG}	SI_{DOLO}	SI_{SID}	SI_{HEM}
CHM 94A	1.43	0.07	–1.808	640	0.240	0.088	0.264	0.644	13.5
CHM 95B	0.89	0.05	–1.847	635	0.283	0.131	0.459	0.485	12.2
CHM 95D	1.87	0.03	–1.871	616	0.280	0.128	0.442	0.817	10.6
CHM 96A	0.68	0.24	–1.739	631	0.135	-0.170	0.041	0.179	13.4
CHM 96B	0.84	0.13	–1.791	647	0.211	0.059	0.207	0.332	13.4
CHM 96C	1.73	0.13	–1.554	661	0.048	-0.104	–0.122	0.465	12.2
NIWC 55	0.91	0.05	–1.929	592	0.245	0.092	0.417	0.522	12.8
NIWC 57	1.31	0.02	–2.013	583	0.252	0.100	0.440	0.753	13.6
NIWC 58	1.11	0.02	–2.064	550	0.261	0.108	0.459	0.692	13.2
Detection limits	0.009	0.009	NA	NA	NA	NA	NA	NA	NA

Sample	$SI_{Fe(OH)_3}$	TC (cfu/ml)	Ent. (cfu/ml)	FC (cfu/ml)	TA (cfu/ml)	NVOC (mg/L)	Log pCO_2 CH_4 (mmol/L)	CO_2 (mmol/L)	TU
CHM 94A	0.272	0	0	0	10	2.1	4.64×10^{-3}	1.47×10^{-1}	<0.40
CHM 95B	–0.340	0	0	0	207	2.0	2.98×10^{-2}	1.08×10^{-1}	ND
CHM 95D	–1.173	0	0	0	108	2.2	2.81×10^{-1}	2.17×10^{-1}	ND
CHM 96A	0.255	0	0	0	88	2.4	1.21×10^{-3}	2.07×10^{-1}	<0.66
CHM 96B	0.257	0	0	0	10	1.4	1.12×10^{-3}	1.62×10^{-1}	ND
CHM 96C	–0.338	0	0	0	90	2.2	5.19×10^{-3}	5.96×10^{-1}	ND
NIWC 55	–0.028	0	0	0	8	2.0	1.76×10^{-1}	3.51×10^{-1}	<0.42
NIWC 57	0.366	ND	ND	ND	10	3.5	4.90×10^{-1}	3.62×10^{-1}	<0.52
NIWC 58	0.172	0	0	0	130	2.7	3.42×10^{-1}	3.22×10^{-1}	ND
Detection limits	NA		1	1	1	1	NA	NA	NA

[1]Eh, redox potential; Sp. cond., specific conductance; Tot. alk., total alkalinity; pCO_2, partial pressure CO_2; TDS, total dissolved solids; calc., calculated; SI, saturation index; CAL, calcite; ARAG, aragonite; DOLO, dolomite; SID, siderite; HEM, hematite; cfu, colony-forming units; TC, total coliforms; Ent., fecal enterococci; FC, fecal coliforms; TA, total aerobic; NVOC, nonvolatile organic carbon; TU, tritium unit; ND, not determined; NA, not applicable.

Response Test Performed in Well NIWC 57

Methods

Well NIWC 57 was not used during the test drilling and installation of observations wells at the site. It was returned to service on August 11, 1999. To take advantage of the month-long off-cycle of NIWC 57 and the recovery of the potentiometric surface in this part of the Mahomet aquifer, the effects of resumed pumping on the water levels in the newly installed observation wells were monitored. Using an air line, water-level fluctuations in NIWC 57 were also measured. Well 57 was pumped at 1,650 to 1,750 gpm according to instantaneous measurements of flow at the pump head and at 1,744 gpm according to calculations based on totalizer gage reading pumping. The results of this response test can be used to conduct an aquifer test using well NIWC 57 in the future.

Water levels in monitoring wells NIWC 57-1G and NIWC 57-1M were periodically measured from July 21 through August 30, 1999, with an electric water-level meter. Water levels were measured from the top of the casing within the steel manhole at each well. Water levels in monitoring wells NIWC 57-2G and NIWC 57-2M were periodically measured from July 26 through August 30, 1999, using an electric water-level meter. Data loggers and pressure transducers were installed in monitoring wells NIWC 57-2G and NIWC 57-2M on August 10, 1999, and in monitoring well NIWC 57-1M on August 16, 1999. These instruments were programmed to record water levels, initially every hour and subsequently every minute. A pressure transducer was placed in NIWC 57-2M at a depth of 35.62 feet. Water levels in these wells were not measured with electric water-level meters while the data loggers were in place. Brian Good (IL-AWC) organized data collection, supervised the operation of NIWC 57, and provided data on the quantity of water pumped from NIWC 57 and other NIWC wells in the west well field.

When the data logger in NIWC 57-2M was retrieved for reprogramming

Table A3 Water level measurements for response test on observation wells adjacent to well NIWC 57. Water levels were measured with electric water level meters.

Well	Date	Time	Depth to water (ft below top of casing)	Change in depth to water
NIWC 57-1G	07/21/99	13:27	158.77	-
	07/23/99	17:08	158.66	0.11
	07/23/99	19:09	158.65	0.01
	07/26/99	08:22	157.29	1.36
	08/10/99	12:18	157.26	0.03
	08/11/99	15:32	157.46	–0.20
	08/12/99	09:15	157.53	–0.07
	08/12/99	14:58	157.36	0.17
	08/13/99	08:41	157.28	0.08
	08/13/99	10:27	157.26	0.02
	08/14/99	19:05	157.66	–0.40
	08/15/99	17:19	157.70	–0.04
	08/16/99	10:00	157.76	–0.06
	08/17/99	15:26	157.64	0.12
	08/18/99	08:51	157.67	–0.03
	08/18/99	10:30	157.66	0.01
	08/20/99	12:30	157.72	-0.06
	08/20/99	13:25	157.72	0.00
	08/23/99	10:47	157.50	0.22
	08/25/99	12:39	157.49	0.01
	08/30/99	14:10	157.96	-0.47
NIWC 57-1M	07/21/99	13:22	167.08	-
	07/23/99	17:04	167.97	–0.90
	07/23/99	19:04	169.90	–1.93
	07/26/99	08:18	166.12	3.78
	08/10/99	12:15	165.84	0.28
	08/11/99	15:21	185.44	–19.60
	08/12/99	09:11	184.78	0.66
	08/12/99	14:55	184.90	–0.12
	08/13/99	08:38	185.72	–0.82
	08/13/99	10:23	185.80	–0.08
	08/14/99	19:01	183.21	2.59
	08/15/99	17:15	183.09	0.12
	08/16/99	09:56	184.07	–0.98
	Data logger installed on 8/16/99; no measurements until 8/20/99			
	08/20/99	13:28	164.23	19.84
	08/23/99	10:44	165.20	–0.97
	08/25/99	12:37	166.35	–1.15
	08/30/99	14:08	168.88	–2.53
NIWC 57-2G	07/26/99	08:40	154.70	-
	08/10/99	09:45	154.74	–0.04
	Data logger installed on 8/10/99; no measurements until 8/20/99			
	08/20/99	13:37	155.22	–0.48
	08/23/99	10:56	154.99	0.23
	08/25/99	12:45	154.97	0.02
	08/30/99	14:03	155.45	–0.48
NIWC 57-2M	07/26/99	08:37	163.00	-
	08/10/99	09:47	162.91	0.09
	Data logger installed on 8/10/99; no measurements until 8/18/99. Removed data logger 8/18/99; reprogrammed to measure submergence more frequently in preparation for well NIWC 57 being turned off			
	08/18/99	08:42	170.09	–7.18
	08/18/99	08:58	170.12	–0.03
	Data logger reinstalled in 8/18/99; monitor water level change when well NIWC 57 turned off			
	08/20/99	13:40	161.55	8.57
	08/23/99	10:53	162.49	–0.94
	08/25/99	12:43	163.60	–1.11
	08/30/99	14:00	166.80	–3.20

during the response test, bentonite was detected at a depth of 138 to 139 feet. The bentonite may have entered the well because of a loose joint in the casing or a missing or broken O-ring at the joint. The bentonite was flushed from the observation well at that time.

Results

Water levels measured in the monitoring wells completed in the Glasford aquifer were consistently higher than those measured in the two monitoring wells completed in the Mahomet aquifer (table A3). The water level in NIWC 57-1G varied by 1.51 feet, from a high of 157.26 feet to a low of 158.77 feet below the top of the well casing. Water levels in NIWC 57-2G varied by 0.75 feet, from a high of 154.70 feet to a low of 155.45 feet.

Water levels in the observation wells completed in the Mahomet aquifer were measured by electric water level meters when the data loggers were not in place (table A3). The water level in NIWC 57-1M varied by 21.57 feet, from a high of 164.23 feet to a low of 185.80 feet. Water levels in NIWC 57-2M varied by 8.57 feet, from a high of 161.55 feet to a low of 170.12 feet. The water level measured in monitoring wells NIWC 57-1M and NIWC-2M indicate the Mahomet aquifer is under confined conditions. Water-level data indicate a downward vertical hydraulic gradient between the Glasford aquifer and the Mahomet aquifer. When NIWC 57 was turned off, measured water levels in both shallow monitoring wells were 7 to 9 feet higher than those in the deep monitoring wells. While NIWC 57 was being pumped, the measured water level in NIWC 57-1M was about 25 to 29 feet lower than NIWC 57-1G. Data loggers were monitoring the water level in NIWC 57-2G and NIWC 57-2M during this time.

When well NIWC 57 was returned to service and pumped at 1,650 to 1,750 gpm, the water level in NIWC 57-2M was immediately lowered. Water-level data collected using data loggers in NIWC 57-2G and NIWC 57-2M show the immediate effect of pumping on the water level in NIWC 57-2M (fig. A3), but little, if any, change of the water level in NIWC 57-2G (not shown). In addition, NIWC 57-2G did not respond to changes in atmospheric pressure. The data logger in NIWC 57-2M collected data for 10,200 minutes after pumping started. At this time it was retrieved from the well and reprogrammed to take a measurement every minute instead of every hour. These data were collected to determine the magnitude of water-level fluctuation in monitoring well NIWC 57-2M in anticipation of conducting an aquifer test in the future. As figure A3 shows, the pressure transducer used with the data logger could not recognize a water level higher than 35.62 feet above the transducer. Thus, water-level fluctuations higher than the initial water level were not recorded. The fluctuations observed in figure A3 most likely are the result of change in barometric pressure or possibly minor variations in the pumping rate of well NIWC 57. Although the data are less than ideal, they yield information on the magnitude of change in water level during pumping and will be helpful for planning future pumping tests.

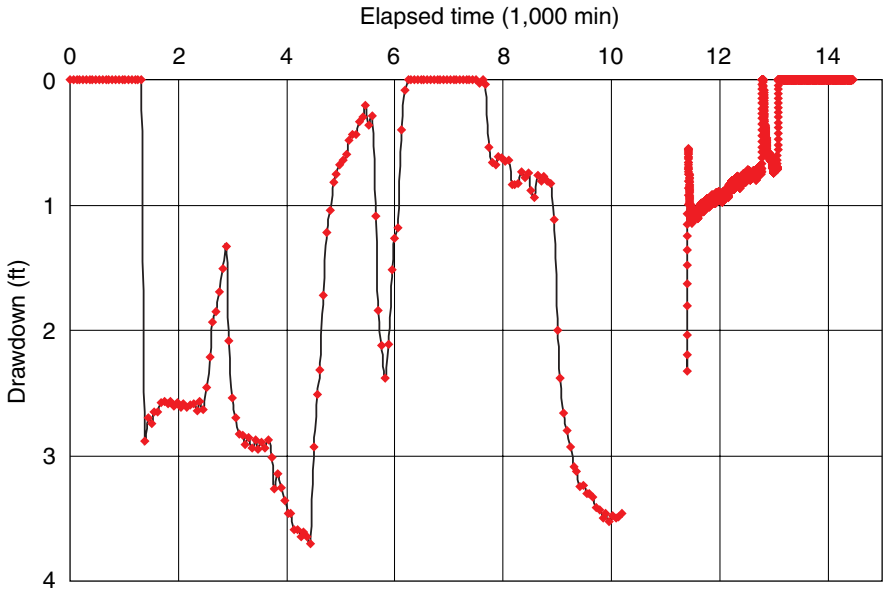

Figure A3 Plot of water-level fluctuations recorded in monitoring well NIWC 57-2M during a response test. The water level in the well, completed in the Mahomet aquifer, is a response to pumping of well NIWC 57.

The response of the water level in NIWC 57-1G and NIWC 57-1M also was monitored using water-level meters. No appreciable change was observed in NIWC 57-1G. The lowest water level in NIWC 57-1M measured during the test was 185.80 feet on August 13, 1999. This level was 19.96 feet lower than the highest water level of 165.84 feet measured before pumping started. The results of this response test provide a good example of how pumping decreases hydrostatic pressure close to the well, which results in outgassing of CO_2 from the groundwater.